

2014

Assessment and optimisation of N-nitrosamine rejection by reverse osmosis for planned potable water recycling applications

Takahiro Fujioka
University of Wollongong

Recommended Citation

Fujioka, Takahiro, Assessment and optimisation of N-nitrosamine rejection by reverse osmosis for planned potable water recycling applications, Doctor of Philosophy thesis, School of Civil, Mining, and Environmental Engineering, University of Wollongong, 2014.
<http://ro.uow.edu.au/theses/4050>

UNIVERSITY OF WOLLONGONG

COPYRIGHT WARNING

You may print or download ONE copy of this document for the purpose of your own research or study. The University does not authorise you to copy, communicate or otherwise make available electronically to any other person any copyright material contained on this site. You are reminded of the following:

Copyright owners are entitled to take legal action against persons who infringe their copyright. A reproduction of material that is protected by copyright may be a copyright infringement. A court may impose penalties and award damages in relation to offences and infringements relating to copyright material. Higher penalties may apply, and higher damages may be awarded, for offences and infringements involving the conversion of material into digital or electronic form.



School of Civil, Mining, and Environmental Engineering

Faculty of Engineering and Information Sciences

**Assessment and Optimisation of N-nitrosamine
Rejection by Reverse Osmosis for Planned Potable
Water Recycling Applications**

A thesis submitted in fulfilment of the
requirements for the award of the degree of

DOCTOR OF PHILOSOPHY

From

The University of Wollongong

By

Takahiro Fujioka

April 2014

UNIVERSITY OF WOLLONGONG

COPYRIGHT WARNING

You may print or download ONE copy of this document for the purpose of your own research or study. The University does not authorise you to copy, communicate or otherwise make available electronically to any other person any copyright material contained on this site. You are reminded of the following:

Copyright owners are entitled to take legal action against persons who infringe their copyright. A reproduction of material that is protected by copyright may be a copyright infringement. A court may impose penalties and award damages in relation to offences and infringements relating to copyright material. Higher penalties may apply, and higher damages may be awarded, for offences and infringements involving the conversion of material into digital or electronic form.

Certificate of Originality

I hereby declare that this submission is my own work and that it contains no material previously published or written by any other person nor material which to substantial extent has been accepted for the award of any other degree or diploma at the university of Wollongong or any other educational institution.

Takahiro Fujioka

Thesis supervisor

A/Prof. Long Duc Nghiem, University of Wollongong, School of Civil, Mining, and Environmental Engineering, Wollongong, Australia. longn@uow.edu.au

Abstract

A comprehensive assessment focusing on the rejection of eight N-nitrosamines by reverse osmosis (RO) membranes was conducted for planned potable water recycling applications. The effects of feed solution characteristics, operating conditions, fouling, chemical cleaning and membrane characteristics on the rejection of N-nitrosamines were first examined at laboratory scale. Field sampling campaigns were carried out at full-scale water recycling plants to provide longitudinal and spatial insights to the rejection of N-nitrosamines. For the prediction of the rejection of N-nitrosamines by spiral-wound RO membrane systems, a mathematical model was developed based on the irreversible thermodynamic principle and hydrodynamic calculation. The model was validated with the results obtained from a pilot-scale RO system.

The results reported here indicate that the rejection of N-nitrosamines by a given membrane increased in the order of increasing molecular weight, suggesting that steric hindrance was a dominating rejection mechanism of N-nitrosamines. The results also indicate that pH, ionic strength, and temperature of the feed solution can exert an influence on the rejection of N-nitrosodimethylamine (NDMA) and in some cases other N-nitrosamines. An increase in the feed temperature led to a significant decrease in the rejection of all N-nitrosamines and the impact was more pronounced for the small molecular weight N-nitrosamines. In general, the rejection of N-nitrosamines increased when the membranes were fouled by tertiary effluent. The rejection of low molecular weight N-nitrosamines was most affected by membrane fouling. From the results reported here, it appears that low molecular weight foulants present in the tertiary effluent can restrict the solute pathway within the active skin layer of membranes, resulting in the observed increase of solute rejection. Caustic chemical cleaning resulted in an increase in membrane permeability but caused a notable decrease in the rejection of N-nitrosamines. The impact of caustic cleaning was not permanent and could be significantly reduced by a subsequent acidic cleaning step. In general, the rejection of NDMA and N-nitrosomethylethylamine (NMEA) increased with decreasing membrane permeability. The impact of membrane permeability became less important for higher

molecular weight N-nitrosamines. In addition to the mean free-volume hole-radius of RO membranes which was measured by the positron annihilation lifetime spectroscopy (PALS), other membrane parameters and properties such as the free-volume hole-radius distribution and thickness of the active skin layer can also play a role in governing the rejection of small and uncharged solutes by RO membranes.

During the sampling campaigns at three full-scale water recycling plants, NDMA was detected in all RO feed samples varying between 7 and 32 ng/L. Overall rejection of NDMA among the three RO systems varied widely from 4 to 47%. Data presented here suggest that the feed temperature can influence rejection of NDMA. A considerable variation in NDMA rejection across the three RO stages (14-78%) was also observed. Overall N-nitrosomorpholine (NMOR) rejections were consistently high ranging from 81 to 84%. On the other hand, overall rejection of N-nitrosodiethylamine (NDEA) varied from negligible to 53%, which was considerably lower than values reported in previous laboratory-scale studies.

The developed model was able to accurately describe the rejection of N-nitrosamines under a range of permeate flux and system recovery conditions. The modelled N-nitrosamine rejections were in good agreement with values obtained experimentally using a pilot-scale RO filtration system. The modelling results also revealed that an increase in recovery caused a decrease in the rejection of these N-nitrosamines, which is consistent with the experimental results. Further modelling investigations suggested that NDMA rejection by a spiral-wound system can drop from 49 to 35% when the overall recovery increased from 10 to 50%. The model developed from this study can be a useful tool for water utilities and regulators for system design and evaluating the removal of N-nitrosamines by RO membranes.

Acknowledgements

I would like to express the deepest appreciation to Associate Professor, Long Nghiem who continually and persuasively conveyed a spirit of adventure and tremendous supports in regard to research. Without his supervision and constant help this achievement on my PhD work would not have been possible.

My PhD work was also made possible by the Australian Research Council (ARC) Linkage Project LP0990705 (with industry support from Veolia Water and Seqwater). I am most grateful to have had the opportunity to work in this ARC project. I would also like to thank the University of Wollongong for a PhD scholarship.

I would like to express my special thanks to the collaborators of the ARC project. A/Prof Stuart Khan and Dr James McDonald (UNSW) are thanked for providing their generous helps for the analysis of trace organic chemicals and sharing their valuable knowledge. I would also like to express my gratitude and thanks to Ms Annalie Roux (Seqwater) and Mr Yvan Poussade (Veolia Water) for providing us various supports and sharing their priceless experiences. I would like to express my special gratitude to Professor Jorg Drewes (TU München) for his critical advices on the research plan and publications and his continuous engagement through the progress of my PhD work.

I would like to express my gratitude to persons who provides me analytical information using state-of-the-art instruments. Dr Rita Henderson (UNSW) is thanks for allowing us to see the details of organic matter in water using the LC-OCD technique (Chapter 5). Dr Nagayasu Oshima and Dr Ryoichi Suzuki (National Institute of Advanced Industrial Science and Technology, Japan) are also thanked for providing us the insights of polymer membranes using the PALS technique (Chapter 8).

My thanks and appreciations also go to my colleagues in the same laboratory who have willingly helped me out with their abilities. I specially acknowledge Kha Tu for his assistance with ICP-MS analysis. I would like to express my thanks to technical officers of the Faculty of Engineering and Information Sciences, Robert Rowlan, Frank Crabtree and Ling Tie for their generous supports.

A special thank must be given to my wife Sandrine for her understanding and help on my work. I was able to devote myself to my research work thanks to her help.

Table of Contents

Chapter 1 Introduction.....	1
Chapter 2 Literature review	4
1 <i>Introduction.....</i>	4
2 <i>Indirect potable water reuse and N-nitrosamines.....</i>	6
2.1 Water reclamation process.....	6
2.2 Occurrence of N-nitrosamines in water recycling schemes.....	9
2.3 Health-based water quality guidelines and standards for N-nitrosamines.....	14
2.4 N-nitrosamine quantification using chemical analysis	17
2.5 Removal of N-nitrosamines during Water Reclamation.....	18
3 <i>N-nitrosamine removal by RO membranes</i>	18
3.1 Rejection of N-nitrosamines in laboratory-scale studies	18
3.2 Rejection of N-nitrosamines and N-nitrosamine precursors in pilot- and full-scale installations	20
3.3 Factors affecting N-nitrosamine rejections.....	24
3.4 Research gaps	29
4 <i>Conclusions</i>	30
Chapter 3 Materials and Methods	32
1 <i>Introduction.....</i>	32
2 <i>Selected NF/RO membranes</i>	32
3 <i>Chemicals.....</i>	33
4 <i>Filtration system.....</i>	36
4.1 Bench-scale filtration system.....	36
4.2 Pilot-scale filtration system.....	36
5 <i>Water chemistry analytical techniques</i>	38
5.1 N-nitrosamine concentration analysis.....	38
5.2 Basic analytical techniques	39
6 <i>Membrane characterisation</i>	39
6.1 Contact angle measurement.....	39
6.2 Zeta potential measurement	40
6.3 Surface chemistry.....	41
Chapter 4 Effects of feed solution characteristics.....	42
1 <i>Introduction.....</i>	42

2	<i>Materials and methods</i>	43
2.1	NF/RO membranes	43
2.2	Chemicals.....	43
2.3	Bench-scale filtration system.....	43
2.4	Experimental protocols	43
2.5	Analytical methods	44
2.6	Transport model description	44
3	<i>Results and discussion</i>	47
3.1	Separation behaviour of N-nitrosamines	47
3.2	Modelling the transport of N-nitrosamines during RO filtration.....	49
3.3	Effects of RO feed solution chemistry.....	52
4	<i>Conclusions</i>	57
Chapter 5 Effects of membrane fouling		58
1	<i>Introduction</i>	58
2	<i>Materials and methods</i>	59
2.1	NF/RO membranes	59
2.2	Chemicals.....	59
2.3	Tertiary treated effluent	59
2.4	Membrane filtration system	59
2.5	Experimental protocols	59
2.6	Analytical techniques.....	61
3	<i>Results and discussion</i>	62
3.1	Characteristics of the tertiary effluent and model foulants	62
3.2	Membrane fouling behaviour.....	64
3.3	Characteristics of fouled membranes.....	67
3.4	Effects of membrane fouling on inorganic salt retention.....	69
3.5	Effects of membrane fouling on N-nitrosamine rejection	70
4	<i>Conclusions</i>	74
Chapter 6 Membrane exposure to chemical cleaning reagents		75
1	<i>Introduction</i>	75
2	<i>Materials and methods</i>	76
2.1	RO membranes	76
2.2	Chemicals.....	76
2.3	Membrane filtration system	77
2.4	Simulated chemical cleaning protocols	77
2.5	Filtration experiments	79
2.6	Analytical methods	79

3	<i>Results and discussion</i>	79
3.1	Effects of membrane cleaning on membrane characteristics.....	79
3.2	Effects of chemical cleaning on rejection performance of RO membranes ..	85
3.3	Sequential cleaning	88
4	<i>Conclusions</i>	89
Chapter 7 Effects of membrane characteristics.....		90
1	<i>Introduction</i>	90
2	<i>Materials and methods</i>	91
2.1	RO membranes	91
2.2	Chemicals.....	91
2.3	Membrane filtration system	91
2.4	Filtration experiments	91
2.5	N-nitrosamine analytical methods	92
2.6	Transport model description	92
3	<i>Results and discussion</i>	93
3.1	N-nitrosamine rejection by NF/RO membranes	93
3.2	Effects of filtration conditions	97
4	<i>Conclusions</i>	102
Chapter 8 Role of free-volume hole-space of RO membranes.....		103
1	<i>Introduction</i>	103
2	<i>Materials and methods</i>	104
2.1	RO membranes	104
2.2	Chemicals.....	104
2.3	Membrane filtration system	104
2.4	Experimental protocols	105
2.5	Analytical technique	105
3	<i>Results and discussion</i>	107
3.1	PALS analysis.....	107
3.2	Rejection of boric acid and N-nitrosamines.....	109
3.3	Rejection mechanisms	110
4	<i>Conclusions</i>	112
Chapter 9 Full-scale monitoring		114
1	<i>Introduction</i>	114
2	<i>Materials and methods</i>	115
2.1	RO systems	115
2.2	Sampling protocol.....	117

2.3	Analytical technique	118
2.4	Calculation	119
3	<i>Results and discussion</i>	119
3.1	Organic and inorganic constituent removal	119
3.2	N-nitrosamine removal	122
3.3	Rejections by RO membranes.....	128
4	<i>Conclusions</i>	131
Chapter 10 Mathematical model development and validation		132
1	<i>Introduction</i>	132
2	<i>Theoretical background</i>	133
2.1	Membrane element characteristics.....	133
2.2	Hydrodynamics	134
2.3	Solute permeation through membranes	137
3	<i>Materials and methods</i>	139
3.1	Pilot-scale filtration system and RO element.....	139
3.2	Chemicals.....	140
3.3	Filtration experiments	140
3.4	Analytical technique	141
4	<i>Results and discussion</i>	141
4.1	Determination of model parameters.....	141
4.2	N-nitrosamine rejection	142
4.3	Impact of recoveries.....	144
5	<i>Conclusions</i>	146
Chapter 11 Conclusions		148
Chapter 12 Future research		152
Glossary		154
List of symbols.....		155
References.....		158

List of Publications

Thesis Related Publications

T. Fujioka, L.D. Nghiem, S.J. Khan, J.A. McDonald, Y. Poussade, J.E. Drewes, Effects of feed solution characteristics on the rejection of N-nitrosamines by reverse osmosis membranes, *J. Membr. Sci.*, 409–410 (2012) 66-74.

T. Fujioka, S.J. Khan, Y. Poussade, J.E. Drewes, L.D. Nghiem, N-nitrosamine removal by reverse osmosis for indirect potable water reuse – A critical review based on observations from laboratory-, pilot- and full-scale studies, *Sep. Purif. Technol.*, 98 (2012) 503-515.

T. Fujioka, S.J. Khan, J.A. McDonald, R.K. Henderson, Y. Poussade, J.E. Drewes, L.D. Nghiem, Effects of membrane fouling on N-nitrosamine rejection by nanofiltration and reverse osmosis membranes, *J. Membr. Sci.*, 427 (2013) 311-319.

T. Fujioka, S.J. Khan, J.A. McDonald, A. Roux, Y. Poussade, J.E. Drewes, L.D. Nghiem, N-nitrosamine rejection by nanofiltration and reverse osmosis membranes: The importance of membrane characteristics, *Desalination*, 316 (2013) 67-75.

T. Fujioka, N. Oshima, R. Suzuki, S.J. Khan, A. Roux, Y. Poussade, J.E. Drewes, L.D. Nghiem, Rejection of small and uncharged chemicals of emerging concern by reverse osmosis membranes: The role of free volume space within the active skin layer, *Sep. Purif. Technol.*, 116 (2013) 426-432.

T. Fujioka, S.J. Khan, J.A. McDonald, A. Roux, Y. Poussade, J.E. Drewes, L.D. Nghiem, N-nitrosamine rejection by reverse osmosis membranes: A full-scale study, *Water Res.*, 47 (2013) 6141-6148.

T. Fujioka, S.J. Khan, J.A. McDonald, A. Roux, Y. Poussade, J.E. Drewes, L.D. Nghiem, N-nitrosamine rejection by RO: Effects of exposing the membrane to chemical cleaning reagents, *Desalination*, 343 (2014) 60-66.

T. Fujioka, S.J. Khan, J.A. McDonald, A. Roux, Y. Poussade, J.E. Drewes, L.D. Nghiem, Modelling the rejection of N-nitrosamines by a Spiral-Wound Reverse Osmosis System: Mathematical model development and validation, *J. Membr. Sci.*, 454 (2014) 212-219.

Other Publications

K.C. Wijekoon, **T. Fujioka**, J.A. McDonald, S.J. Khan, F.I. Hai, W.E. Price, L.D. Nghiem, Removal of N-nitrosamines by an aerobic membrane bioreactor, *Bioresource Technology*, 141 (2013) 41-45.

K.L. Tu, **T. Fujioka**, S.J. Khan, Y. Poussade, A. Roux, J.E. Drewes, A.R. Chivas, L.D. Nghiem, Boron as a surrogate for N-nitrosodimethylamine (NDMA) rejection by reverse osmosis membranes in potable water reuse applications, *Environ. Sci. Technol.*, 47 (2013) 6425–6430.

T. Fujioka, L.D. Nghiem, Modification of a polyamide reverse osmosis membrane by heat treatment for enhanced fouling resistance, *Water Sci. Technol. Water Supply*, 13 (2013) 1553-1559.

T. Fujioka, S.J. Khan, J.A. McDonald, L.D. Nghiem, Ozonation of N-nitrosamines in the Reverse Osmosis Concentrate from Water Recycling Applications, *Ozone: Science & Engineering*, 36 (2014) 174-180.

T. Fujioka, S.J. Khan, J.A. McDonald, A. Roux, Y. Poussade, J.E. Drewes, L.D. Nghiem, Rejection of small solutes by reverse osmosis membranes for water reuse applications: A pilot-scale study, Manuscript submitted to *Desalination*.

T. Fujioka, N. Oshima, R. Suzuki, M. Higgins, W.E. Price, R.K. Henderson, L.D. Nghiem, Modification of reverse osmosis membrane by heat treatment for the improvement of boron rejection and fouling resistance, Manuscript submitted to *Desalination*.

Chapter 1

Introduction

Background

Potable water reuse has been recognised as an effective and reliable measure to augment the supply of drinking water in many parts of the world where fresh water resources are under severe stress [1]. This practice can be implemented by replenishing reservoirs or underground aquifers with high quality reclaimed water. In most cases, the reclamation of water for potable purposes is accomplished by an array of several advanced treatment processes such as reverse osmosis (RO), activated carbon adsorption, and advanced oxidation [1, 2]. The deployment of these advanced treatment processes is to ensure effective removal of pathogenic agents and trace organic chemicals of concern [1, 3-5]. Notable examples of these trace organic chemicals are N-nitrosodimethylamine (NDMA) and several other N-nitrosamines. NDMA is a disinfection by-product formed during the chloramination of biologically treated effluent [6] and is often found in the RO feed at up to a few hundred parts per trillion [7]. Other N-nitrosamines that have previously been reported in treated wastewater include N-nitrosomethylethylamine (NMEA), N-nitrosopyrrolidine (NPYR), N-nitrosodiethylamine (NDEA), N-nitrosodipropylamine (NDPA), N-nitrosodi-n-butylamine (NDBA), N-nitrosopiperidine (NPIP), N-nitrosomorpholine (NMOR), and N-Nitrosodiphenylamine (NDPhA) [8-12]. Some of these N-nitrosamines have also been identified as potential human carcinogens by the US EPA [13] and their concentrations in reclaimed water intended for potable reuse have been regulated in Australia and several other countries at 10 ng/L or less [14].

Research Rationale

RO is a key treatment process in water reclamation applications for the removal of organic matter, inorganic salts and trace organic chemicals [3, 15, 16]. Due to its high performance on solute separation, RO process in water reclamation plants is also

accounted for some degrees of N-nitrosamine removal from the reclaimed water which is used for the augmentation of drinking water source. Nevertheless, the removal of NDMA by RO process appears to be highly variable. For example, NDMA rejections by the same type of RO membranes reported from full-scale studies range from negligible to 60% [8, 12, 17, 18]. Moreover, the effectiveness of RO membranes for the rejection of NDMA and other N-nitrosamines is still poorly understood.

Research objectives

The goal of this study was to understand and optimise N-nitrosamine rejections by RO membranes. Specific objectives of this study are to:

- 1) Evaluate the rejection of N-nitrosamines by RO membranes under a range of operating conditions;
- 2) Examine the impact of fouling and chemical cleaning on N-nitrosamine rejection;
- 3) Elucidate the mechanisms of permeation of N-nitrosamines through RO membranes; and
- 4) Develop a full-scale rejection model of N-nitrosamines and validate the model using a pilot-scale RO system.

Thesis outline

The structure of this thesis is schematically described in Figure 1.1. A series of chapters starts with Chapter 2 which provides a comprehensive literature review on the current knowledge of N-nitrosamines and their rejections by RO membranes. Descriptions of membranes, chemicals and filtration system used in this investigation as well as analytical techniques are summarised in Chapter 3. This is followed by seven chapters which include experimental results and discussions. The results in regard to the effects of feed solution characteristics, fouling and chemical cleaning on N-nitrosamine rejection are presented in Chapter 4, 5, and 6, respectively. The mechanisms of N-nitrosamine rejection were explored focusing on the properties of RO membranes in Chapter 7 and 8. The results regarding the removal of N-nitrosamines in full-scale RO system are presented in Chapter 9. A developed model for the prediction of N-nitrosamine rejection and the validation of the model using a pilot-scale RO system are

reported in Chapter 10. The findings in this thesis are summarised in the Conclusion (Chapter 11). Recommendations and suggestions for future research are provided in the last chapter (Chapter 12).

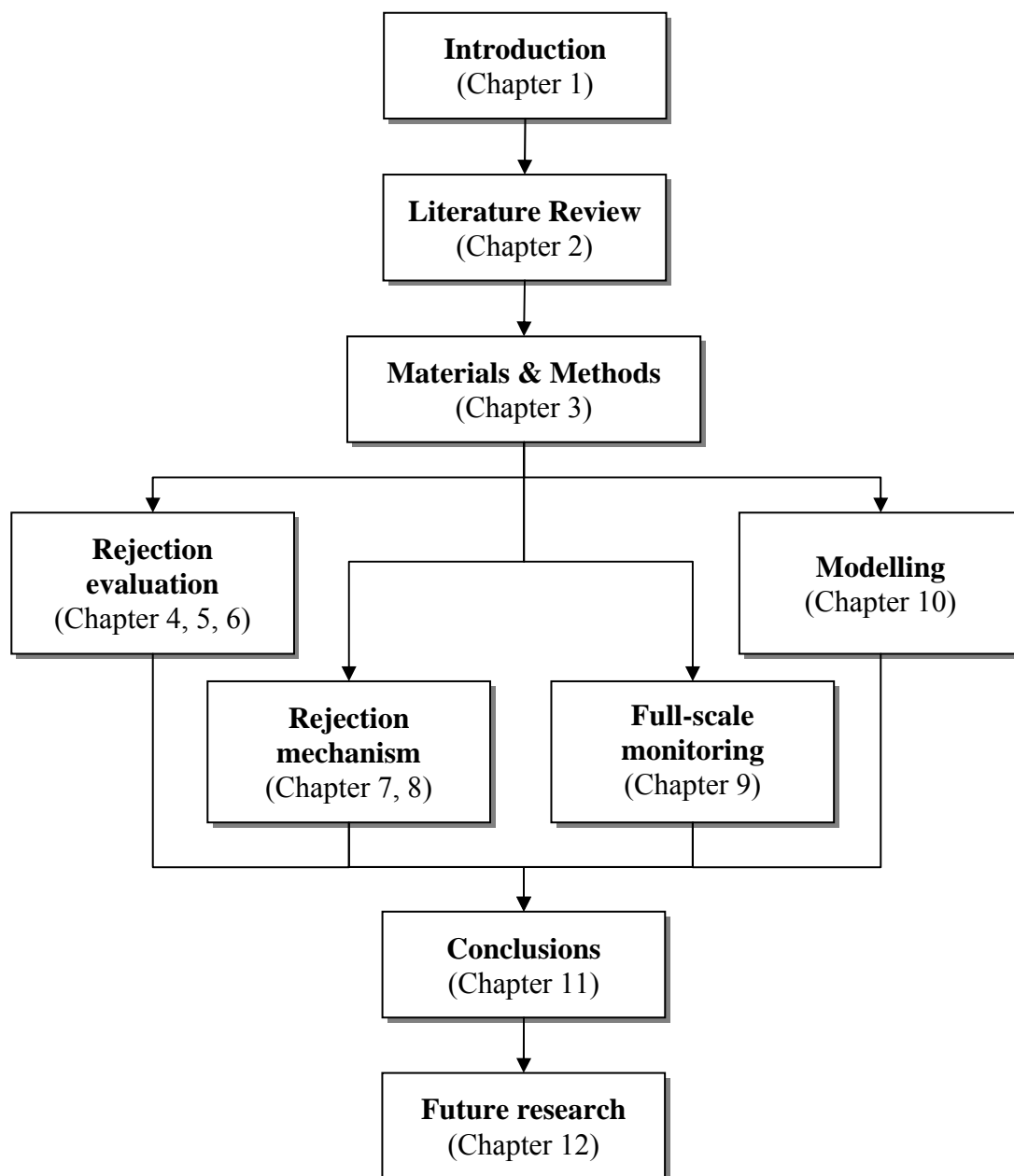


Figure 1.1: Schematic diagram of the thesis “Assessment and Optimisation of N-nitrosamine Rejection by Reverse Osmosis for Planned Potable Water Recycling Applications”.

Chapter 2

Literature review

This chapter has been published as:

T. Fujioka, S.J. Khan, Y. Poussade, J.E. Drewes, L.D. Nghiem, N-nitrosamine removal by reverse osmosis for indirect potable water reuse – A critical review based on observations from laboratory-, pilot- and full-scale studies, Sep. Purif. Technol., 98 (2012) 503-515.

1 Introduction

Water reuse has grown significantly in recent years in response to the increasing demand for water brought about by population increase, urbanisation, and diminishing and uncertain availability of freshwater resources. Many water utilities around the world have now recognised the potential value of water reuse after experiencing severe droughts as well as the environmental and economic costs of imported water [1, 19, 20]. Since the quality of reclaimed water for potable reuse is stringently regulated, reverse osmosis (RO) treatment has become an increasingly common component of the water reclamation process. RO membranes can successfully remove a wide range of contaminants including inorganic salts and trace organic chemicals [3, 16]. However, the rejection of N-nitrosodimethylamine (NDMA) by RO membranes appears to be highly variable [18, 21]. N-nitrosamines including NDMA can readily be formed during the disinfection of biologically-treated effluent using chlorine or chloramines [22, 23]. Given the probable carcinogenic potency of NDMA and several other N-nitrosamines [24, 25], the fate of these compounds in water reclamation applications is of significant interest to both the scientific community and water utilities.

For indirect potable water reuse applications involving the use of the RO process, concentration of NDMA in the final product water can be controlled via several strategies. NDMA concentration can be minimised by reducing the formation of NDMA

during the chloramination process. This can be achieved by dosing pre-formed chloramine [12] and reducing the contact time of chloramination [26, 27]. However, reducing the NDMA formation may not be sufficient if a higher NDMA concentration than the regulatory level occurs in the inflow of the wastewater treatment plant (WWTP). An alternative approach is to use an additional treatment process for the removal of NDMA. Possible treatment technologies include UV/H₂O₂ treatment process, natural attenuation during aquifer recharge, and RO filtration.

Advanced oxidation using a combination of UV radiation and dosed hydrogen peroxide (H₂O₂) to form hydroxyl radicals has been proven to be effective for the removal of NDMA and has been applied following RO filtration in several water reclamation schemes around the world [2, 21]. However, the energy consumption required by UV/H₂O₂ treatment for the control of NDMA is high and can have a negative consequence of increasing the carbon footprint of the water reuse scheme. Moreover, it is still necessary to control the concentration of NDMA by other processes during wastewater reclamation since the removal of NDMA by UV/H₂O₂ treatment is sometimes incomplete [21]. At a water reuse facility in Southern California, there were some periods when reclaimed water after UV/H₂O₂ treatment had to be blended with other non-recycled sources to reduce NDMA concentration in the final product to below the 10 ng/L notification level [18].

Natural attenuation over an extended retention time in an aquifer or surface reservoir has been shown to be effective for the removal of NDMA and other N-nitrosamines [28, 29]. For example, Drewes et al. [29] reported that half-lives of N-nitrosamines in laboratory-scale soil-column ranged from 1.3 to 7 days. Although natural attenuation is likely to play a significant role as a post RO treatment process for the removal of NDMA and other N-nitrosamines, most water utilities are still reluctant to exclusively rely on this passive treatment technique. A reliable removal efficiency of NDMA and other N-nitrosamines remains a major focus for the control of these contaminants in indirect potable water recycling practices.

RO membranes are widely used for the treatment of reclaimed water for indirect potable reuse and other applications. However, the effectiveness of RO membranes for the

rejection of NDMA and other N-nitrosamines is still poorly understood. Broad discrepancy exists in the existing scientific literature regarding the rejection of NDMA by RO membranes. For instance, NDMA rejection by a commonly used RO membrane (TFC-HR, Koch Membranes) was reported to be 50% at the West Basin Municipal Water District water recycling plant in California, USA [21]. At the Scottsdale Water Campus (Arizona, USA), NDMA rejections by the same type of RO membrane (TFC-HR) were reported to be 10 and 70% during two separate sampling events [21]. Compared to NDMA, little is known about the fate of other N-nitrosamines in water reclamation due to the scarcity of sampling data. This chapter provides a comprehensive review on the fate of N-nitrosamines and their rejections by RO treatment during water reclamation.

2 Indirect potable water reuse and N-nitrosamines

2.1 Water reclamation process

Indirect potable water reuse is generally performed through a ‘multiple barrier’ approach that incorporates both engineered and natural treatment processes as well as non-treatment measures. These multiple barriers may variably include (1) residential/industrial source control; (2) conventional wastewater treatment; (3) advanced water treatment; (4) environmental buffer and blending; and (5) drinking water treatment [20].

A notable approach for the advanced treatment of reclaimed water is the use of integrated membrane systems (Table 2.1). Since secondary effluents have high fouling propensity against RO membranes [30], microfiltration (MF) or ultrafiltration (UF) treatment is usually used as a pretreatment step to minimise membrane fouling in the subsequent RO process. The RO process substantially reduces the concentration of dissolved solids including macro-organic molecules and inorganic salts [31]. RO membranes can also achieve an excellent removal of a large range of trace organic chemicals [16, 17, 31, 32]. Although RO membranes can remove bacteria and viruses [33, 34], it is still common to deploy either UV- or chlorine-based disinfection processes as a ‘redundant’ post treatment to inactivate human pathogens (Table 2.1). Because the rejection of NDMA by RO membranes is highly variable and can be quite

low, the advanced oxidation UV/H₂O₂ process may also be used for the destruction of NDMA that can permeate through the RO membrane.

Table 2.1: Examples of advanced water treatment processes for indirect potable water reuse.

Treatment processes	Location (Commissioning year)	Final water use	Capacity [m ³ /day]	Ref.
MF/UF → RO	Scottsdale, AZ, USA (1999)	Groundwater recharge	53,000	[20]
	Terminal Island, CA, USA (2001)	Groundwater recharge	18,900	[35]
MF/UF → RO → UV	Vander Lans, CA, USA (2001)	Groundwater recharge	12,000	[35]
	Torreele, Belgium (2002)	Groundwater recharge	8,800	[8]
	NeWater, Singapore Kranji (2002), Bedok (2002), Seletar (2004), Ulu pandan (2007)	Surface water augmentation into a dam	216,000	[20]
MF/UF → RO → UV+H ₂ O ₂	Groundwater Replenishment Project, Orange County, CA, USA (2007)	Groundwater recharge	265,000	[20]
	Western Corridor project, Australia Bundamba (2007), Luggage Point (2008), Gibson Island (2008)	Planned future surface water augmentation into a dam	232,000	[36]

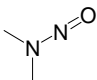
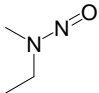
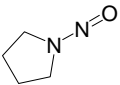
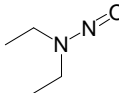
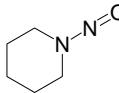
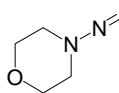
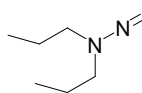
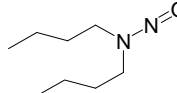
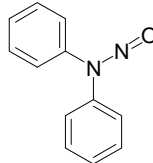
2.2 Occurrence of N-nitrosamines in water recycling schemes

2.2.1 Presence of N-nitrosamines in wastewater

In addition to NDMA, other N-nitrosamines known to occur in secondary effluent include N-nitrosomethylethylamine (NMEA), N-nitrosopyrrolidine (NPYR), N-nitrosodiethylamine (NDEA), N-nitrosopiperidine (NPIP), N-nitrosomorpholine (NMOR), N-nitrosodipropylamine (NDPA), N-nitrosodi-n-butylamine (NDBA) and N-Nitrosodiphenylamine (NDPhA) [29, 37, 38]. The chemical structure of N-nitrosamines is generally described as $R_1R_2N-N=O$. These N-nitrosamines are neutral and small molecules ranging from 74 to 198 g/mol and most N-nitrosamines have high solubilities (Table 2.2). N-nitrosamines are considered hydrophilic (i.e. $\log K_{ow} < 3$) with N-nitrosodiphenylamine being the only exception (Table 2.2). Of these N-nitrosamines, much of the recent research has focused on the fate of NDMA during wastewater treatment and water reuse.

N-nitrosamines can be found in both domestic and industrial wastewater. Cosmetic and toiletry products contain NDMA and NMOR [39] and NDMA concentration in the range of 17 to 63 ng/L has been reported in raw residential sewage [21, 40, 41]. Industrial discharge is another potentially major pathway for NDMA to enter the sewage system. N-nitrosamines including NDMA can be formed as impurities during various manufacturing activities, such as the production of rubber, high-energy batteries, some lubricants, antifreezers, and cutting fluids [21]. Due to industrial activities, NDMA concentrations as high as 1,000 ng/L have been reported in an industrial sewer system [41]. Sedlak and Kavanaugh [21] investigated the inflow of several WWTPs in California and suggested that NDMA concentrations in the inflow could vary significantly depending on the degree of industrial sewer inflow. They reported that NDMA concentration in the inflow of WWTPs located in residential areas ranged between 50 and 100 ng/L whereas an average of 150 ng/L NDMA concentrations was found at WWTPs where the contribution of the industrial discharge was over 10%. NMOR concentrations in the wastewater effluent reported in literature [7] are variable in the ranged from 130 to 12,700 ng/L which may have occurred due to the industrial activities.

Table 2.2: Physicochemical properties of the selected nitrosamines.

Compound	NDMA	NMEA	NPYR	NDEA	NPIP	NMOR	NDPA	NDBA	NDPhA
Structure									
Molecular Formula	C ₂ H ₆ N ₂ O	C ₃ H ₈ N ₂ O	C ₄ H ₈ N ₂ O	C ₄ H ₁₀ N ₂ O	C ₅ H ₁₀ N ₂ O	C ₄ H ₈ N ₂ O ₂	C ₆ H ₁₄ N ₂ O	C ₈ H ₁₈ N ₂ O	C ₁₂ H ₁₀ N ₂ O
Molecular Weight [g/mol]	74.05	88.06	100.06	102.08	114.08	116.06	130.11	158.14	198.22
Henry's law constant at 25 °C ^a [atm m ³ /mol]	1.20×10 ⁻⁶	1.44×10 ⁻⁶	1.99×10 ⁻⁷	1.73×10 ⁻⁶	2.81×10 ⁻⁷	2.13×10 ⁻¹⁰	3.46×10 ⁻⁶	9.96×10 ⁻⁶	1.38×10 ⁻⁵
Solubility in water at 20 °C ^b [g/L]	1,000	300	780	147	49	4,714	9.9	1.2	0.035
LogK _{ow} ^b	-0.64	-0.15	0.23	0.34	0.74	-1.39	1.35	2.31	3.16

^a EPI Suite™ v4.10, US EPA, <http://www.epa.gov/opptintr/exposure/pubs/episuite.htm>^b GSI Environmental Inc., <http://www.gsi-net.com/en/publications/gsi-chemical-database.html>

2.2.2 NDMA precursors

Together with the increasingly reported occurrence of NDMA in domestic and industrial wastewater, the abundance of NDMA precursors in both domestic and industrial wastewater discharge has been widely reported in the literature. For the evaluation of the maximum NDMA formation that can occur in an aqueous solution, the NDMA formation potential can be used [6]. NDMA formation potentials ranging from 25 to 55 $\mu\text{g/L}$ were reported in domestic wastewater in California by Sedlak and Kavanaugh [21]. They also reported NDMA formation potentials of as high as 82.5 $\mu\text{g/L}$ in an industrial wastewater.

A number of substances have been identified as NDMA precursors. These include both heterogeneous organic mixtures such as humic substances found in the natural environment [42] and some specific organic compounds containing the amine functional group such as dimethylamine, triethylamines, and dimethylaminobenzene (Figure 2.1). These amine bearing organic compounds can be readily converted to NDMA during chloramination [43]. Some pharmaceuticals and personal care products (PPCPs) containing dimethylamine (DMA) or diethylamine (DEA) functional groups can also act as NDMA precursors. For example, Shen and Andrews [44] reported higher than 1% molar conversion of eight PPCPs containing these functional groups to NDMA during chloramination.

Since DMA occurs naturally in urine and faeces, DMA is ubiquitous in domestic wastewater [21, 45]. In fact, faeces and urine contain an average DMA concentration of 0.4 and 15.9 mg/L , respectively [46]. Numerous studies have used DMA to elucidate mechanisms of NDMA formation [26, 45, 47]. Gerecke and Sedlak [48] reported that the yield of NDMA from the reaction between DMA and chloramine was only approximately 0.6%. Similarly, in the primary effluent of the Orange County Sanitation District facility (CA, USA) approximately 80 $\mu\text{g/L}$ of DMA was found while NDMA formation potential was only 5 $\mu\text{g/L}$ in the same sample [40].

Several other compounds such as DEA, dipropylamine (PYP), pyrrolidine (PIP) and diphenylamine (DPhA) are also suspected to be the precursor of NDEA, NPYP, NPIP

and NDPhA, respectively. Amongst them, DEA, PYP and PIP are excreted through faeces and urines in the range of 0.03-9 mg/L [46], and DPhA can be found in an insecticide, a storage preservative for apples and a rubber antioxidant [49]. To date, however, most N-nitrosamine precursor studies have focused exclusively on the formation of NDMA during chloramination, and information regarding the precursors of the other N-nitrosamines is rather scarce.

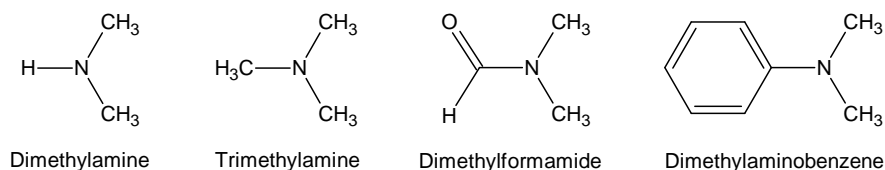
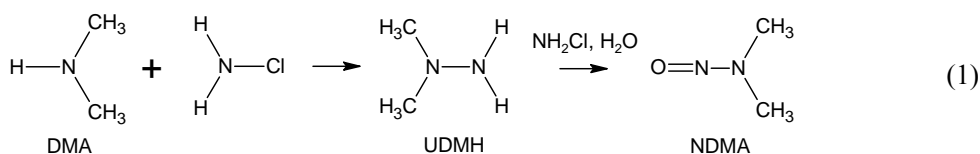


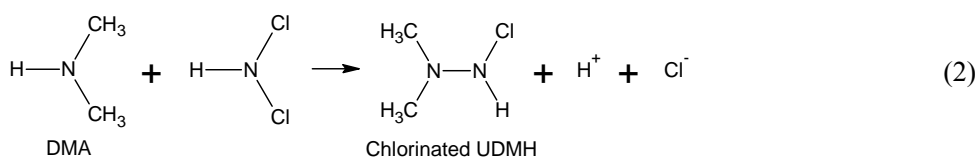
Figure 2.1: NDMA precursors found in wastewater.

2.2.3 NDMA formation

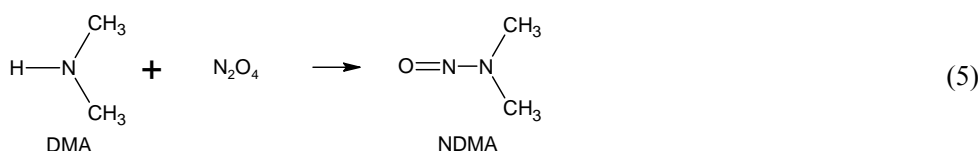
In general, oxidation of N-nitrosamine precursors by strong oxidants such as chlorination, chloramination, ozone, and potassium permanganate leads to a formation of NDMA [26, 50-53]. Several mechanisms of NDMA formation during chloramination have been proposed [54], and they usually involve two major pathways. Unsymmetrical dimethylhydrazine (UDMH) is initially formed from NDMA precursors such as DMA by a reaction with monochloramine (NH_2Cl). Then UDMH is transformed into NDMA by the oxidation of monochloramine, as shown in Equation 1 [45, 47]. The yield of NDMA formation from DMA is less than 3% and the oxidation is a gradual process taking several days [6, 26].



Schreiber and Mitch [26] have revised this formula to take into account the significant enhancement in NDMA formation by dichloramine (NHCl_2), as shown in Equation 2. Another study proposed that the chlorinated UDMH intermediates can be oxidised by both dissolved oxygen and chloramines. This is attributed to the weak and non-polar property of the N-Cl bond contained in the chlorinated UDMH intermediates [55].



Choi and Valentine [56] proposed another pathway for NDMA formation in the presence of DMA and chlorine. It was hypothesised that dinitrogen tetroxide (N_2O_4) is firstly formed by nitrosation enhanced by chlorine, and then a reaction between N_2O_4 and DMA leads to the formation of NDMA as shown in Equations 3 - 5.



The formation of NDMA by chloramination can vary significantly depending on the conditions of the chloramination process. In fact, several studies reported that NDMA concentration substantially increased with increasing reaction time and chloramine (or chlorine) dosage [22, 23, 45, 47]. Farré et al. [12] investigated the impact of chloramination contact time on NDMA formation in the feed of a full-scale RO plant. They reported that 20 – 22 hours of chloramination contact time led to 170 ± 20 ng/L NDMA concentration, while 1 to 2 hours of chloramination exposure resulted in only 7 ± 2 ng/L NDMA concentration. Laboratory-scale experiments conducted by the authors also showed that NDMA formation significantly decreased as chloramine dose [12].

The disinfection process can be optimised to minimise the formation of NDMA. It has been demonstrated that adding ammonium chloride followed by chlorine into the wastewater forms less NDMA than adding chlorine followed by ammonium chloride [26, 27]. This is because dichloramine, which forms more NDMA than monochloramine, is generated less when ammonium chloride is added earlier into the wastewater, reducing the transient occurrence of high chlorine/ammonia ratios. These findings are consistent with another laboratory-scale study where dosing pre-formed monochloramine into the wastewater led to far less NDMA formation potential (< 1

ng/L) compared with dosing ammonium chloride and sodium hypochlorite into the wastewater (6 ng/L) [12]. Although the formation of NDMA during water reclamation can be minimised with an appropriate chloramination conditions, a subsequent treatment process is often necessary for further removal of NDMA.

2.3 Health-based water quality guidelines and standards for N-nitrosamines

The occurrence of N-nitrosamines in drinking water has attracted significant scientific and regulatory attention in recent years since some have been classified as probable human carcinogens by the US Environmental Protection Agency [25] and the International Agency for Research on Cancer [24]. The occurrence of NDMA is of particular concern amongst all N-nitrosamines because NDMA concentration exceeding some enforced regulatory levels has been detected in drinking water [52, 57, 58]. Based on a calculated excess lifetime cancer risk of 1 in 10^6 , the California Office of Environmental Health Hazard Assessment have set a public health goal for NDMA in drinking water of 3 ng/L [59] (Table 2.3). The California Department of Public Health (CDPH) also established a notification level for NDMA, NDEA and NDPA of 10 ng/L [59]. Outside the US, an interim action level of NDMA has been determined at 9 ng/L by the Ontario Ministry of the Environment [60], while a NDMA guideline value of the World Health Organisation [61] and Australian Drinking Water Guidelines [62] is as high as 100 ng/L. The regulation of N-nitrosamines in indirect potable water reuse can be more stringent than that in conventional drinking water. Health-based guideline values of 10 ng/L for NDMA, 10 ng/L for NDEA and 1 ng/L for NMOR have been established in the Australian Guidelines for Water Recycling [14]. Although an increasing number of authorities have regulated N-nitrosamine concentrations for drinking or recycled water (Table 2.3), many water utilities have not been able to monitor their concentrations in the product water on a regular basis. Under the USEPA Unregulated Contaminant Monitoring Rule 2 (UCMR 2), an extensive screening exercise was conducted between 2008 and 2010 to identify key contaminants of concern for future monitoring and regulation [58]. From 1,196 public water supplies and approximately 17,150 samples, NDMA was the most frequently detected contaminant in the samples from 25% of the public water supplies or 10% of the total samples in

which a maximum concentration of 630 ng/L was reported [58]. Five N-nitrosamines (i.e., NDMA, NDEA, NDPA, NPYR and NDPhA) have also been included in the third Contaminant Candidate List 3 (CCL3) proposed by the US EPA [63]. These N-nitrosamines are likely to be regulated in the future under the Safe Drinking Water Act of the United States [64].

Table 2.3: Risk level and guideline level of N-nitrosamines.

Compound	US EPA classification ^a	IARC classification ^b	US EPA, IRIS 10 ⁻⁶ risk level [ng/L]	CDPH 10 ⁻⁶ risk level [ng/L]	CDPH notification level [ng/L]	Ontario MOE interim action level [ng/L]	WHO guideline value [ng/L]	ADWG guideline value [ng/L]	AGWR guideline value [ng/L]
NDMA ^{c, d}	B2	2A	0.7	3	10	9	100	100	10
NMEA ^c	B2	2B	2	1.5	-	-	-	-	-
NPYR ^{c, d}	B2	2B	20	15	-	-	-	-	-
NDEA ^{c, d}	B2	2A	0.2	1	10	-	-	-	10
NPIP	-	2B	-	3.5	-	-	-	-	-
NMOR	-	2B	-	5	-	-	-	-	1
NDPA ^{c, d}	B2	2B	5	5	10	-	-	-	-
NDBA ^c	B2	2B	6	3	-	-	-	-	-
NDPhA ^d	B2	3	7,000	-	-	-	-	-	-
Ref.	[25]	[24]	[25]	[59]	[59]	[60]	[61]	[62]	[14]

^a B2: probable human carcinogen.^b 2A: probable human carcinogen; 2B: possibly human carcinogen; 3: unclassifiable chemical as to its carcinogenicity to humans.^c Chemical is on US EPA's list of the UCMR 2.^d Chemical is on US EPA's list of the CCL3.

2.4 N-nitrosamine quantification using chemical analysis

Quantifying NDMA and other N-nitrosamines at the part-per-trillion level (ng/L) is a challenging task and to date most reported detection limits are only marginally lower than their regulated values. High analytical cost is also a hurdle to engage in intensive monitoring efforts for N-nitrosamines in addition to regulatory requirements. To address the low concentration analysis, most currently available methods involve a solid-phase extraction (SPE) procedure followed by quantification using chromatographic-mass spectrometric analytical instruments.

For quantitative determination of N-nitrosamines in water samples, many recent methods use gas chromatography coupled with different detection techniques such as mass spectrometry (GC-MS) [65, 66], tandem mass spectrometry (GC-MS/MS) [67-69] or high resolution mass spectrometry (GC-HRMS) [70, 71]. These methods use deuterated N-nitrosamines (i.e. d_6 -NDMA and d_{14} -NDPA) as an internal standard for calibrations and/or surrogate for recoveries. The US EPA has defined that Method 521 [67] be used for analysing N-nitrosamines under the USEPA Unregulated Contaminant Monitoring Rule 2. Method 521 is based on coconut charcoal SPE, GC-MS/MS, large volume injector and chemical ionization (CI) operation mode with CI reagent gas (methanol or acetonitrile). Method 521 provides a reporting detection limit of 1.6 ng/L for NDMA and the reporting detection limits of the other N-nitrosamines (NMEA, NDEA, NDPA, NDBA, NPYR and NPIP) range from 1.2 to 2.1 ng/L. The Ontario Ministry of Environment sets a different testing method for Ontario drinking water samples using GC-HRMS after an SPE procedure using the Amborsorb 572 adsorbent [70]. In the method, the reporting detection limit of NMDA is 0.99 ng/L. Recent developments in N-nitrosamine analysis include a simple technique using selective ion storage mode of GC/MS with chemical ionisation [72], a sensitive GC-MS/MS technique using electron ionisation [73] and high-field asymmetric waveform ion mobility spectrometry with time-of-flight mass spectrometry [74].

Analytical techniques using liquid chromatography (LC) have been increasingly developed to analyse N-nitrosamine concentration in water. Compared to GC methods, LC technique particularly has an advantage on detecting both thermally stable and

unstable N-nitrosamines (i.e. NDPhA) [75]. To date several LC-MS/MS techniques have been reported [18, 37, 76]. Positive electrospray ionisation (ESI) combined with multiple reaction monitoring mode is used in these methods. Zhao et al. [37] investigated nine N-nitrosamines in water samples using SPE-LC(ESI)-MS/MS and reported that detection limits of N-nitrosamines are in the range from 0.1 to 10.6 ng/L with 41 to 111% recoveries. Another SPE-LC(ESI)-MS/MS technique has been developed with a detection limit of 2 ng/L NDMA and over 90% recovery [18]. The other recent techniques include a method using SPE and LC(ESI)-HRMS detection [76] and SPE-LC-MS/MS with atmospheric pressure chemical ionisation [77]. Although these LC-MS/MS or LC-HRMS methods can be an alternative technique to GC-based techniques, very few water utilities have affordable routine access to LC-MS/MS and LC-HRMS.

2.5 Removal of N-nitrosamines during Water Reclamation

N-nitrosamines have relatively low molecular weights and are stable in aqueous solution, and thus are not sufficiently removed by most conventional water and wastewater treatment processes. The removal of NDMA by secondary treatment is poor and highly variable [21] and the removal of NDMA by coagulation has been reported to be negligible [78]. Less than 10% NDMA removal by UF treatment was reported at a full-scale plant [12]. Granular activated carbon adsorption also exhibited limited effectiveness for NDMA removal [79, 80], with the removal of NDMA in the range of 20 – 50% [81]. Although RO membranes have been proven for complete or near complete removal of a large range of trace organic chemicals, there exists significant discrepancy in NDMA rejections both from laboratory- and full-scale data. This discrepancy will be further discussed in the next section.

3 *N-nitrosamine removal by RO membranes*

3.1 Rejection of N-nitrosamines in laboratory-scale studies

N-nitrosamines are neutral compounds at the typical environmental pH range of 4 to 10. In general, the rejection of N-nitrosamines is primarily governed by steric hindrance (size exclusion) (Figure 2.2). It is noteworthy that all of the RO membranes listed in

Figure 2.2 are typically used for brackish water desalting and softening. There is a strong correlation between molecular weight of N-nitrosamines and their rejections for a given membrane [38, 82]. An overall trend of increasing rejection in the increasing order of molecular width of the N-nitrosamines has also been demonstrated by Miyashita et al. [82]. A strong correlation between the rejection of N-nitrosamines by a NF membrane (NF270) and the Stokes radius of the N-nitrosamines was also reported by Bellona et al. [83]. The rejection of NDMA, the smallest compound amongst all N-nitrosamines, was consistently found to be lowest by all types of membrane reported in the literature.

Laboratory-scale studies available to date have consistently indicated that the rejection of NDMA by RO membranes (i.e. BE, BW30, and LFC3 membranes) was between 55% and 70% (Figure 2.2). On the other hand, NDMA rejection by NF membrane (i.e. NF90) reported in a laboratory-scale study was below 15%. The impact of membrane type on N-nitrosamine rejection is less profound with higher molecular weight N-nitrosamines. It is noted that the rejection of NDPhA has not been reported in the literature.

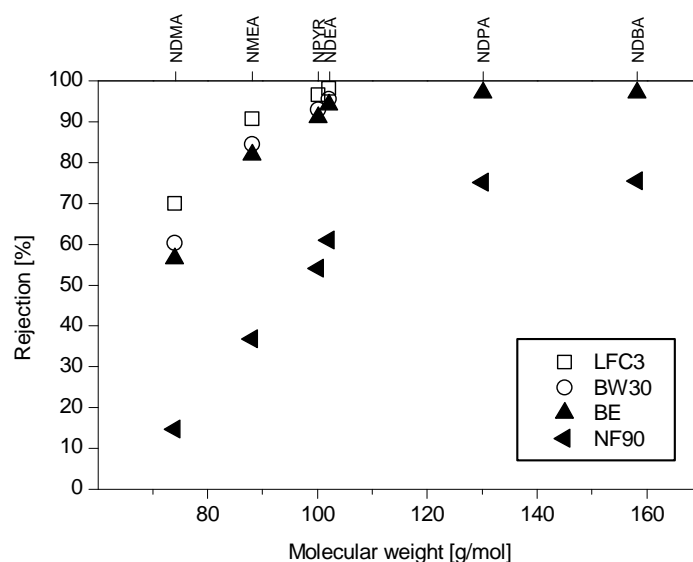


Figure 2.2: Rejection of N-nitrosamines by three RO (LFC3, BW30, BE) and one NF (NF90) membranes obtained from laboratory-scale studies [38, 82].

3.2 Rejection of N-nitrosamines and N-nitrosamine precursors in pilot- and full-scale installations

3.2.1 *Rejection of N-nitrosamines*

In comparison to other trace organic chemicals, pilot- and full-scale data regarding the rejection of N-nitrosamines by RO membranes are very scarce. To date, monitoring effort in pilot- and full-scale investigations has focused almost exclusively on NDMA. The rejections of other N-nitrosamines are rarely reported in the literature. While NDMA rejection by RO membranes reported in most laboratory-scale studies was in the range of 50 to 70% (Section 3.1), it is striking to note a substantial discrepancy in the rejection of NDMA recorded from pilot- and full-scale RO plants (Table 2.4). These plants had similar pretreatment processes and were operated with almost identical water recovery ratios and average RO permeate fluxes. In these water reclamation plants, chloramination was performed by injecting sodium hypochlorite (NaOCl) and ammonia simultaneously prior to MF or UF to control biofouling. The concentration of chloramine in the RO feed was usually maintained at between 1 and 5 mg/L. The average permeate flux and water recovery of all RO plants were approximately 20 L/m²h and 80 – 85%, respectively (Table 2.4).

In general, the rejection of trace organic chemicals by RO membranes is very high (e.g. over 90%) [32]. Nevertheless, the rejection of NDMA by the same membrane reported at different RO plants can be very low and significantly variable. For example, NDMA rejection by the TFC-HR membrane in the range of 14 to 70% was reported at the Bundamba Advanced WTP (Queensland, Australia), the West Basin Municipal Water District WTP (California, USA), and the Scottsdale Water Campus (Arizona, USA) (Table 2.4). Similarly, there also exists substantial discrepancy in NDMA rejection ranging from 22 to 86% at three different plants using the ESPA2 membrane (Table 2.4). It is also worth noting that substantial difference in NDMA rejection can be found even at the same plant. Two distinct NDMA rejections (10% and 70%) were recorded at different sampling occasions at the Scottsdale Water Campus [21]. Approximately 30% difference in NDMA rejection was also reported at the Interim Water Factory 21 (USA) [18, 21]. As discussed above, although these plants were operated with a similar water recovery and average permeate flux, the exact operating conditions may vary

significantly from one another. In order to account for variability in rejection performance by a single plant, Khan and McDonald [84] have demonstrated the use of probability density functions to more comprehensively describe the RO rejection of NDMA, NDEA and NDPA. The variation in the removal of NDMA by the RO process demonstrated in Table 2.4 can be attributed to such differences in operating conditions amongst the different plants or sampling events. Further discussion of the impact of operating conditions on the rejection of NDMA and other N-nitrosamines is provided in Section 3.3.

Table 2.4: NDMA rejection by pilot and full-scale RO plants.

Location	Pretreatment processes ^a	RO Membrane	RO stages	RO recovery [%]	RO permeate flux [L/m ² h]	NDMA in RO feed [ng/L]	NDMA in RO permeate [ng/L]	NDMA rejection by RO [%]	Reference
El Segundo – train 3, West Basin Water Recycling Plant, USA	SEC - NaOCl - MF - RO	TFC-HR	3	85	17	90 60	40 43	56 28	[21] [85]
Scottsdale Water Campus, USA	SEC - NaOCl/NH ₄ ⁺ - MF - RO	TFC-HR	3	85	18.2	330 200	100 180	70 10	[21, 85]
Bundamba AWTP, Australia	SEC - NaOCl/NH ₄ ⁺ - COAG - UF - RO	TFC-HR	3	85	NA	190	170	11	[12, 86]
	SEC - NH ₄ ⁺ - COAG - NaOCl - UF - RO					7	6	14	
El Segundo - train 4, West Basin Water Recycling Plant, USA	SEC - NaOCl - MF - RO	ESPA2	2	85	19.4	32	21	34	[35, 85]
Interim Water Factory 21, USA	SEC - NaOCl - MF - RO	ESPA2	NA	85	20.5	18 45	14 20	22 55	[18]
Beenyup Pilot Plant, Australia	SEC - HOCl/NH ₄ ⁺ - MF - RO	ESPA2	2	80	19.7	11 6.7	< 1.6 2.5	> 86 63	[87]

^aSEC: Secondary effluent; COAG: Coagulation process; NaOCl/HOCl: Chlorine addition; NH₄⁺: Ammonia addition; MF/UF: MF/UF process; RO: RO process.

3.2.2 Rejection of *N*-nitrosamine precursors

To measure the rejection of NDMA precursors by RO membranes, NDMA formation potential is usually used as a surrogate. Results reported from laboratory- and pilot-scale studies show that the rejection of NDMA formation potential by most RO membranes is more than 97% [8, 22, 43]. Farré et al. [86] reported over 98.5% NDMA formation potential rejection by the TFC-HR membrane at the Bundamba AWTP (Australia). It is noteworthy that the elevated NDMA formation potential in the RO concentrate can be reduced using a nitrification-denitrification process [86]. NDMA formation potential may also be rejected to a certain extent by MF and UF membranes. At the Torreele plant (Belgium), up to 10% NDMA formation potential rejection by an UF membrane was reported [8]. Similarly, NDMA formation potential rejection in the range of 10 to 90% by a MF membrane was reported in a pilot study at the Interim Water Factory 21 [21].

Because NDMA formation potential can occur at high concentration (i.e., 500 – 3,200 ng/L) prior to RO filtration [21, 43, 86], some NDMA formation potential may still be detected in the RO permeate. For example, approximately 6 ng/L of NDMA formation potential was reported in the RO permeate treated by the TFC-HR membrane at the Bundamba AWTP [86]. On the other hand, NDMA formation potential in the range from 12 to 52 ng/L was also detected in the RO permeate in a pilot study at the Interim Water Factory 21 [21]. Because NDMA yield from NDMA formation potential by chloramination and chlorination is very low (Section 2.2.2), the remaining NDMA precursors in the RO permeate is not likely to adversely impact the RO permeate quality.

The investigation of NDMA precursor is frequently carried out with DMA. In a typical water recycling application, it occurs in the feed water to the RO process in the range of 3 to 12 µg/L [21, 43]. The molecular weight of DMA is low (45 g/mol), however, its basicity constant (pK_b) is 3.36 and thus it is positively charged at pH below or near neutral pH ($(CH_3)_2NH + H_2O \rightleftharpoons (CH_3)_2NH_2^+ + OH^-$). As a result, DMA is very well rejected by RO membranes. Mitch and Sedlak [43] reported over 99% DMA rejection (from 8-11 µg/L to below 0.09 µg/L) at a WWTP using an unspecified RO membrane. In a laboratory-scale study, Miyashita et al. [82] also demonstrated a very high DMA

rejection of 99.5% and 99.2% by RO (Saehan BE) and NF (NF90) membranes, respectively. Despite the similarity in rejection between NDMA formation potential and DMA, Mitch and Sedlak [43] suggested an average contribution of only 14% of DMA into the total dissolved NDMA formation potential in secondary effluent. Although the majority of NDMA formation potential found in the feed to the RO process have been reported to be small and low molecular weight compounds (< 2.5 kDa) [8, 88], there is very little information available regarding specific NDMA precursors prior to RO treatment.

The rejection data of the other N-nitrosamine formation potential using pilot- or full-scale RO treatment is scarcely available. Krauss et al. [8] reported over 98% of NPYR formation potential rejection and over 94% of NPIP formation potential rejection by an RO membrane, showing a similar rejection efficiency to the rejection of NDMA.

3.3 Factors affecting N-nitrosamine rejections

3.3.1 Feed concentration

Although most RO plants (Table 2.4) are operated with similar water recovery and average permeate flux, the exact operating conditions may vary significantly from one to another. A notable parameter is the concentration of NDMA in the feed, which may vary over a wide range from 7 to 330 ng/L (Table 2.4). However, recent laboratory-scale studies have conclusively demonstrated that the impact of feed concentration on the rejection of NDMA is negligible [82]. Miyashita et al. [82] reported less than 5% variation in NDMA rejection by the Saehan BE membrane when the feed concentration of NDMA varied from 0.4 to 900 $\mu\text{g/L}$.

Previous studies using NF membranes also reported that solute concentration in the feed does not affect its rejection [89, 90]. Transport of uncharged solutes such as N-nitrosamines through porous membranes is governed by diffusive and convective flows inside the pores, which is commonly expressed with the hydrodynamic model (Equation 6) [91, 92].

$$J_s = -D_p \frac{dC}{dx} + J_v K_c C \quad (6)$$

where J_s is solute flux; D_p is the diffusion coefficient of the solute in the pore; x is position in a pore from inlet; C is solute concentration at axial position x in the pore; J_v is water flux; and K_c is the hindrance factor for convection. Although RO membranes generally have non-porous active skin layer, free-volume spaces in the membrane polymer chains can be considered as fictive pore radius [93] and the hydrodynamic model may be still effective [92]. In fact, the free-volume hole-size in the active skin layer of RO membranes have been analysed by previous studies [94, 95] using the positron annihilation lifetime spectroscopy technique. In the hydrodynamic model, the solute rejection (R_j) is expressed as Equation 7 [92].

$$R_j = 1 - \frac{C_p}{C_f} = 1 - \frac{\Phi K_c}{1 - [1 - \Phi K_c] \exp\left(-\frac{K_c J_v \Delta x}{D_p}\right)} \quad (7)$$

where C_p is solute concentration in the permeate; C_f is solute concentration in the feed; and Φ is steric partition factor. The solute rejection, which is associated with the membrane polymer matrix, water flux and solute characteristics, is solute concentration independent and this may explain the negligible impact of feed concentration on NDMA rejection described above.

3.3.2 Permeate flux

Permeate flux is an important operating parameter for a membrane filtration system. Miyashita et al. [82] examined the rejection of six N-nitrosamines by RO membranes (BE membrane) using a laboratory-scale filtration system and reported that their rejections increased with increasing permeates flux. They reported that NDMA rejections increased from 42 to 52% as permeate flux increased from 17 to 28 L/m²h.

Water flux (J_v) and solute flux (J_s) can be described with Equation 8 and 9 in the solute-diffusion model [96].

$$J_v = A(\Delta P - \Delta \pi) \quad (8)$$

$$J_s = B(C_{fo} - C_{pl}) \quad (9)$$

where A is called the water permeability constant; B is called the salt permeability constant; ΔP is the difference in hydrostatic pressure across the membrane; $\Delta\pi$ is the difference in osmotic pressure across the membrane; C_{fo} is the feed solute concentration at the interface of the membrane surface; and C_{pl} is the permeate solute concentration at the interface of the membrane in the permeate side. According to these equations, water flux increases with applied feed pressure, while solute flux is not pressure-dependent. Solute rejection thus increases when water flux increases by increasing pressure. In practice, the average permeate flux of RO systems used for water recycling is usually set at approximately 20 L/m²h (Table 2.4). However, differences in the local permeate flux amongst different elements in an RO pressure vessel can be intensified by feed pressure loss, osmotic pressure increase and membrane fouling [30, 97]. Thus, variations in permeate flux that occur in an RO pressure vessel is likely to affect the rejection of low molecular weight compounds such as NDMA.

3.3.3 Feed pH

The influence of feed pH on the rejection of seven N-nitrosamines was investigated in a laboratory-scale study using the ESPA3 membrane [38]. They revealed higher NDMA rejection (56%) at pH 10 than at pH 3 (49%). For the other six N-nitrosamines, the impact of feed pH was not pronounced.

The rejection of small and neutral compounds can be influenced by the feed solution pH and the rejection usually increases with increasing pH [98, 99]. It is assumed that high pH causes an extended chain conformation of the membrane polymer matrix which results in narrower pore size of membrane, and the rejection of neutral compounds thus increases. On the other hand, chain groups existing on the membrane surface lose electrostatic repulsion at low pH range, resulting in looser pore size and low rejections [99, 100]. It can be inferred from these studies that an increase in feed pH led to tighter membrane pore structure that results in an increase in the rejection of small N-nitrosamines (i.e., NDMA and NMEA). In general, changes in feed pH of full-scale water reclamation plants only occur in a small range (i.e. pH 5-8) [101] and most full-scale RO plants adjust feed pH to 6.3-6.5 to minimize scaling. Thus, feed pH is unlikely to be a major cause of the variations in NDMA rejection in full-scale RO plants.

3.3.4 Total dissolved solids concentration

Total dissolved solids (TDS) concentration can induce an observable impact on the rejection of N-nitrosamines. Steinle-Darling et al. [38] investigated the impact of TDS (ionic strength) on the rejections of the seven N-nitrosamines using a laboratory-scale system and the ESPA3 membrane. They reported that NDMA rejections with deionised feed solution and 100 mM NaCl feed solution were 56 and 41%, respectively. On the other hand, the rejections of the other six N-nitrosamines for the two TDS feed solutions were equivalent.

TDS concentration of RO feed for water recycling applications can vary across a range of 10 to 30 mM [102-104]. Therefore, it is likely that feed TDS variations will play a role in NDMA rejection variations. In addition to TDS variations in the RO feed, and TDS are gradually accumulated in the feed toward a tail-element (the last membrane element amongst serially-connected membrane elements in a vessel) because salt rejection by RO membrane is well over 90% [17]. This concentration effect results in a significant variation in total TDS concentration within RO system. The permeability of a membrane and the rejection of salts typically decrease as TDS concentration increases [105, 106]. Drewes et al. [31] demonstrated that the conductivity of the feed substantially increased from 1,249 to 5,164 $\mu\text{S}/\text{cm}$ after passing through two subsequent RO stages during water reclamation. Consequently, the conductivity of the various membranes permeates throughout the RO system increased from 22 $\mu\text{S}/\text{cm}$ (1st stage permeate) to 65 $\mu\text{S}/\text{cm}$ (3rd stage permeate). Several studies demonstrated that an increase in TDS concentration in the RO feed also resulted in a decrease in neutral solute rejections [107-109]. They suggested that the decreasing solute rejection resulted from the enlargement in pore sizes of a membrane and changes of the solute size caused by increasing TDS concentration in the feed. It is thus reasonable to hypothesize that a high TDS concentration can decrease NDMA rejection by RO membranes.

3.3.5 Feed temperature

Some seasonal and diurnal variation in the temperature of the feed solution is inevitable in most WWTPs. To the best of our knowledge, so far there is only one laboratory-scale

study available regarding the impact of feed temperature on the rejection of N-nitrosamines.

Ben Amar et al. [110] investigated the impact of feed temperature on the rejection of neutral solutes using a thin-composite polyamide NF membrane and found that their rejections increased with increasing feed temperature due partly to the increasing diffusivity of the solutes. In addition to the increased diffusivity, effective pore radius of a NF organic membrane has been suggested to increase with increasing feed temperature due to thermal expansion of pores within the active skin layer, which causes more passage of neutral solutes through membranes [111, 112]. In fact, Ben Amar et al. [110] also reported that the rejection of neutral solute (arabinose) decreased from 50 to 42% when the feed temperature increased from 22 to 30 °C using an organic NF membrane (Desal 5 DK). These mechanisms reported in the literature may explain the observed decrease in the rejection of N-nitrosamines by RO membranes with an increase in feed temperature. In any water reclamation plants, the seasonal variation in RO feed temperature can be over 10 °C [113]. Thus, changes in the feed temperature can possibly account for up to 25% variation in NDMA rejection.

3.3.6 *Membrane fouling and membrane ageing*

Membrane fouling is inevitable in most if not all NF/RO filtration processes. The separation of small organic molecules by NF/RO filtration can be significantly influenced by membrane fouling [114-117]. Surprisingly, apart from a study by Steinle-Darling et al. [38] who investigated the rejection of several N-nitrosamines by an RO membrane artificially fouled with sodium alginate, to date little attention has been given to the effects of membrane fouling on the rejection of N-nitrosamines. Nevertheless, data reported by Steinle-Darling et al. [38] confirms that the impact of membrane fouling caused by alginate on NDMA rejection can be significant. Due to membrane fouling, the permeate flux decreased by 15% and the rejections of NDMA and NMEA decreased from 56 to 39% and 79 to 68%, respectively [38]. The authors attributed the decrease in NDMA and NMEA rejection to the cake-enhanced concentration polarisation phenomenon as previously reported in the literature [115, 118]. It is noteworthy that some of the reduction in NDMA and NMEA rejection observed by

Steinle-Darling et al. [38] can also be attributed to a decrease in the permeate flux as discussed previously in section 3.3.2. Further investigation is required to separate the impact of membrane fouling and flux decline and to develop a systematic understanding of the influence of other forms of membrane fouling on the rejection of N-nitrosamines.

Of a particular note is the dearth of information regarding the influence of membrane ageing on the rejection of N-nitrosamines. Membrane ageing caused by prolonged exposure to hypochlorite has been shown to have a negative impact on the rejection of inorganic salts and several trace organic compounds [119, 120]. The membrane ageing process can also be exacerbated by occasional chemical cleaning which is used to restore the permeate flux once the membrane has been fouled. A recent study reported by Simon et al. [121] demonstrated that caustic cleaning at pH 12 could lead to a significant reduction in the rejection of carbamazepine which is a pharmaceutically active compound from 80 to 50%. These recent results highlight the need for a systematic investigation of the impact of membrane ageing on the rejection of N-nitrosamines. Thus, the impact of membrane ageing may also account for some of the variations in the rejection of NDMA that have been observed in the literature.

3.4 Research gaps

The significant variations in the rejection of NDMA and the lack of rejection data of other N-nitrosamines and their precursors discussed above underscore the current research gap regarding the fate and transport of these contaminants during RO treatment for indirect potable water reuse. Thus, in addition to the core research objectives described in Chapter 1, the following research gaps will also be addressed in this thesis:

- 1) Impact of membrane fouling and membrane ageing on the rejection of N-nitrosamines is unclear;
- 2) Modelling of N-nitrosamine rejection at pilot- or full-scale level taking into account the changes in feed water composition and hydraulic variation throughout the system has not been performed by previous studies; and
- 3) Identifying a suitable surrogate parameter for routine assessment of NDMA rejection is required.

Research gaps I and II will be addressed in Chapters 5, 6, 10 of this thesis. Research gap III has also been addressed as part of another PhD project (K.L. Tu, **T. Fujioka**, et al., *Environmental Science & Technology*, 47 (2013) 6425–6430) and thus the results will not be presented here.

As discussed above, future studies addressing the impact of membrane fouling and membrane ageing on the rejection of N-nitrosamines could also explain for some of the variations in their rejection amongst different pilot/full scale RO plants. Recent research has confirmed that the rejection of N-nitrosamines can be simulated using the existing irreversible thermodynamic model. However, such modelling capacity is limited to a flat-sheet membrane sample at the laboratory scale. Further expansion of this modelling capacity is needed to take into account variation in the hydraulic condition along the spiral wound membrane element and between different membrane elements in the system and thus allowing for a systematic evaluation of the impact of permeate flux on the rejection of NDMA and other N-nitrosamines. The monitoring of N-nitrosamines rejection in pilot- and full-scale RO plants is severely hindered by the difficulties associated with the analysis of NDMA at the regulatory levels (Section 2.4). Because the rejection of NDMA by RO membranes is governed mostly by steric hindrance, it may be possible to identify a solute that both has similar rejection behaviour to that of NDMA and ubiquitously occurs in reclaimed water at a sufficiently high concentration for routine analysis. Such a surrogate, if it can be identified, is not expected to completely replace the need for the actual analysis of NDMA. However, it will be of immense benefit to the study of NDMA rejection at the pilot- and full-scale level and can serve as an early warning when low NDMA rejection occurs.

4 *Conclusions*

Data represented in the literature suggest that steric hindrance appears to be the primary mechanism governing the rejection of N-nitrosamine by RO membranes. The rejection of N-nitrosamines by RO membranes can be described by the irreversible thermodynamic model. Considering all N-nitrosamines, studies available to date have focused mostly on the rejection of NDMA. Several investigations focusing on other N-nitrosamines have revealed that their rejection by RO membranes can be significantly

higher than that of NDMA (which has the lowest molecular weight amongst all N-nitrosamines). This review reveals significant variation in NDMA rejection amongst laboratory-, pilot- and full-scale studies (sometimes even by the same RO membrane). The rejection of NDMA by a typical brackish water RO membrane obtained from laboratory-scale studies ranged from 50 to 70%. In contrast, the rejections of NDMA reported at pilot- and full-scale varied significantly, from negligible to over 70%. The variation in NDMA rejection observed across studies can be partially explained by the differences in operating conditions (i.e. recovery, permeate flux, and feed pH) and feed solution characteristics (i.e. ionic strength and temperature). In particular, evidence reported in the literatures suggests that seasonal changes in feed water temperature are likely to play an important role in NDMA rejection. For example, an increase in feed temperature by 10 °C could account for as much as 25% reduction in NDMA rejection by a conventional RO membrane. However, the combined effects of all operating parameters cannot fully account for the variations in NDMA rejection that were observed at full-scale RO installations. The impact of membrane fouling and chemical cleaning on rejection of N-nitrosamines has not yet been systematically investigated. In addition, further research on the development of a predictive model is also needed to allow for the full understanding and optimisation of NDMA rejection in full-sale RO systems.

Chapter 3

Materials and Methods

1 *Introduction*

Experimental work in this study was carried out using laboratory-, pilot-, or full-scale RO filtration system. In this chapter, the physicochemical properties of the selected membranes and N-nitrosamines were examined. These data were obtained from literature review, simulation using computer software and laboratory-scale experiments. Chemicals and their sample preparations were described in details. Filtration systems and experimental protocols were also included. In addition, each analytical technique used in this investigation was fully explained.

2 *Selected NF/RO membranes*

Eight NF/RO membranes selected here are thin film composite membranes with a thin polyamide active skin layer on a porous polysulfone supporting layer. The NF90 and ESPA1 membranes are typically used for brackish water treatment. The ESPA2, LFC3, TFC-HR and 70LW are low pressure reverse osmosis (LPRO) membranes which have been widely employed for water reclamation applications [8, 86, 122, 123]. The ESPAB is another LPRO membrane which is particularly designed to achieve a high rejection of boron during second pass seawater desalination. A sea water reverse osmosis (SWRO) membrane (namely SWC5) was also used in this study. The nominal salt rejection values of these membranes are summarised in Table 3.1. It is noteworthy that for comparison purposes, the pure water permeability values of the different membranes were measured under the same filtration condition (Table 3.1). Given the variety of membranes used in this study, our filtration condition is not necessarily identical to the filtration protocol used by each manufacturer to specify the performance of their membranes. Moreover, membrane properties such as permeability are not always uniform in a membrane sheet. As a result, the pure water permeability values reported in Table 3.1 may differ from what specified by the manufacturer by up to 20%.

Table 3.1: Properties of the membranes used in this study (salt rejection values were specified by the manufacturers).

Membrane	Membrane type	Manufacturer	NaCl rejection [%]	MgSO ₄ rejection [%]	Pure water permeability ^f [L/m ² hbar at 20°C]	Contact angle ^g [°]
NF90	NF	Dow/Filmtec	-	> 97 ^e	12.6 (±0.2)	69
ESPA1	LPRO	Hydranautics	99.3 ^a	-	8.1 (±0.3)	61
ESPA2	LPRO	Hydranautics	99.6 ^a	-	5.2 (±0.2)	53
LFC3	LPRO	Hydranautics	99.7 ^a	-	2.9 (±0.3)	35
TFC-HR	LPRO	KMS	99.6 ^b	-	2.8 (±0.3)	52
70LW(TML)	LPRO	Toray	99.7 ^c	-	2.5 (±0.2)	41
ESPAB	LPRO	Hydranautics	99.3 ^a	-	4.3 (±0.5)	47
SWC5	SWRO	Hydranautics	99.8 ^d	-	1.9 (±0.1)	61

^a Filtration condition: 1,500 ppm NaCl, 1.05 MPa, 25 °C and pH 6.5 - 7.0.

^b Filtration condition: 2,000 ppm NaCl, 1.55 MPa, 25 °C and pH 7.5.

^c Filtration condition: 2,000 ppm NaCl, 1.55 MPa, 25 °C and pH 7.0.

^d Filtration condition: 32,000 ppm NaCl, 5.5 MPa, 25 °C and pH 6.5 - 7.0.

^e Filtration condition: 2,000 ppm MgSO₄, 0.48 MPa, 25 °C and pH 8.

^f Determined with Milli-Q water at 1,000 kPa and 20 °C feed temperature. Errors represent the standard deviation of two replicates.

^g Measured with a Rame-Hart Goniometer (Model 250, Rame-Hart, Netcong, NJ, USA) using the standard sessile drop method.

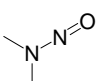
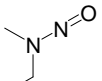
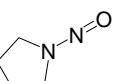
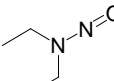
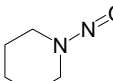
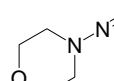
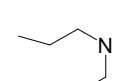
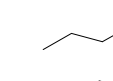
3 Chemicals

The eight N-nitrosamines used in this study were of analytical grade and were purchased from Sigma-Aldrich (St Louis, MO, USA). These N-nitrosamines include N-nitrosodimethylamine (NDMA), N-nitrosomethylethylamine (NMEA), N-nitrosopyrrolidine (NPYR), N-nitrosodiethylamine (NDEA), N-nitrosodipropylamine (NDPA), N-nitrosodi-n-butylamine (NDBA), N-nitrosopiperidine (NPIP), and N-nitrosomorpholine (NMOR). Their physicochemical properties have been described in Table 3.2. N-nitrosamine stock solution was prepared in pure methanol with 250 µg/L of each N-nitrosamine. A deuterated surrogate standard was used for each N-nitrosamine under investigation. These surrogate standards include N-nitrosodimethylamine-D6, N-nitrosomethylethylamine-D3, N-nitrosopyrrolidine-D8, N-nitrosodiethylamine-D10, N-nitrosopiperidine-D10, N-nitrosomorpholine-D8, N-nitrosodipropylamine-D14 and N-nitrosodi-n-butylamine-D9, and were purchased from

CDN isotopes (Pointe-Claire, Quebec, Canada). A surrogate stock solution containing 100 µg/L of each deuterated N-nitrosamine was prepared in pure methanol. The stock solutions were stored at -18 °C and used within one month of preparation. The stock solutions were kept at -18 °C in the dark. All stock solutions were used within 1 month of preparation.

Analytical grade boric acid was obtained from by Sigma-Aldrich (St Louis, MO, USA). A stock solution of boric acid of 1 g-boron/L was prepared in Milli-Q. Analytical grade NaCl, CaCl₂ and NaHCO₃ were purchased from Ajax Finechem (Taren Point, NSW, Australia) and used as the background electrolytes for the filtration experiments. Stock solutions of these background electrolytes were also prepared in Milli-Q water at 2M (NaCl) and 0.1M (CaCl₂ and NaHCO₃) concentrations.

Table 3.2: Physicochemical properties of the selected N-nitrosamines.

Compound	NDMA	NMEA	NPYR	NDEA	NPIP	NMOR	NDPA	NDBA
Structure								
Molecular Formula	C ₂ H ₆ N ₂ O	C ₃ H ₈ N ₂ O	C ₄ H ₈ N ₂ O	C ₄ H ₁₀ N ₂ O	C ₅ H ₁₀ N ₂ O	C ₄ H ₈ N ₂ O ₂	C ₆ H ₁₄ N ₂ O	C ₈ H ₁₈ N ₂ O
Molecular Weight [g/mol]	74.05	88.06	100.06	102.08	114.08	116.06	130.11	158.14
Molecular Width ^a [nm]	0.270	0.306	0.318	0.322	0.325	0.317	0.365	0.405
Diffusion coefficient in water ^b [cm ² /s]	9.7×10 ⁻⁶	8.0×10 ⁻⁶	8.0×10 ⁻⁶	8.0×10 ⁻⁶	8.6×10 ⁻⁶	9.2×10 ⁻⁶	8.2×10 ⁻⁶	8.0×10 ⁻⁶
LogK _{ow} ^b	-0.64	-0.15	0.23	0.34	0.74	-1.39	1.35	2.31
Solubility in water at 20 °C ^b [g/L]	1,000	300	780	147	49	4,714	9.9	1.2
Dipole moment ^c [Debye]	3.71	3.71	3.74	3.72	3.73	2.68	3.77	3.82

^a Calculated using Molecular Modeling Pro (ChemSW Inc., Fairfield, CA, USA).^b GSI chemical properties database (GSI ENVIRONMENTAL INC), <http://www.gsi-net.com/en/publications/gsi-chemical-database.html>.^c Millsian 2.1 software (Millsian INC).

4 Filtration system

4.1 Bench-scale filtration system

A bench-scale cross flow membrane filtration system was used in this study (Figure 3.1). The system consists of a rectangular stainless steel membrane cell, a high pressure pump (Hydra-Cell, Wanner Engineering Inc., Minneapolis, MN, USA), and a stainless steel reservoir. The membrane cell has an effective membrane area of 40 cm^2 ($4 \text{ cm} \times 10 \text{ cm}$) and channel height of 2 mm. Permeate flow rate and cross flow velocity were monitored using a digital flow meter (FlowCal, GJC Instruments Ltd, Cheshire, UK), which was connected to a PC and a rotameter, respectively. The concentrate flow was controlled using a back pressure regulating valve (Swagelok, Solon, OH, USA) and a bypass valve. Feed pressure indicated by a pressure gauge was also recorded during the filtration experiments. Feed temperature was controlled by a temperature control unit (Neslab RTE 7, Thermo Scientific Inc., Waltham, MA, USA) equipped with a stainless steel heat exchanger coil which was submerged directly into the feed reservoir. The retention time between the exit of the membrane cell and the feed reservoir was within a few seconds and the pipe work is insulated. The impact from the atmospheric temperature would be thus negligible.

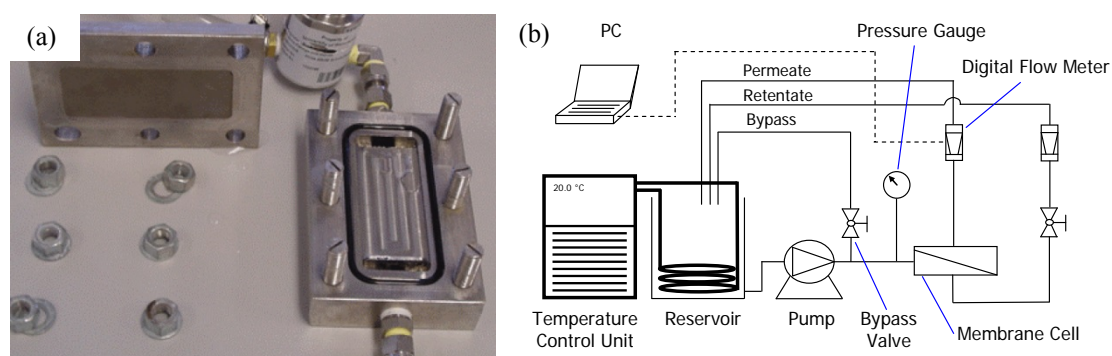


Figure 3.1: (a) A picture of the membrane cell; and (b) schematic diagram of the laboratory-scale filtration system.

4.2 Pilot-scale filtration system

A pilot-scale cross-flow RO filtration system was used in this investigation. The pilot system comprises three 4 inch glass-fibre pressure vessels, 300 L feed reservoir, stainless steel pipes in the feed stream and PVC pipes in the permeate stream (Figure

3.2). Each pressure vessel holds one 4 inch \times 40 inch RO membrane element. The feed solution was delivered from the feed reservoir to the first stage by a pump (CRN 3-25, Grundfos, Bjerringbro, Denmark) and the concentrate of the first stage was transferred to the second stage followed by the third stage. The permeate and concentrate streams were returned back into the feed reservoir. The permeate flow rate and cross flow rate were both monitored by flow meters and regulated by a globe valve and speed controller of the pump. Feed solution temperature was conditioned in the feed reservoir using stainless steel heat exchanging pipes connected to a chiller/heater unit (Aqua Cooler S360PD-CT, Chester Hill, NSW, Australia).

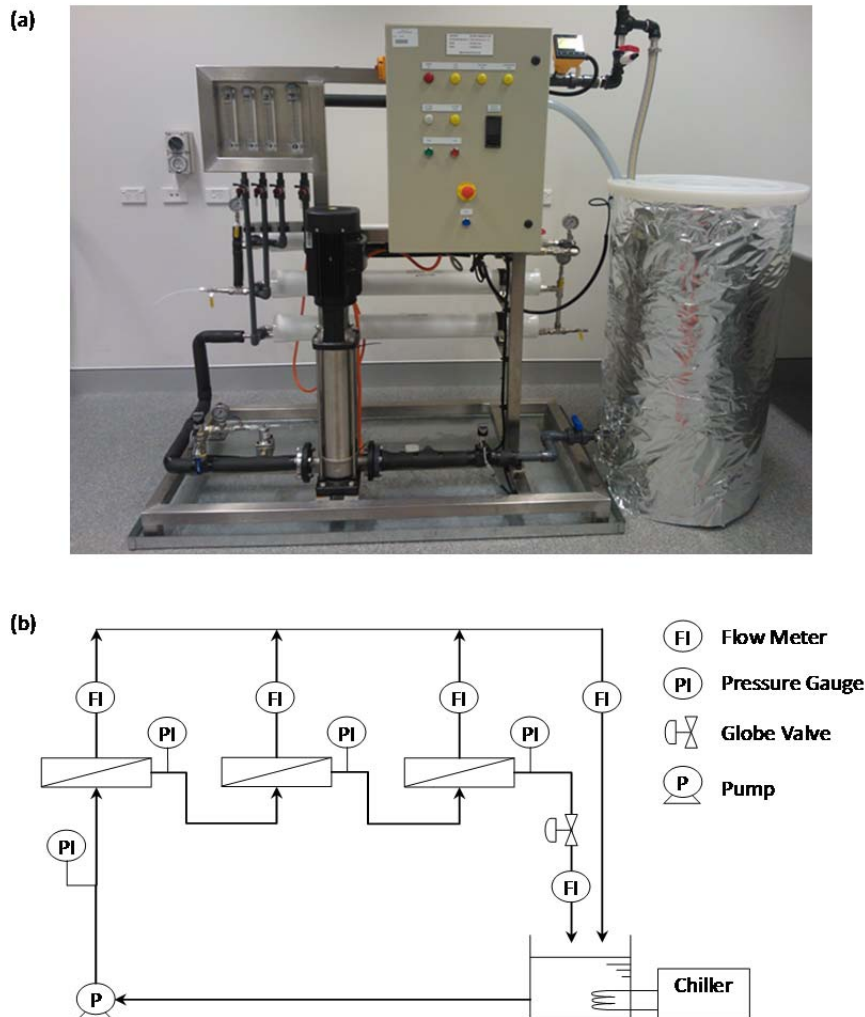


Figure 3.2: (a) A picture of the pilot system; and (b) schematic diagram of the pilot system.

5 *Water chemistry analytical techniques*

5.1 N-nitrosamine concentration analysis

The analysis of each N-nitrosamine concentration in this study is based on the gas chromatography coupled with tandem mass spectrometry (GC-MS/MS) technique using electron ionisation in a combination with the solid phase extraction (SPE) method previously described by McDonald et al [73]. Prior to the SPE procedure, 100 µL surrogate stock solution was spiked into the sample to obtain 50 ng/L of each N-nitrosamine surrogate. SupelcleanTM Coconut Charcoal SPE cartridges (2 g), supplied by Supelco (St Louis, MO, USA), were used for the SPE process. Thereafter, the SPE cartridges were cleaned with 6 mL dichloromethane, 6 mL methanol and 12 mL of Milli-Q water. Accurate quantitation (accounting for incomplete SPE recovery) was undertaken by direct-analogue isotope dilution for all nitrosamines by adding 100 µL surrogate stock solution into 200 mL of each sample to make up 50 ng/L of each N-nitrosamine surrogate. N-nitrosamines in the samples were then extracted by SPE at a flow rate of 5 mL/min. The cartridges were rinsed with 3 mL Milli-Q water and dried with high purity nitrogen gas for at least 60 minutes. The dried SPE cartridges were then eluted using 12 mL dichloromethane, and 100 µL of toluene was added in the eluent. The eluent was then concentrated to 1 mL with a Turbovap LV (Caliper Life Sciences, Hopkinton, MA, USA) under a gentle nitrogen stream. The concentrations of N-nitrosamines were quantified using an Agilent 7890A gas chromatograph (GC) coupled with an Agilent 7000B triple quadrupole mass spectrometer (MS/MS) (Figure 3.3). Calibration curves were established for each N-nitrosamine in the range of 1-400 ng/L. The detection limits of N-nitrosamines established for this analytical method are 5 ng/L for NDMA, NDEA, NPIP, and NMOR, and 10 ng/L for NMEA, NPYR, NDPA, and NDBA.



Figure 3.3: A picture of GC-MS/MS.

5.2 Basic analytical techniques

Turbidity was analysed using a 2100N laboratory turbidity meter (Hach, USA). Conductivity and pH were measured using an Orion 4-Star Plus pH/conductivity meter (Thermo scientific, USA). Total organic carbon (TOC) concentration was determined using a TOC-VSH analyser (Shimadzu, Japan) based on the non-purgeable organic carbon (NPOC) method. Cations and anions were analysed using an Inductive Coupled Plasma – Mass Spectrometer (7500CS, Agilent Technologies, Wilmington, DE, USA) and an ion chromatography (IC) system (Shimadzu, Tokyo, Japan), respectively.

6 Membrane characterisation

6.1 Contact angle measurement

Contact angle of membrane surface was measured using the standard sessile drop method. This was performed with a Rame-Hart Goniometer (Model 250, Rame-Hart, Netcong, NJ) (Figure 3.4). Prior to the measurement, virgin and fouled membrane samples were dried for over 24 h in the dark. The dry membrane was fixed on the stage of the instrument and contact angle of the membrane was measured with a water droplet (Milli-Q water). The contact angle of each membrane was determined from ten droplets.



Figure 3.4: A picture of Rame-Hart Goniometer.

6.2 Zeta potential measurement

The streaming potential of the membrane surface was measured using a SurPASS electrokinetic analyser (Anton Paar GmbH, Graz, Austria) (Figure 3.5). The measurement of the streaming potential was performed in 1 mM KCl background electrolyte solution. The background solution was first adjusted to pH 9.5 using a KOH (0.1 M) solution. Subsequently, the background pH was reduced to pH 3 by a stepwise automatic titration using HCl (0.1 M) solution. The zeta potential of the membrane surface was calculated with the measured streaming potential using the Fairbrother-Mastin method [124]. During the analysis, the background solution temperature was maintained at 25 ± 1 °C.

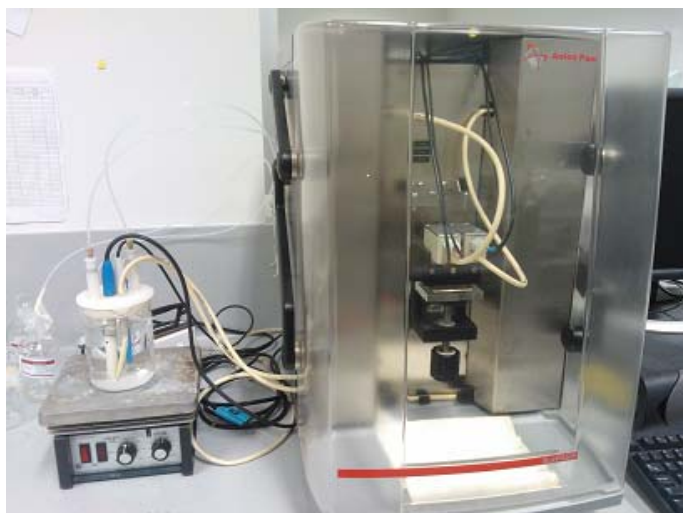


Figure 3.5: A picture of SurPASS electrokinetic analyser.

6.3 Surface chemistry

Functional groups of RO membranes were analysed obtaining Fourier transform infrared spectroscopy (FTIR) spectra using an IRAffinity-1 (Shimazu, Kyoto, Japan) equipped with a diamond crystal plate. The active skin layer of each dried membrane sample was fixed on the diamond crystal plate with the same press force. The spectrum was obtained in the range of 400-4000 cm^{-1} at 2 cm^{-1} resolution.

Chapter 4

Effects of feed solution characteristics

This chapter has been published as:

T. Fujioka, L.D. Nghiem, S.J. Khan, J.A. McDonald, Y. Poussade, J.E. Drewes, Effects of feed solution characteristics on the rejection of N-nitrosamines by reverse osmosis membranes, J. Membr. Sci., 409–410 (2012) 66–74.

1 Introduction

Variations in the feed solution characteristics are expected at full-scale RO plants. For example, wastewater temperature is a seasonally variable parameter and is typically in the range of 15 to 30°C [125]. However, to date, studies focusing on the impact of feed temperature on the rejection of N-nitrosamines by RO membranes have not been reported. Although feed solution pH is usually adjusted to pH 6 – 8 prior to RO treatment [101], the impact of such feed pH setting variation on the rejection of N-nitrosamines is not well understood. Total dissolved solid or ionic strength of the feed has also been found as an important feed solution characteristic which may affect solute separation during RO filtration [108, 109, 126]. While ionic strength as well as N-nitrosamine concentration in the feed can increase considerably on the brine side of an RO pressure vessel and between different stages, there is no data available to systematically elucidate these effects on the rejection of N-nitrosamines by RO membranes.

This study investigated the rejection of eight N-nitrosamines by NF/RO membranes. The effects of feed solution characteristics on the rejection of these trace organic chemicals were elucidated by examining the rejection of N-nitrosamines under various operational conditions (i.e. permeate flux, feed concentration, pH, temperature, and ionic strength). The overall objective of this study was to provide insight into the separation behaviour of a complete set of N-nitrosamines by RO membranes. The study

also aimed to reconcile the highly variable rejection values of NDMA by RO membranes previously reported in the literature.

2 Materials and methods

2.1 NF/RO membranes

One NF (NF90) and two RO (SWC5 and TFC-HR) membranes were used in this study. Properties of these membranes are summarized in Table 3.1 (Chapter 3).

2.2 Chemicals

Properties of eight N-nitrosamines are summarized in Table 3.2 (Chapter 3).

2.3 Bench-scale filtration system

A bench-scale cross flow membrane filtration system was used (Figure 3.1). Specification of the bench-scale filtration system is described in Chapter 3, Section 4.1.

2.4 Experimental protocols

Prior to each experiment, the membrane sample was rinsed with Milli-Q water to remove any preservative coating layer. The membrane was then compacted using Milli-Q water at 1,800 kPa for at least one hour until stable permeate flux had been achieved. Unless otherwise stated, the cross flow velocity and solution temperature were kept constant at 0.42 m/s and $20 \pm 0.1^\circ\text{C}$, respectively. Once the membrane had been compacted, the pressure was reduced to 1,000 kPa for the measurement of the pure water permeability. The Milli-Q water used for compaction and pure water permeability measurement was then replaced with 10 L of a solution containing 20 mM NaCl, 1 mM CaCl_2 and 1 mM NaHCO_3 as background electrolytes. Background electrolytes of 20mM NaCl and 1mM CaCl_2 were selected to simulate the typical composition of monovalent and divalent ions in secondary treated effluent, and 1mM NaHCO_3 was selected and to maintain a constant pH. Similar synthetic feed solutions have been widely adopted in previous studies [38, 127, 128]. Unless otherwise stated, the permeate flux was adjusted to 20 L/m²h, which is a typical value used in most RO plants for water reclamation applications [18, 85]. Stock solutions containing 250 µg/L of each N-nitrosamine were then spiked into the feed reservoir to obtain the desirable

concentration of each target compound. Throughout the experiment, both permeate and retentate were circulated back to the feed reservoir. The system was continuously operated for 12 hours before any samples were taken for analysis to ensure that the stabilisation of N-nitrosamine rejection has been achieved. Experiments with variable permeate flux were conducted by first adjusting the permeate flux to 60 L/m²h, and then it was stepwise decreased to 5 L/m²h. To study the effect of feed concentration on the rejection of N-nitrosamines, stock solutions of N-nitrosamines were incrementally added to the feed reservoir to increase the concentration from 250 to 1,500 ng/L. Experiments with variable pH were conducted by first adjusting the feed solution pH to 9 using NaOH (1 M). The pH was then incrementally reduced to approximately 3.5 by the addition of HCl (1 M). For experiments with variable temperature, the feed temperature was incrementally increased from 10 to 40 °C. Once the temperature set point had been achieved, the permeate flux was adjusted to 20 L/m²h by gently regulating the feed pressure. Experiments with variable ionic strength were conducted in the range from 26 to 260 mM by a stepwise addition of the electrolytes (NaCl, CaCl₂ and NaHCO₃ with the molar ratio of 20:1:1 respectively) to the feed reservoir. In all experiments described above, once the target parameter has been adjusted, the filtration system was stabilised for one hour prior to the collection of feed and permeate samples for analysis. At each sampling event, 200 mL of feed and permeate samples were collected simultaneously and solid phase extraction (SPE) was conducted immediately.

2.5 Analytical methods

N-nitrosamine concentrations were analysed using an analytical method described in Chapter 3, Section 5.1. Solution pH and electrical conductivity of the feed and permeate samples were measured using an Orion 4-Star Plus pH/conductivity meter (Thermo Fisher Scientific, Waltham, MA, USA).

2.6 Transport model description

According to the irreversible thermodynamics model previously developed by Kedem and Katchalsky [129], the transport of solvent (J_v) and solute (J_s) through an NF/RO membrane can be expressed as the following equations:

$$J_v = L_p(\Delta P - \sigma \Delta \pi) \quad J_v = L_p(\Delta P - \sigma \Delta \pi) \quad (1)$$

$$J_s = P_s(C_m - C_p) + (1 - \sigma) \bar{C} J_v \quad J_s = P_s \Delta x \left(\frac{dC}{dx} \right) + (1 - \sigma) C J_v \quad (2)$$

where L_p = pure water permeability, ΔP = pressure difference between the feed and permeate sides, σ = reflection coefficient, $\Delta \pi$ = osmotic pressure difference between the feed and permeate sides, P_s = solute permeability coefficient, Δx = membrane thickness and C = concentration. The reflection coefficient (σ) represents the fraction of solute reflected by the membrane in convective flow and ranges from 0 (no rejection of solutes) to 1 (no passage of solutes), while the solute permeability coefficient (P_s) represents the effective diffusivity of a solute inside a pore [130]. Reflection coefficient (σ), solute permeability coefficient (P_s) and pure water permeability (L_p) are transport coefficients representing membrane characteristics. Equation (2) can be expressed as the following equation (3), using reverse osmosis conditions ($J_s = C_p J_v$, C_p = permeate concentration):

$$P_s \Delta x \left(\frac{dC}{dx} \right) + [(1 - \sigma)C - C_p] J_v = 0 \quad (3)$$

Equation (3) is integrated with boundary limits as follows:

$$x = 0, C = C_p \text{ and } x = \Delta x, C = C_m \quad (4)$$

$$\int_{C_p}^{C_m} \frac{dC}{(1 - \sigma)C - C_p} + \int_0^{\Delta x} \frac{J_v dx}{P_s \Delta x} = 0 \quad (5)$$

where C_m is membrane concentration. Integration of equation (5) gives the following equation:

$$\log \left\{ \frac{[C_p - C_m(1 - \sigma)]}{\sigma C_p} \right\} + \frac{(1 - \sigma)}{P_s} J_v = 0 \quad (6)$$

Real rejection can be expressed by the following Spiegler-Kedem equation [131]:

$$R_{real} = 1 - \frac{C_p}{C_m} = \frac{\sigma(1-F)}{(1-\sigma F)} \quad (7)$$

$$F = \exp\left(-\frac{(1-\sigma)}{P_s} J_v\right) F = \exp\left(-\frac{(1-\sigma)}{P_s} J_v\right) F = \exp\left(-\frac{(1-\sigma)}{p} J_v\right) \quad (8)$$

Due to the concentration polarisation phenomenon, the solute accumulates at the membrane surface and the solute concentration on the membrane surface (C_m) is higher than that in the feed (C_b). Therefore, the real rejection (R_{real}) can be calculated from the observed rejection (which is defined as $R_{obs}=1-C_p/C_b$) by taking into account the concentration polarisation effect [132]:

$$R_{real} = \frac{R_{obs} \exp\left(\frac{J_v}{k}\right)}{1 + R_{obs} \left[\exp\left(\frac{J_v}{k}\right) - 1 \right]} \quad (9)$$

where k = mass transfer coefficient. Mass transfer coefficient (k) can be calculated by Sherwood number (Sh). When the filtration experiment is carried out under laminar flow conditions (Reynolds number (Re) < 2000) and the length of the entry region ($L^* = 0.029d_h Re$) is larger than the length of the membrane (L), the Schmidt number (Sc) can be expressed by Grover equation [133]:

$$Sh = \frac{d_h k}{D} = 0.664 Re^{0.5} Sc^{0.33} \left(\frac{d_h}{L} \right)^{0.33} \quad (10)$$

where $Re = (d_h u / \nu)$, $Sc = (\nu / D)$, d_h = hydraulic diameter, u = feed velocity, ν = kinematic viscosity and D = diffusion coefficient.

3 Results and discussion

3.1 Separation behaviour of N-nitrosamines

3.1.1 Rejection of N-nitrosamines by NF/RO membranes

Solute separation by NF/RO membranes can be governed by electrostatic interactions and steric hindrance. The former is not expected to occur for the eight N-nitrosamines investigated here since they are uncharged at neutral pH. Steric exclusion relates directly to the molecular size (for which molecular weight can be used as an approximate surrogate measure) of these compounds. In general, the rejection of N-nitrosamines by all three NF/RO membranes selected in this study increased in the increasing order of their molecular weight (Figure 4.1a). Results reported here are consistent with previous bench-scale studies [38, 82]. However, it is striking to note a peculiarity regarding the rejection of NMOR. Despite the similarity in molecular weight between NMOR (116 g/mol) and NPIP (114 g/mol), NMOR rejection by the TFC-HR and NF90 membrane was 2% and 16% lower than that of NPIP, respectively. NMOR was not used in either of the previous studies [38, 82] and this appears to be the first time the rejection of NMOR has been reported and compared to that of other N-nitrosamines.

An overall trend of increasing rejection in the increasing order of molecular width can also be observed (Figure 4.1b). The molecular width is defined as half of the square root of the rectangle minimum area that encloses the projection of N-nitrosamine on a perpendicular plane [134]. In this study, the molecular width was calculated using the Molecular Modeling Pro software package (ChemSW Inc., Fairfield, CA, USA). The molecular width has been suggested to correlate better with the rejection of neutral solutes than molecular weight [134, 135]. There is a good correlation between molecular width and the rejection of N-nitrosamines with NMOR being the only exception (Figure 4.1b). Although the molecular width of NMOR is similar to that of NPYR and NDEA (NMOR: 0.317 nm, NPYR: 0.318 nm and NDEA: 0.322 nm), rejections of these three compounds by the NF90 varied over a wide range, from 33 to 52%. Similarly, their rejections by the TFC-HR were in the range of 90 to 95%.

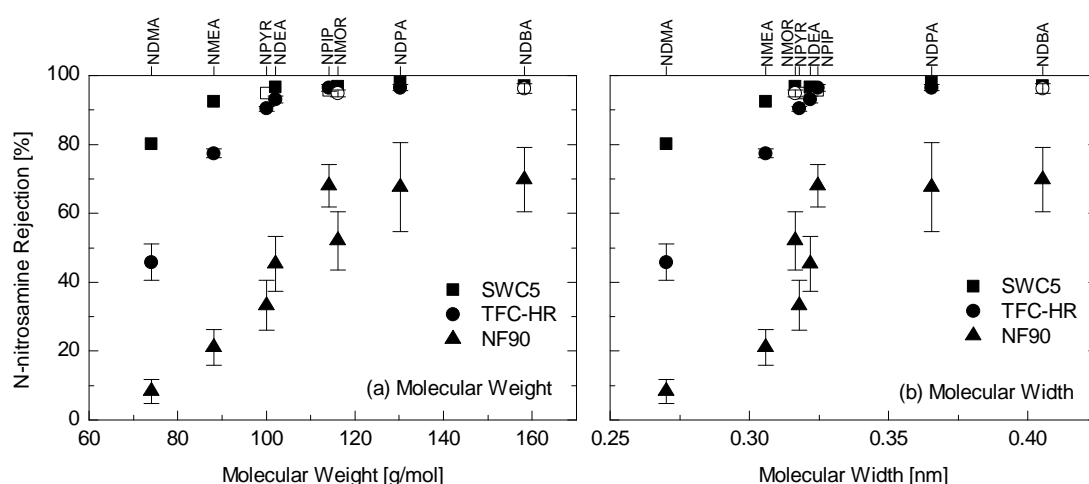


Figure 4.1: Rejection of N-nitrosamines by the SWC5, TFC-HR and NF90 membranes as a function of (a) their molecular weight and (b) molecular width (20 mM NaCl, 1 mM NaHCO₃, 1 mM CaCl₂, permeate flux 20 L/m²h, cross flow velocity 40.2 cm/s, feed pH 8.0 ± 0.1, feed temperature 20.0 ± 0.1°C). Open symbol (□ and ○) indicates that the permeate concentration was below the instrumental detection limit. Error bars show the standard deviation of three replicate experiments.

The small difference in the rejection behaviour of NMOR compared to other N-nitrosamines (Figure 4.1) can probably be explained by the fact that it is the only N-nitrosamine that has an ether functional group (Table 3.2). Because the ether functional group can also participate in hydrogen bonding with water, NMOR is the most hydrophilic and water soluble compound of all eight N-nitrosamines investigated in this study. In fact, the hydrophobicity (determined by $\log K_{ow}$) of all other N-nitrosamines increases linearly as the molecular weight increases, but this correlation cannot be applied to NMOR (Figure 4.2).

Membrane type also exhibited a significant impact on the rejection of N-nitrosamines (Figure 4.1a). Under the same experimental condition, the rejection of NDMA by the NF90 membrane was 8%, while NDMA rejection by the TFC-HR and SWC5 RO membranes were 46% and 80%, respectively. The impact of membrane type on rejection of N-nitrosamines was less pronounced for the higher molecular weight chemicals. In fact, when comparing the TFC-HR and SWC5 membranes, there was no discernible difference in the rejection of NDEA, NPIP, NMOR, NDPA and NDBA by RO membranes. Although further investigation is still necessary to identify key membrane characteristics that determine the extent of N-nitrosamine rejection, the

results reported here indicate that the rejection of low molecular weight N-nitrosamines, and particularly NDMA, can be improved by appropriate membrane selection.

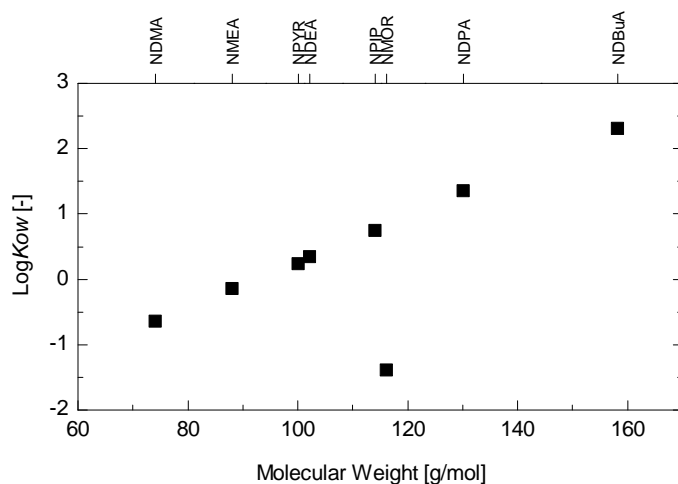


Figure 4.2: Correlation between hydrophobicity ($\log K_{ow}$) and molecular weight of N-nitrosamines.

3.2 Modelling the transport of N-nitrosamines during RO filtration

N-nitrosamine rejections by the TFC-HR membrane increased with increasing permeate flux (Figure 4.3), which is consistent with the findings of a previous study [82]. In addition, the impact of permeate flux on rejection appears more pronounced for low molecular weight N-nitrosamines. Changes in the permeate flux from 5 to 60 L/m²h resulted in an increase in NDMA and NMEA rejection from 25 to 63% and from 49 to 89%, respectively. The impact of permeate flux on rejection was less pronounced for the larger molecular weight N-nitrosamines. In fact, the influence of permeate flux on the rejection of N-nitrosamines with molecular weight higher than 114 g/mol (NPIP, NMOR, NDPA, and NDBA) was negligible. The impact of permeate flux on N-nitrosamine rejection also varied depending on a range of permeates flux and was most sensitive in the range of less than 20 L/m²h. Nevertheless, it is noteworthy that most full scale RO plants for water recycling applications operate at an average permeate flux of 20 L/m²h or less [16, 25]. At the same permeate flux of 20 L/m²h, N-nitrosamine rejection data obtained from variable and constant flux experiments are very similar (Table 4.1). The variation was less than 5% and it could be confirmed that stepwise

changes in permeate flux did not induce any significant systematic bias to the rejection of N-nitrosamines.

The irreversible thermodynamic model was used to further elucidate the rejection behaviour of N-nitrosamines by NF/RO membranes. The real rejection (R_{real}) at different permeate flux was calculated from the observed rejection data and the mass transfer co-efficient (k) which is a property of the cross flow cell using Equation 9. The reflection coefficient (σ) and solute permeability coefficient (P_s) were obtained by fitting the real rejection data to the irreversible thermodynamic model (Equations 7 and 8) and the data are summarised in Table 4.2. Because NPIP and NDPA concentrations in the permeate were below the instrument analytical limit, these two compounds were excluded from this modelling exercise. The irreversible thermodynamic model could describe very well the rejection of N-nitrosamines by the TFC-HR (Figure 4.4). While the reflection coefficient (σ) of each N-nitrosamine was high (> 0.95), a decrease in the solute permeability coefficient (P_s) was observed for an increase in molecular weight (Table 4.2). The reported results indicate that solute permeability of N-nitrosamines may be an important factor that governs their rejection by RO membranes.

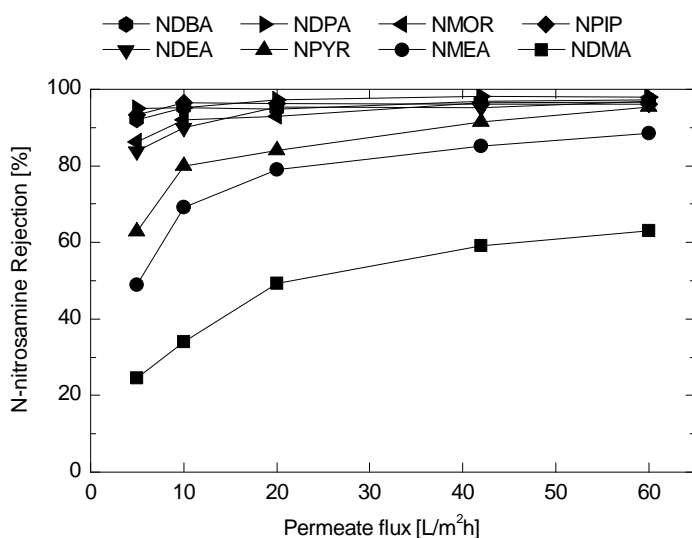


Figure 4.3: N-nitrosamine rejection and feed pressure by the TFC-HR membrane as a function of permeate flux (20 mM NaCl, 1 mM NaHCO₃, 1 mM CaCl₂, crossflow velocity 40.2 cm/s, feed pH 8.0 ± 0.1 , feed temperature $20.0 \pm 0.1^\circ\text{C}$).

Table 4.1: Impact of step-wise changes in permeate flux on the rejection of N-nitrosamines at 20 L/m²h permeate flux by the TFC-HR membrane (20 mM NaCl, 1 mM NaHCO₃, 1 mM CaCl₂, cross flow velocity 40.2 cm/s, feed pH 8.0 ± 0.1, feed temperature 20.0 ± 0.1 °C).

	Rejection [%] from variable flux experiment	Rejection [%] from constant flux experiment*
NDMA	49.3	47.6 (±5.2)
NMEA	79.0	77.4 (±1.3)
NPYR	84.0	90.4 (±0.7)
NDEA	95.3	93.0 (±1.0)
NPIP	96.2	96.6 (±1.0)
NMOR	93.0	94.9 (±1.0)
NDPA	97.3	96.5 (±0.9)
NDBA	94.8	96.3 (±1.4)

* Errors show the standard deviation of three replicate experiments.

Table 4.2: Transport parameters of N-nitrosamines through the TFC-HR membrane and the fitting coefficient of determination (R^2) of the irreversible thermodynamics model.

N-nitrosamine	k [m/s]	σ [-] (95% confidence bounds)	P [m/s] (95% confidence bounds)	R^2 [-]
NDMA	2.26×10^{-5}	0.949 (0.800, 1.10)	4.15×10^{-6} (2.88×10^{-6} , 5.41×10^{-6})	0.99
NMEA	1.99×10^{-5}	0.968 (0.805, 1.13)	1.07×10^{-6} (4.97×10^{-7} , 1.64×10^{-6})	0.98
NPYR	1.99×10^{-5}	0.989 (0.869, 1.11)	6.74×10^{-7} (3.59×10^{-7} , 9.88×10^{-7})	0.98
NDEA	1.99×10^{-5}	0.998 (0.968, 1.03)	2.49×10^{-7} (1.95×10^{-7} , 3.02×10^{-7})	0.99
NMOR	2.18×10^{-5}	0.988 (0.957, 1.02)	1.99×10^{-7} (1.37×10^{-7} , 2.60×10^{-7})	0.97
NDBA	1.99×10^{-5}	0.983 (0.962, 1.01)	1.01×10^{-7} (5.34×10^{-8} , 1.47×10^{-7})	0.92

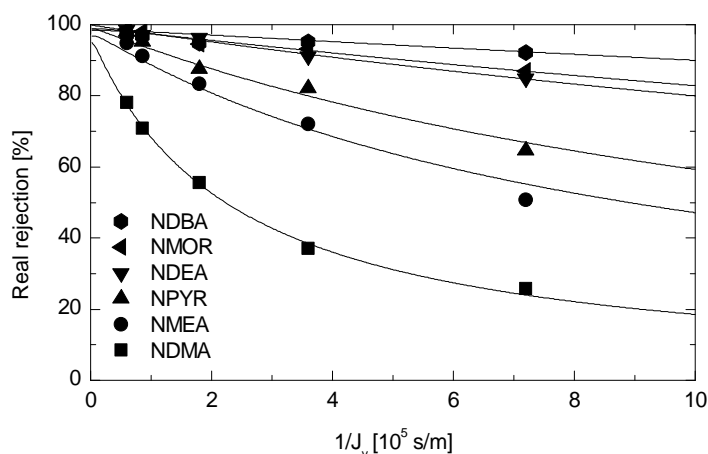


Figure 4.4: Real rejection of N-nitrosamines by the TFC-HR membrane as a function of reciprocal permeate flux. Experimental conditions are as described in Figure 4.3.

3.3 Effects of RO feed solution chemistry

3.3.1 *N-nitrosamine concentrations*

All N-nitrosamines investigated here are hydrophilic (Table 3.2) and thus they are not expected to adsorb to the membrane. Indeed, in all experiments of this study, N-nitrosamine concentrations in the feed were stable indicating that the adsorption of N-nitrosamines to the membrane was negligible and that the filtration process of N-nitrosamines would reach a steady state condition in a short period. Miyashita et al. [82] reported that steady state conditions in the rejection of N-nitrosamines by NF/RO membranes were achieved within less than 45 minutes of N-nitrosamine addition in the feed. Similarly, Steinle-Darling et al. [38] reported that the rejection of N-nitrosamines by the LFC3 membrane reached a steady state condition ($\pm 5\%$ of the final rejection value) within 5 minutes of operation.

Changes in the feed concentration of N-nitrosamine (250-1,500 ng/L) did not have any apparent effect on their rejections (Figure 4.5), which is in agreement with a previous study by Miyashita et al. [82]. Because concentration of the solute in the feed solution is not an input parameter to the irreversible thermodynamic model previously described in section 2.6, solute rejection (which is an output of the model) is expected to be independent of the feed solute concentration. The results reported here suggest that the

irreversible thermodynamics model can be used to adequately describe the separation of N-nitrosamines during NF/RO filtration processes.

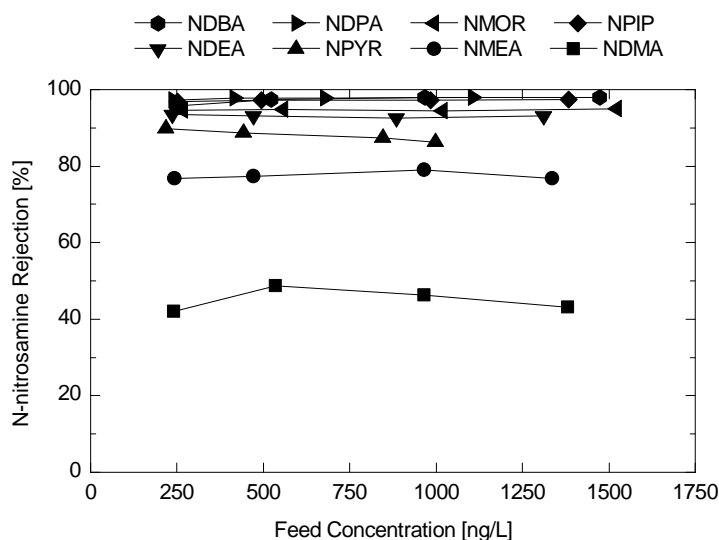


Figure 4.5: Rejection of N-nitrosamines by TFC-HR as a function of nitrosamine concentration in the feed (20 mM NaCl, 1 mM NaHCO₃, 1 mM CaCl₂, permeate flux 20 L/m²h, crossflow velocity 40.2 cm/s, feed pH 8.0 ± 0.1, feed temperature 20.0 ± 0.1°C).

3.3.2 Feed pH

The rejections of NDMA and NMEA (which exhibits the lowest molecular weight among the eight N-nitrosamines selected in this study) were sensitive to the feed solution pH (Figure 4.6). Their rejection by the TFC-HR membrane decreased gradually as the feed solution pH decreased from 9 to 3.5. The active skin layer of the TFC-HR is made of polyamide which has both carboxylic and amine functional groups. Changes in the solution pH can lead to speciation of these functional groups and thus changes in the conformation of the membrane polymeric matrix. In fact, it has been reported that the membrane pore size can become larger as the solution pH decreases due to changes in the conformation of the membrane polymer matrix [99, 100]. Bellona and Drewes [136] found that the rejection of negatively charged organic acids, 2-Naphthalenesulfonic acid and 1,5-Naphthalenedisulfonic acid, by the NF90 and NF200 membranes increased with increasing feed solution pH. Similarly, Verliefde et al. [98] reported that the feed solution pH could influence the rejection of the small and neutral pharmaceutical compound phenazon by the Desal HL membrane. Although the changes in NDMA and NMEA rejection observed in this study are likely to be caused by the changes in the

membrane pore size, it is noteworthy that no discernible changes in the membrane permeability as a function of feed solution pH could be observed. It can be inferred from the results reported here that small variations in feed pH in the range from pH 6 to 8, which can occur in a full-scale RO plant [101], have only a small impact upon the rejection of NDMA and NMEA. The impact of feed solution pH on other N-nitrosamines with molecular weight larger than that of NMEA is expected to be negligible.

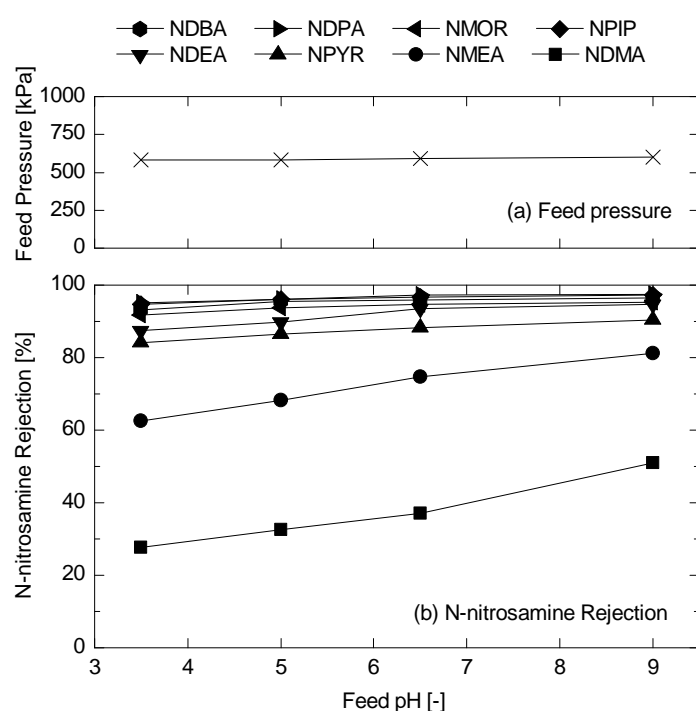


Figure 4.6: (a) Feed pressure and (b) N-nitrosamine rejection by the TFC-HR membrane as a function of feed pH (20 mM NaCl, 1 mM NaHCO₃, 1 mM CaCl₂, permeate flux 20 L/m²h, crossflow velocity 40.2 cm/s, feed temperature 20.0 ± 0.1°C).

3.3.3 Ionic strength

Higher feed ionic strength necessitated higher feed pressure to maintain permeate flux, due to the increased osmotic pressure (Figure 4.7). Changes in ionic strength mainly affected the rejection of NDMA, which is consistent with results reported in a previous study [38]. As the ionic strength increased by a factor of ten (from 26 to 260 mM), NDMA rejection by the TFC-HR decreased from 52 to 34%. Although several other N-nitrosamines also exhibited changes in their rejection as the ionic strength of the feed

solution increased, the extent of the decreased rejection was small (e.g. from 90 to 83% for NPYR). Similar to the impact of the feed solution pH on N-nitrosamine rejection previously discussed in section 3.2.2, the impact of feed solution ionic strength was only apparent for NDMA. It has been suggested that an increase in ionic strength can increase the membrane pore size (or porosity) and reduce the size of neutral solutes, resulting in decreasing rejection of neutral solutes [107-109]. Therefore, the changes in NDMA rejection reported here can possibly be caused by changes in the membrane internal structure. Since ionic strength of the feed solution increases on the brine side toward the end of an RO pressure vessel, NDMA rejection can be reduced as RO treatment progresses.

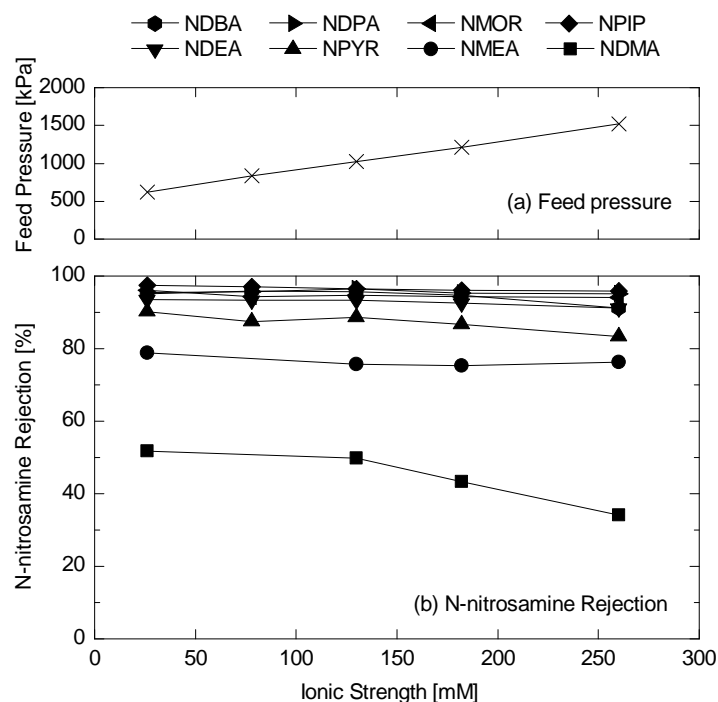


Figure 4.7: (a) Feed pressure and (b) N-nitrosamine rejection with TFC-HR as a function of feed ionic strength (permeate flux 20 L/m²h, crossflow velocity 40.2 cm/s, feed pH 8.0 ± 0.1, feed temperature 20.0 ± 0.1°C).

3.3.4 Feed temperature

At a higher feed temperature, a lower feed pressure was required to maintain a permeate flux of 20 L/m²h. The increase in feed temperature caused a decrease in the rejection of all N-nitrosamines (Figure 4.8). The impact of feed temperature on rejection was more

pronounced for smaller N-nitrosamines. For example, an increase in the feed temperature in the range from 20 to 30°C caused a significant drop in the rejection of NDMA, NMEA and NPYR from 49 to 24%, 81 to 62% and 90 to 74%, respectively.

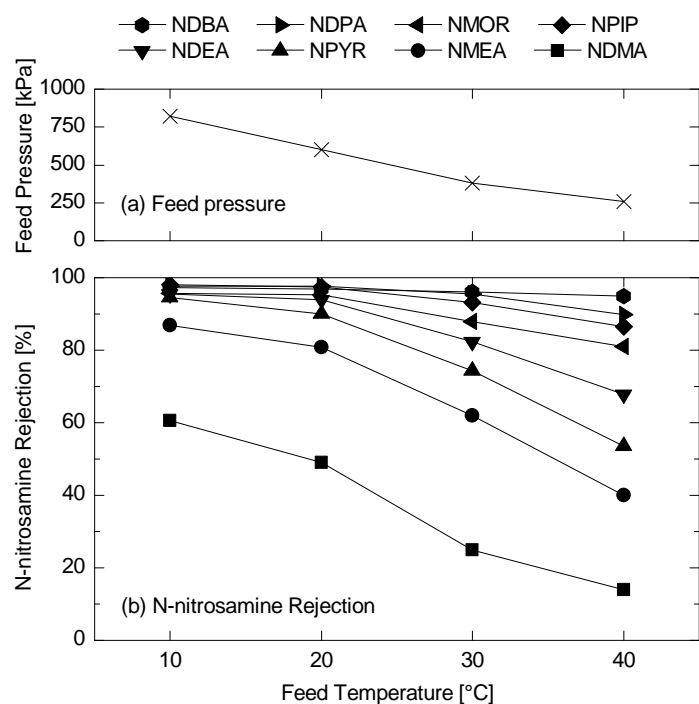


Figure 4.8: (a) Feed pressure and (b) N-nitrosamine rejection by the TFC-HR membrane as a function of feed temperature (20 mM NaCl, 1 mM NaHCO₃, 1 mM CaCl₂, permeate flux 20 L/m²h, crossflow velocity 40.2 cm/s, feed pH 8.0 ± 0.1).

A decreasing trend in neutral solute rejection in response to an increase in the feed temperature has been reported in several previous studies. The permeability coefficients of neutral solutes (raffinose, alcohols, sugars and polyethylene glycols) through inorganic NF membranes were reported to increase with increasing feed temperature [130, 132]. For polymeric membranes, it has been reported that an increase in the feed temperature could lead to changes in the polymer structure of the membrane active layer, reflected by an increase in the membrane average pore size and a higher passage of neutral solute [111]. The low rejection of N-nitrosamines at high feed temperature observed in this study is, therefore, likely to have been caused by both the increased permeability coefficient of N-nitrosamines and the increased pore size of the organic RO membrane. This finding is important because temperature variation in the range

from 20 to 30°C is likely to occur at many water reclamation plants employing RO membranes and is usually difficult to control.

4 Conclusions

The rejection of specific N-nitrosamines increased in the order of NF (NF90), low pressure RO (TFC-HR), and seawater RO (SWC5) membranes. Similarly, the rejection of N-nitrosamines increased in the order of increasing molecular weight. Results reported in this study indicate that steric hindrance is a major rejection mechanism and is mainly associated with the molecular dimensions or molecular weight of N-nitrosamines. However, a small but nevertheless discernible difference in the rejection behaviour between NMOR and the other N-nitrosamines was also observed. The irreversible thermodynamics model was able to describe the separation of N-nitrosamines by the TFC-HR membrane. In good agreement with this model, changes in the feed concentration in the range from 250 – 1,500 ng/L did not lead to any discernible influence on their rejection. An increase in the feed solution pH (i.e. from 6 to 8) led to a small but clearly discernible increase in the rejection of NDMA and NMEA, which are the two smallest N-nitrosamines. A ten-fold increase in the feed solution ionic strength (from 26 to 260 mM) led to a discernible decrease in NDMA rejection (from 52 to 34%), while there was no apparent impact of ionic strength on all other N-nitrosamines. It is important to note that an increase in the feed temperature caused a considerable decrease in the rejection of all N-nitrosamines. The impact of feed solution temperature on the rejection was more severe for the low molecular weight N-nitrosamines. When the feed temperature increased from 20 to 30°C, the rejection of NDMA, NMEA and NPYR decreased from 49 to 24%, 81 to 62%, and 90 to 74%, respectively. Results reported here indicate that pH, ionic strength, and temperature of the feed solution can exert some influence on the rejection of NDMA and in some cases other N-nitrosamines. The combined effects of these feed solution characteristics, particularly feed solution temperature, may account for some of the variation of NDMA rejection by RO membranes previously reported in the literature.

Chapter 5

Effects of membrane fouling

This chapter has been published as:

T. Fujioka, S.J. Khan, J.A. McDonald, R.K. Henderson, Y. Poussade, J.E. Drewes, L.D. Nghiem, *Effects of membrane fouling on N-nitrosamine rejection by nanofiltration and reverse osmosis membranes, J. Membr. Sci., 427 (2013) 311-319.*

1 Introduction

Municipal wastewater usually contains a large amount of organic and inorganic matter, resulting in the formation of organic and colloidal fouling, bio-fouling and inorganic scales on RO membranes [101, 116]. It has been established in the literature that membrane fouling can either increase or decrease the separation efficiency of NF/RO membranes [114, 116, 117, 137]. However, apart from a laboratory-scale study conducted by Steinle-Darling et al. [38] who investigated the rejection of several N-nitrosamines by an RO membrane (ESPA3) artificially fouled with sodium alginate, to date little attention has been given to the effects of membrane fouling on the rejection of N-nitrosamines. Steinle-Darling et al. [38] reported that membrane fouling by sodium alginate on the ESPA3 membrane caused a reduction in NDMA rejection (from 56 to 37%).

The aim of this work was to provide insights into the effects of membrane fouling on the rejection of N-nitrosamines by NF/RO membranes. The effects of membrane fouling were investigated by comparing the rejections of N-nitrosamines by clean and fouled membranes. Tertiary treated effluent and four different model foulants (namely sodium alginate, bovine serum albumin, humic acid and colloidal silica) were used to induce membrane fouling. The tertiary treated effluent and model foulants were characterised in detail to systematically elucidate the effects of membrane fouling on the rejection of N-nitrosamines by NF/RO membranes.

2 Materials and methods

2.1 NF/RO membranes

Three NF/RO membranes – namely the NF90, ESPA2, and ESPAB – were used in this investigation. Properties of these membranes are summarized in Table 3.1 (Chapter 3).

2.2 Chemicals

Properties of eight N-nitrosamines are summarized in Table 3.2 (Chapter 3). Sodium alginate (SA), bovine serum albumin (BSA), humic acid (HA) and colloidal silica (Ludox CL, 30% weight suspension in water) were selected as model foulants to simulate polysaccharides, proteins, refractory organic matter and colloidal particles, respectively. The source of SA was alginic acid sodium salt from brown algae. These model foulants were purchased from Sigma-Aldrich (St Louis, MO, USA). The Ludox CL is a positively charged silica particle whose surface is coated with a layer of aluminium [138]. The hydrodynamic diameter of the Ludox CL is from approximately 40 nm at below pH 6 to 233 nm at pH 10 due to aggregation effects in different pH solutions [138].

2.3 Tertiary treated effluent

Tertiary treated effluent sample was collected from an advanced water recycling plant in New South Wales, Australia. The treatment train of the plant prior to the sampling point includes screening, bioreactor and sand filtration, and the sample was collected after sand filtration.

2.4 Membrane filtration system

A bench-scale cross flow membrane filtration system was used (Figure 3.1). Specification of the bench-scale filtration system is described in Chapter 3, Section 4.1.

2.5 Experimental protocols

Rejection measurement and membrane fouling development were sequentially carried out with four steps: (1) compaction; (2) measuring N-nitrosamine rejection without membrane fouling; (3) fouling development; and (4) remeasuring N-nitrosamine

rejection by fouled membrane (Figure 5.1). Because full-scale RO plants are generally operated with a constant (average) permeate flux which is approximately 20 L/m²h [122] and feed pressure increases as fouling progresses to maintain the permeate flux, the constant permeate flux of 20 L/m²h was used to evaluate N-nitrosamine rejection before and after fouling. Throughout the experiments, cross flow velocity and feed temperature in the reservoir were always kept constant at 0.42 m/s and 20 ± 0.1 °C, respectively. The details of these four steps are as follows.

Step 1: The membrane sample was first compacted using Milli-Q water at 1,800 kPa until the permeate flux was stabilised.

Step 2: Following the compaction step, the Milli-Q water in the filtration system was replaced with either the tertiary effluent or synthetic solution containing a particular model foulant (e.g. SA, HA, BSA or Ludox CL) and background electrolytes (20 mM NaCl, 1 mM CaCl₂ and 1 mM NaHCO₃). The concentrations of SA, BSA and HA in the feed solution were adjusted to make up approximately 10 mg/L as total organic carbon (TOC). The Ludox CL was suspended in the same background electrolyte solution (20 mM NaCl, 1 mM CaCl₂ and 1 mM NaHCO₃) to obtain 100 mg/L of colloidal silica. After the replacement of feed solutions, stock N-nitrosamine solution was spiked into the feed solution at environmentally relevant concentration (i.e., 250 ng/L). The permeate flux was also adjusted at 20 L/m²h which is a typical value for most water reclamation RO plants [122]. The system was operated for 1 h prior to the collection of the feed and permeate samples for analysis. This sampling point represents the performance of the membrane under a clean condition.

Step 3: After the first sampling event, membrane fouling was promoted by adjusting the permeate flux to 60 L/m²h. The system was then continuously operated with a constant feed pressure. The fouling development step ended after the permeate flux reached 45 L/m²h (i.e., decreased by 25%).

Step 4: The permeate flux was adjusted to 20 L/m²h and the system was stabilised for 1 h prior to the second sampling of the feed and permeate. This sampling point represents the performance of the membrane under a fouled condition.

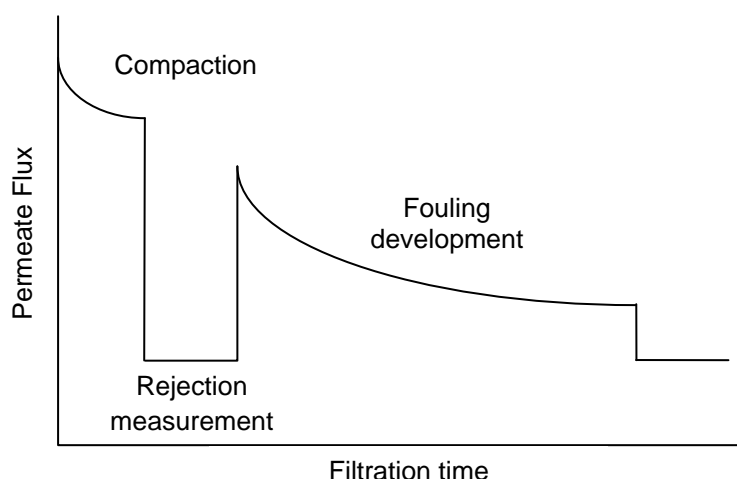


Figure 5.1: Fouling development procedure and N-nitrosamine rejection measurement.

2.6 Analytical techniques

2.6.1 Size exclusion chromatography analyses

Characterisation of dissolved organic carbon (DOC) composition in the tertiary effluent and model foulant solution samples was carried out with a size exclusion chromatography technique using a Liquid Chromatography - Organic Carbon Detection (LC-OCD) Model 8 system (DOC-LABOR, Karlsruhe, Germany). The LC-OCD system is equipped with a UV-detector (254 nm) as well as organic carbon and nitrogen detectors. Chromatographic separation is undertaken using a Toyopearl® TSK HW-50S column (Tosoh Bioscience, Tokyo, Japan). Prior to the analysis, calibration of humic substance molecular weights was conducted using IHSS Humic acid and IHSS Fulvic acid. Calibrations of detectors for total organic carbon and total organic nitrogen were also conducted using potassium hydrogen phthalate and potassium nitrate, respectively. For the analysis, a mobile phase (phosphate buffer, pH 6.37, 2.5 g/L KH_2PO_4 and 1.5g/L $\text{Na}_2\text{HPO}_4 \cdot \text{H}_2\text{O}$) was set at a flow rate of 1.1 mL/min. In the LC-OCD system, an injected sample of 1 mL was pre-filtered with an in-line 0.45 μm PES-filter located in front of the column and detectors. Software provided by the manufacturer (ChromCALC, DOC-LABOR, Karlsruhe, Germany) was used for the quantification of the organic matter compositions. Further details can also be found in previous studies [139, 140].

2.6.2 *N-nitrosamine concentration analysis*

N-nitrosamine concentrations were analysed using an analytical method described in Chapter 3, Section 5.1.

2.6.3 *Basic analytical techniques*

Basic analytical techniques are described in Chapter 3, Section 5.2.

2.6.4 *Contact angle measurement*

Details of contact angle analysis are described in Chapter 3, Section 6.1.

2.6.5 *Zeta potential measurement*

Details of zeta potential analysis are described in Chapter 3, Section 6.2.

3 *Results and discussion*

3.1 *Characteristics of the tertiary effluent and model foulants*

Ionic composition and organic content of the tertiary effluent used in this study (Table 5.1) was similar to that of most water reclamation plants. Nevertheless, the conductivity of this tertiary treated effluent (Table 5.1) was slightly lower than the typical range of 1200-1700 $\mu\text{S}/\text{cm}$, which is often found in the literature [31, 113]. The tertiary effluent used in this study had not been subjected to chloramination, and all other N-nitrosamines, with the exception of NMOR, were not detectable in the tertiary effluent sample. The concentration of NMOR in this tertiary effluent was 1350 ng/L. NMOR can be found in toiletry and cosmetic products [39] and rubber and tire industry, and elevated NMOR concentration of NMOR in treated effluent has previously been reported [7]. The water recycling plant where the tertiary treated effluent was collected is known to have a very high load of industrial wastewaters in its catchment.

Table 5.1: Water quality of the tertiary effluent.

Parameter	Value
Turbidity	0.7 NTU
Conductivity	790 $\mu\text{S}/\text{cm}$
pH	7.8
TOC	9.3 mg/L
Na^+	106 mg/L
Mg^{2+}	14 mg/L
K^+	17 mg/L
Ca^{2+}	23 mg/L
Fe^{2+}	13 mg/L
Cl^-	177 mg/L
NO_3^-	43 mg/L
SO_4^{2-}	46 mg/L

The organic contents of secondary effluents have been generally characterised to comprise a number of size fractions commonly referred to as biopolymers (polysaccharides, proteins and colloidal organics) ($>>20,000$ Da), humic substances (approximately 1000 Da), building blocks (300-500 Da) and low molecular weight (LMW) acids (<350 Da) and neutrals (<350 Da) [139-142]. The building blocks block fraction represents breakdown products, or intermediates during the degradation, of humic substances such as fulvic acid [140, 143]. The tertiary effluent used in this study has a diverse molecular weight distribution (Figure 5.2). The DOC concentration of fractions of biopolymers (10%), humic substances (46%), building blocks (17%) and LMW neutrals (23%) in the tertiary effluent (Table 5.2) was in good agreement with a previous study carried out by Henderson et al. [141]. Model foulants used in this investigation had significant differences in their physicochemical characteristics which were expected to assist in identifying the impact of fouling on membrane separation performance. The major fraction of SA and BSA solutions was biopolymers (>20000 g/mol), which is consistent with a previous study [144] showing a molecular weight of 12000-80000 g/mol (SA) and 67000 g/mol (BSA). The molecular weight of HA analysed here was in the range of approximately 1000 g/mol and this is in good agreement of the average molecular weight of HA (1000 g/mol) reported in the literature [140]. All three organic model foulant also contained some fraction of building blocks (300-500 g/mol) and LMW neutrals (<350 g/mol) (Table 5.2).

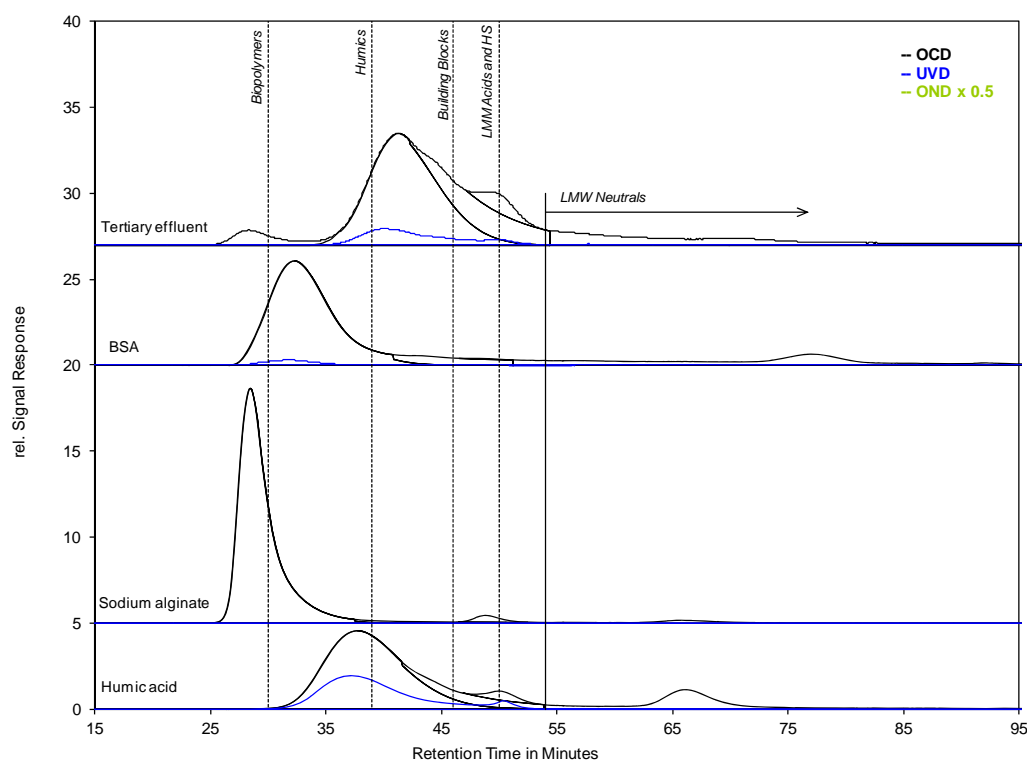


Figure 5.2: LC-OCD chromatograms of tertiary effluent, SA, BSA and HA solutions. OCD and UVD represent organic carbon detection and UV-detection at 254 nm, respectively.

Table 5.2: Organic matter fractions in each feed solution.

	Tertiary effluent	BSA	Sodium alginate	Humic acid
Hydrophobic [%]	11.1	n.q.	2.0	0.4
Hydrophilic				
Biopolymer [%]	9.8	79.5	91.1	5.6
Humics [%]	50.8	n.q.	n.q.	68.4
(Mean MW [g/mol])	(467)			(850)
Building blocks [%]	15.1	8.1	2.2	9.2
LMW neutrals [%]	12.6	22.4	2.6	16.4
LMW acid [%]	0.6	0.2	2.1	n.q.

*n.q., not quantifiable

3.2 Membrane fouling behaviour

Significant membrane fouling was observed with all three membranes investigated in this study when tertiary effluent was used at the elevated initial permeate flux of 60 L/m²h (which is approximately three times the value used in most full scale RO systems

for water recycling applications). The profile of membrane permeability measured before and after fouling is presented in Table 5.3. Membrane fouling behaviour of the NF90 differs significantly from that of the ESPA2 and ESPAB membranes (Figure 5.3). Flux decline was most severe for the NF90 membrane followed by the ESPA2 and ESPAB membranes. The permeate flux of the NF90 membrane dropped by 30% within the first 12 h system operation, and then decreased linearly as filtration progressed. In contrast, the two RO membranes (ESPAB and ESPA2) showed an almost linear flux decline from the beginning of the filtration. The flux decline of the ESPA2 and ESPAB membranes using tertiary effluent reached 30% with 40-50 h and 60 h filtration, respectively. Interestingly, the rate of flux decline amongst the three membranes increased in the order of increasing pure water membrane permeability (Table 3.1). Similar observations were reported in previous laboratory-scale studies [114, 145].

Table 5.3: Membrane permeability by the clean and fouled membranes.

Membrane	Feed solution		Clean [Lm ² h ⁻¹ bar ⁻¹ at 20°C]	Fouled [Lm ² h ⁻¹ bar ⁻¹ at 20°C]
NF90	Tertiary effluent		11.1	5.7
ESPAB	Tertiary effluent		3.3	2.7
ESPA2	Tertiary effluent	1st	4.9	3.6
		2nd	5.0	3.5
	Sodium alginate	1st	4.5	2.6
		2nd	4.6	3.0
	Humic acid	1st	5.0	2.9
		2nd	5.0	3.6
	BSA	1st	4.7	4.0
		2nd	4.7	3.7
	Ludox CL	1st	4.9	3.5
		2nd	4.7	3.3

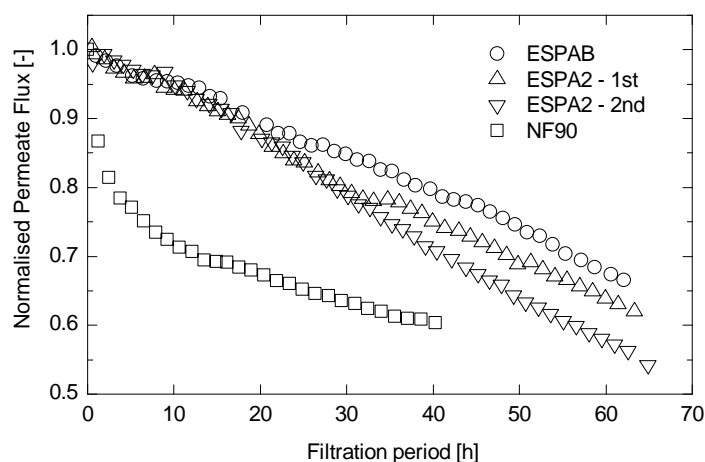


Figure 5.3: Normalised permeate flux of the ESPAB, ESPA2 and NF90 membranes as a function of filtration time using the tertiary effluent (crossflow velocity 40.2 cm/s, feed temperature 20.0 ± 0.1 °C).

When the model foulants were used, significant variation in membrane fouling was observed. When the ESPA2 membrane was fouled with either SA or HA, permeate flux dropped rapidly within 10–20 h of system operation (Figure 5.4a-b). These observed curves of membrane fouling are consistent with a previous study [146]. The rapid flux decline in the early stage may have resulted from the formation of an alginate and humic acid fouling layer on the membrane surface, resulting in a substantial resistance to permeate flow [114, 147]. In fact, it is known that the HA foulant layer can account for a cake layer as thick as 4 μm [148], while a skin layer thickness of RO membrane is usually less than 0.3 μm [107]. In contrast, membrane fouling by BSA used here progressed slowly and linearly until 30 h system operation, and then the slope of the permeate flux decline became steeper (Figure 5.4c). This trend of the permeate flux decline is again in good agreement with a previous study [144]. Permeate flux with Ludox CL dropped significantly within 5 h of system operation, then gradually decreased as filtration progressed (Figure 5.4d). This observation is consistent with a previous laboratory-study from which it was suggested that the hydrophobic interactions and electrostatic attraction forces between charged colloid particles and membrane surface were key causes for colloidal membrane fouling in the early filtration stage [138].

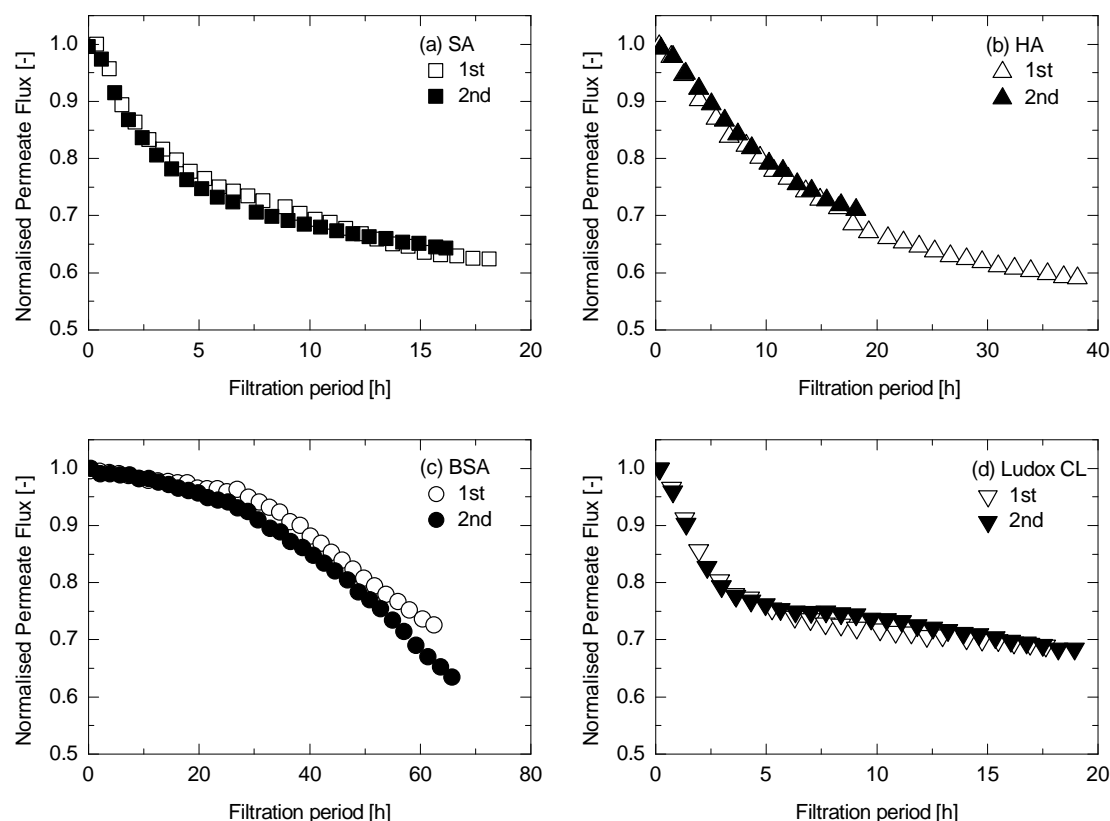


Figure 5.4: Normalised permeate flux of the ESPA2 membrane as a function of filtration time using (a) SA, (b) HA, (c) BSA and (d) Ludox CL (20 mM NaCl, 1 mM NaHCO₃, 1 mM CaCl₂, cross flow velocity 40.2 cm/s, feed pH 8.0 ± 0.1 , feed temperature 20.0 ± 0.1 °C). Open and solid symbol indicates the result of the first and second experiment, respectively.

3.3 Characteristics of fouled membranes

The membrane surface hydrophobicity (measured by contact angle) increased significantly when the NF/RO membranes were fouled by tertiary effluent (Figure 5.5). The contact angle of the ESPA2 membrane increased from 43 to 79° due to the membrane fouling. While the three virgin membranes (NF90, ESPA2 and ESPAB) have a wide range of contact angle values (43-69°), the fouled membrane surface revealed a very similar contact angle (in the range of 66-79°). The type of foulants can also have a major impact on the hydrophobicity of membranes. The hydrophobicity of ESPA2 membranes increased as a result of membrane fouling by SA, HA and BSA, whereas a considerable reduction in hydrophobicity was observed with Ludox CL (Figure 5.5). The contact angle of each fouled membrane analysed here was in good agreement with

results reported by Beyer et al. [146] who also investigated the hydrophobicity of fouled membranes by various model foulants using the NF270 membrane. Results reported here suggest that the hydrophobicity of the fouled membrane surface depends mainly on the hydrophobicity of the foulants.

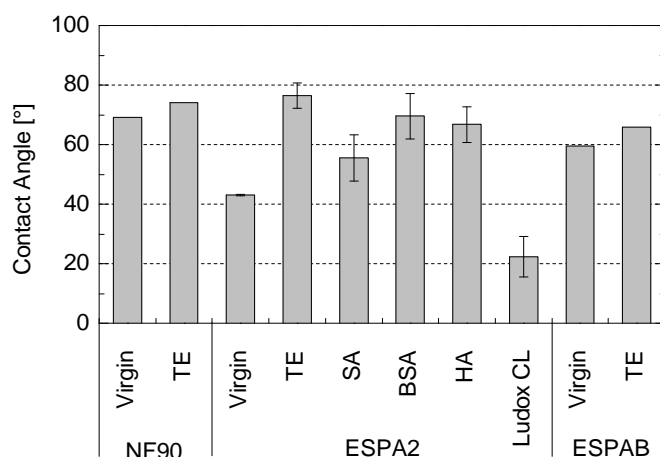


Figure 5.5: Effects of membrane fouling by tertiary effluent (TE) and model foulants (SA, BSA, HA and Ludox CL) on contact angle of the NF90, ESPA2 and ESPAB membranes. Error bars show the standard deviation of two replicate experiments.

The impact of fouling on the membrane surface charge was also examined by analysing zeta potentials of clean and fouled ESPA2 membranes. Consistent with a previous study [148], the zeta potential of the fouled membranes became less negative at high pH (i.e., pH8) and less positive at low pH (Figure 5.6). Amongst the model foulants, the zeta potential of BSA was similar to tertiary effluent at all pH values tested. Although organic matter eluting in tertiary effluent has a high concentration of material with similar molecular size to humic substances (Table 5.2), the measured zeta potential of fouled membranes by the tertiary effluent and HA were distinctly different (Figure 5.6). These results suggest that the material of the tertiary effluent eluting in the humic substance fraction is similar to humic acid and fulvic acid standards in terms of molecular size but has different charge characteristics. It is noted that the zeta potential analysis of the SA fouled membrane was not conducted because of the re-formation of alginate gel which clogged of the flow through cell of the Electrokinetic Analyser.

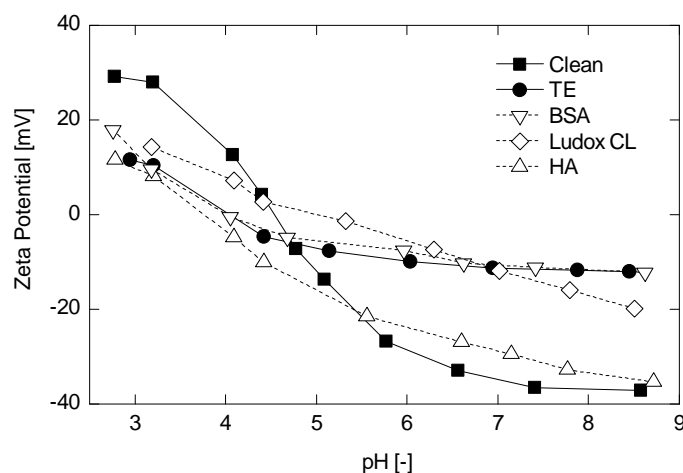


Figure 5.6: Effects of membrane fouling by tertiary effluent (TE) and model foulants (BSA, HA and Ludox CL) on zeta potential of the ESPA2 membrane. The measurement was conducted in 1mM KCl at $25\pm 1^\circ\text{C}$.

3.4 Effects of membrane fouling on inorganic salt retention

Membrane fouling by tertiary effluent led to an increase in conductivity (salt) rejection for all membranes with an exception of Ludox CL used in this investigation (Figure 5.7). In particular, conductivity rejection by the NF90 membrane increased significantly from 87 to 95%. Similarly, when the ESPA2 membrane was fouled by organic model foulants (SA, HA and BSA), conductivity rejection also increased. Because the fouling layer and skin layer surfaces of the RO membranes were negatively charged at pH 8 (Figure 5.6), the conductivity rejection increase may be attributed to an additional repelling force occurring between the fouling layer and salts. Tang et al. [145] investigated the impact of humic acid fouling using several NF/RO membranes and suggested that an increase in conductivity rejection with humic acid fouling may be attributed to an increase in repelling force between Cl^- anions and the cake layer where negatively charged humic acid is deposited (Donnan exclusion mechanism). In addition to the additional repelling force, conductivity rejection can increase when the pathways of the solute such as membrane pore (or so-called free-volume space in polymer chain [94]) and the local defects of the active skin layer are restricted with foulants. Tu et al. [149] reported a considerable increase in boron rejection when organic fouling occurred, and they suggested that the increase in boron rejection was due to the plugging of local defects or hot spots on the membrane active skin layer. In the present work, low

molecular weight organic foulants present in the tertiary effluent may have narrowed down the pores within the active skin layer and/or blocked the local defects on the active skin layer surface. This additional restriction of the solute pathway may explain why the increase in conductivity rejection observed using tertiary effluent was higher than that using BSA despite their similar zeta potential of fouled membrane surface. On the other hand, the results reported here also revealed a reduction in conductivity rejection with Ludox CL fouling. Colloidal cake fouling layer depositing on membrane surface hinders back diffusion of rejected salt from the membrane surface to bulk solution, and the higher concentration gradient across the membrane is likely to result in a decrease in salt rejection (cake enhanced concentration polarisation) [115, 144]. Because the fouled membrane by colloids remarkably decreased salt rejection from 96.3% to 94.9%, the cake enhanced concentration polarisation may have played an important role in salt rejection using the fouled membrane.

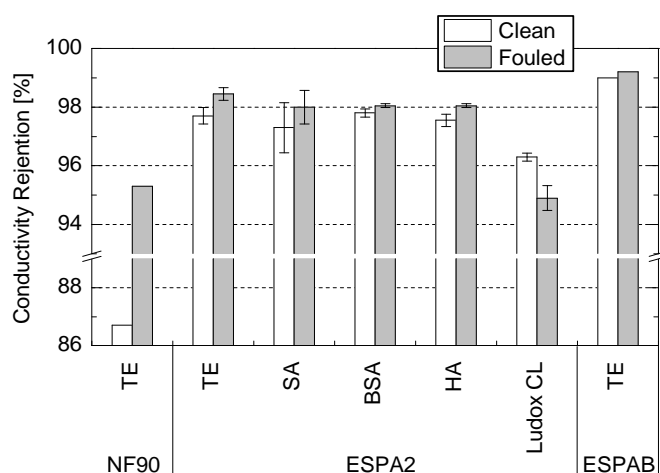


Figure 5.7: Conductivity rejection of the clean and fouled membranes (Permeate flux 20 L/m²h, crossflow velocity 40.2 cm/s, feed temperature 20.0 ± 0.1 °C). Error bars show the standard deviation of two replicate experiments.

3.5 Effects of membrane fouling on N-nitrosamine rejection

The rejection of small organic compounds by NF/RO membranes can be governed by steric hindrance, electrostatic interactions and adsorption onto the membrane surface [3]. All N-nitrosamines used are hydrophilic and uncharged at neutral pH, thus the electrostatic interactions and adsorption effects do not play a major role on their rejection performances. Previous studies also reported that N-nitrosamine rejection by

NF/RO membranes in clean water matrices reached a steady state condition within a 45 min filtration period [38, 82]. Preliminary experimental results (Figure 5.8) revealed no significant changes in the rejection of N-nitrosamines with the exception of NDEA after 1 and 48 h of filtration even in tertiary effluent feed. These results indicate that 1 h filtration is sufficient to evaluate the rejection of most N-nitrosamines in tertiary effluent. During the preliminary experiment, the concentration of some N-nitrosamines (i.e, NDMA, NMEA and NDBA) in the feed decreased as the filtration progressed. These N-nitrosamines have been reported to be readily biodegradable [29], and the reduction in these N-nitrosamines was possibly caused by biodegradation. Fujioka et al. [150] investigated the impact of N-nitrosamine feed concentration on their rejection using a RO membrane (TFC-HR) and reported their negligible impacts in the range from 0.25 to 1.5 $\mu\text{g/L}$ of each N-nitrosamine concentration. Thus, the changes in N-nitrosamine feed concentration are unlikely to play an important role in the evaluation of N-nitrosamine rejections.

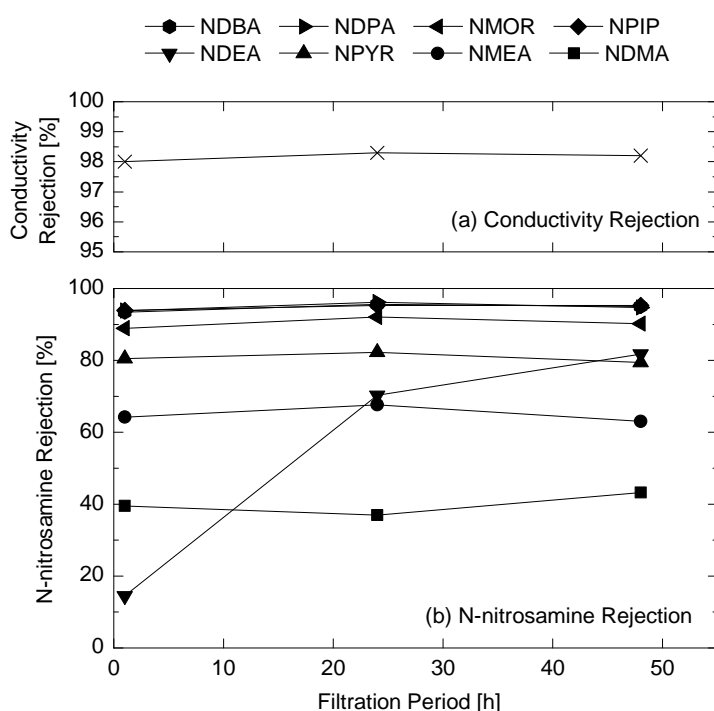


Figure 5.8: (a) Conductivity rejection and (b) N-nitrosamine rejection by the ESPA2 membrane as a function of filtration period (permeate flux 20 $\text{L/m}^2\text{h}$, cross flow velocity 40.2 cm/s , feed temperature 20.0 ± 0.1 $^\circ\text{C}$).

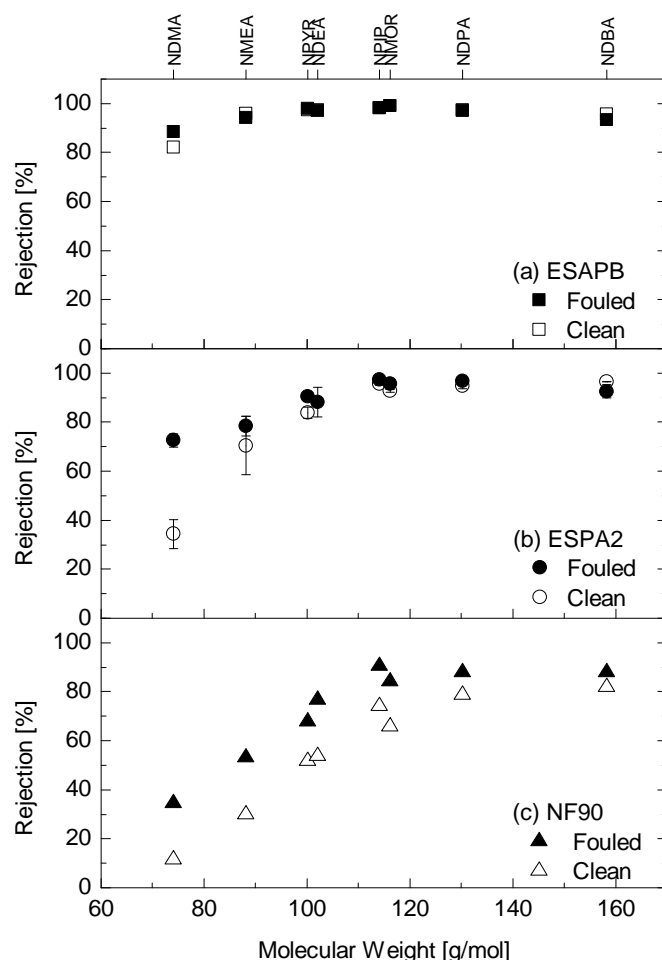


Figure 5.9: Effects of membrane fouling using tertiary effluent on the rejection of N-nitrosamines by (a) ESPAB, (b) ESPA2 and (c) NF90 membranes (permeate flux 20 L/m²h, cross flow velocity 40.2 cm/s, feed temperature 20.0 ± 0.1 °C). Error bars on the ESPA2 membranes show the standard deviation of two replicate experiments. N-nitrosamine concentrations (except NDMA and NMOR) in the permeate of the ESPAB membrane were all below detection limits.

In general, membrane fouling by tertiary effluent caused an increase in N-nitrosamine rejection (Figure 5.9). This was particularly apparent for low molecular weight N-nitrosamines such as NDMA. For example, the rejection of NDMA by the NF90 and ESPA2 membranes increased in the range from 11 to 34% and from 34 to 73%, respectively. In contrast, membrane fouling on the ESPAB membrane resulted in only a slight increase (from 82 to 88%) in NDMA rejection. The results reported here also indicate that the ESPAB membrane is very effective for the removal of N-nitrosamines regardless of membrane fouling. As expected, during these filtration tests the

concentrations of NDMA, NMEA and NDBA in the feed (i.e., tertiary effluent) decreased by up to 82%. The impact of SA fouling was minor, but nevertheless discernible for low molecular weight N-nitrosamines such as NDMA (Figure 5.10). On the other hand, membrane fouling of HA, BSA and Ludox CL had a negligible impact on the rejection of N-nitrosamines.

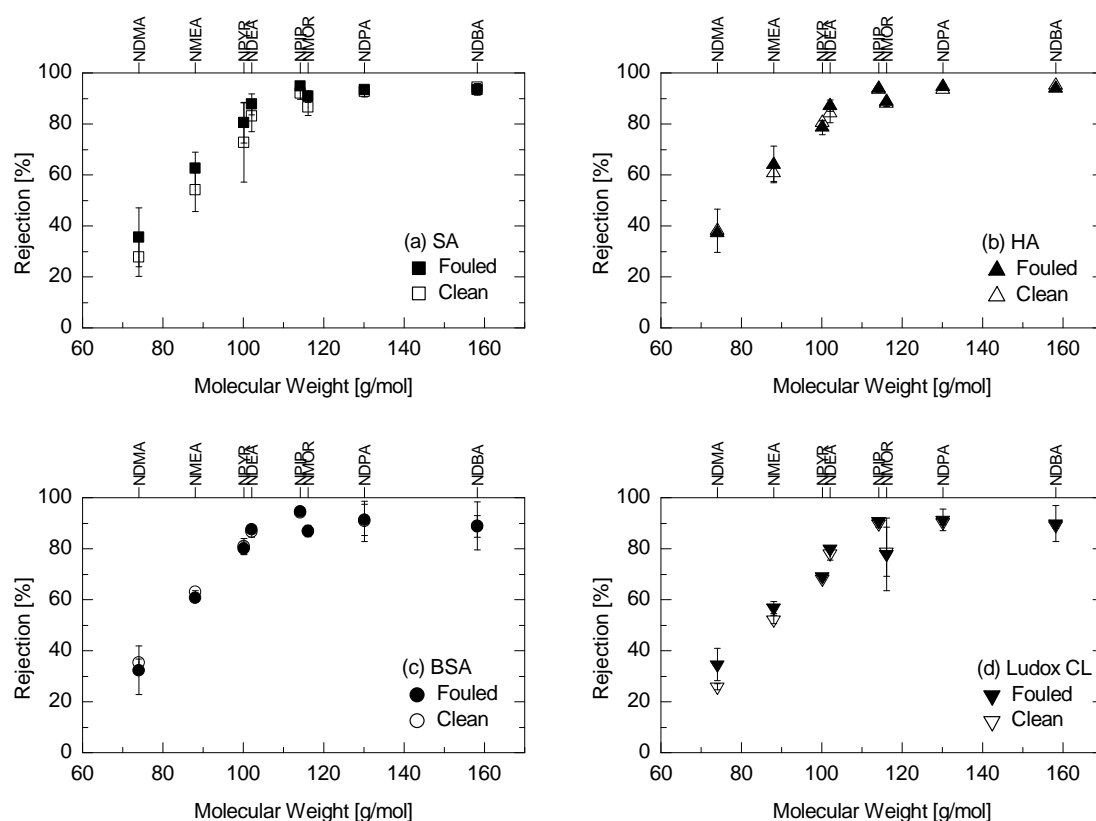


Figure 5.10: N-nitrosamine rejections by the ESPA2 membrane with and without fouling of (a) SA, (b) HA, (c) BSA and (d) Ludox CL. (20 mM NaCl, 1 mM NaHCO₃, 1 mM CaCl₂, permeate flux 20 L/m²h, cross flow velocity 40.2 cm/s, feed pH 8.0 ± 0.1, feed temperature 20.0 ± 0.1 °C). Error bars show the standard deviation of two replicate experiments.

The clear difference in the impact of membrane fouling observed between tertiary effluent (Figure 5.9) and model foulants (Figure 5.10) is intriguing. For the separation mechanism of N-nitrosamines, the rejection of N-nitrosamines by NF/RO membranes has been reported to be mainly governed by steric hindrance where the interaction between N-nitrosamine molecule size and pore size of the active skin layer plays an

important role in their rejection [150]. Because the molecular size of N-nitrosamines does not change under the experimental conditions, the increased rejection of some N-nitrosamines using the tertiary effluent is likely to be attributed to changes in membrane characteristics. As described in Section 3.4, it can be suggested that the pathway of solutes (such as membrane pore and local defects of the active skin layer) on RO membranes can be restricted with foulants present in the tertiary effluent, and these changes in the solute pathway leads to an increase of N-nitrosamine rejection.

4 Conclusions

Membrane fouling by tertiary effluent and organic model foulants (i.e., sodium alginate, bovine serum albumin and humic acid) led to an increase in conductivity rejection due to enhanced electrostatic interactions between the fouling layer and inorganic salts. On the other hand, colloidal fouling using Ludox CL caused a reduction in conductivity rejection. Membrane fouling by tertiary effluent also increased the rejection of N-nitrosamines. The rejection of low molecular weight N-nitrosamines such as NDMA was most affected by membrane fouling and the impact was most pronounced for membranes that have high membrane permeability. Although the ESPA2 and ESPAB membranes were comparable in terms of membrane permeability and fouling susceptibility the rejection of N-nitrosamines by the ESPAB membrane was very high (over 82%) regardless the impact of membrane fouling. In contrast to the results using tertiary effluent, membrane fouling by model foulants revealed only a negligible impact on N-nitrosamine rejection. Because the tertiary effluent used in this investigation contained a high fraction of low molecular weight organic substances, these foulants may have restricted the pathway of solutes on the active skin layer of the RO membrane, resulting in an increase in N-nitrosamine rejection. The present findings provide valuable insights for predicting NDMA rejection variations observed during full-scale RO plant operation. In addition, the results reported here indicate that changes in NDMA rejection may be predicted by analysing conductivity rejection because both rejections increased as fouling progressed.

Chapter 6

Membrane exposure to chemical cleaning reagents

This chapter has been published as:

T. Fujioka, S.J. Khan, J.A. McDonald, A. Roux, Y. Poussade, J.E. Drewes, L.D. Nghiem, *N-nitrosamine rejection by RO: Effects of exposing the membrane to chemical cleaning reagents, Desalination, 343 (2014) 60-66.*

1 Introduction

In addition to feed solution characteristics and operating conditions, the separation performance of RO membranes may also be affected by the alteration of membrane surface characteristics particularly caused by chemical cleaning. Because membrane fouling is an inherent phenomenon in almost all pressure driven membrane processes, chemical cleaning is inevitable. Typical cleaning chemicals include sodium hydroxide (NaOH) citric acid (CA), hydrochloric acid (HCl) and ethylenediaminetetraacetic acid (EDTA) [151, 152]. Although chemical cleaning can frequently restore the performance of RO membranes exposed to wastewater foulants [127, 153], these chemicals may also modify polyamide membrane structures, resulting in an increase in permeability or decrease in salt rejection [151]. Simon et al. [121] recently investigated the effects of chemical cleaning by exposing a NF270 nanofiltration membrane to several cleaning reagents (i.e., NaOH, CA, sodium dodecyl sulphate (SDS) and EDTA) and reported that these chemical cleaning agents (with the exception of CA) increased membrane permeability by up to 30%. Simon et al. [121] reported that the rejection of neutral solutes was more significantly affected by chemical cleaning than that of charged compounds. When the NF270 membrane was exposed to NaOH solution (pH 12), its permeability increased by 30% and the rejection of carbamazepine (molecular weight 253.3 g/mol) decreased from 80 to 50%. From the previous literature mentioned above, periodical chemical cleaning can potentially lead to a decrease in the rejection of N-nitrosamines including NDMA in full-scale RO installations, causing unexpected

deterioration and variation in their rejection. Nevertheless, to date, the impact of chemical cleaning on the rejection of N-nitrosamines by RO membranes has not fully understood.

The aim of this study was to provide a comprehensive understanding of the effects of chemical cleaning on the rejection of N-nitrosamines by RO membranes. The cleaning agents used in this investigation include three general cleaning chemical solutions (NaOH, HCl, CA) and three proprietary cleaning solutions. The impact of chemical cleaning was elucidated by examining the membrane pure water permeability, surface charge through zeta potential measurements, and separation performances of salts and select organic solutes.

2 *Materials and methods*

2.1 RO membranes

Two low pressure RO membranes – namely TFC-HR (Koch Membrane Systems, San Diego, CA, USA) and ESPA2 (Hydranautics, Oceanside, CA, USA) – were used in this study. Properties of these membranes are summarized in Table 3.1 (Chapter 3).

2.2 Chemicals

Properties of eight N-nitrosamines are summarized in Table 3.2 (Chapter 3).

Six chemical cleaning agents were used in this investigation (Table 6.1). Analytical grade NaOH, HCl and CA from Ajax Finechem (Taren Point, NSW, Australia) were used as cleaning reagents based on recommendations from the membrane manufacturers (Table 6.2). The cleaning solution was prepared by dissolving the reagent in Milli-Q water. Three proprietary formulations designed for membrane cleaning in full-scale RO plants were also used. They are referred to as MC3, MC11 and PC98. Flocclean[®] MC3 is an acidic based while Flocclean[®] MC11 and PermaClean[®] PC98 are caustic based chemical cleaning formulations. MC3 and MC11 were supplied in powder form and the cleaning solution was prepared at 25 g/L as recommended by the manufacturer. PC98 was supplied in liquid form and was prepared at 4% (w/w) as recommended by the manufacturer.

Table 6.1: Properties of the selected cleaning solutions.

Chemical	pH	Chemical formula/ingredients	Abbreviation
Sodium hydroxide	12.0	NaOH	NaOH
Chloridric acid	2.1	HCl	HCl
Citric acid	2.1	C ₆ H ₈ O ₇	CA
Floclean [®] MC3	3.3	Organic acids and chelating agents containing tripolyphosphate (SDP)	MC3
Floclean [®] MC11	11	Detergent builders, pH buffer, chelating agents containing EDTA, SDP and sodium trisodium phosphate	MC11
PermaClean [®] PC98	10.7	Amphoteric surfactant and chelating agents containing EDTA	PC98

Table 6.2: Typical chemical cleaning for RO membrane elements recommended by the membrane manufacturer.

Frequency	3-12 months
Caustic	NaOH (pH = 11.5 and 30 °C) NaOH + SDS (pH = 11.5 and 30 °C) Na-EDTA + sodium tripolyphosphate (pH 10 and 40 °C)
Acid	2% Citric acid (40 °C) HCl (pH = 2.5 and 35 °C)
Cleaning period	1-8 h/stage

* Hydranautics, Foulants and Cleaning Procedures for composite polyamide RO

Membrane Elements (ESPA, ESNA, CPA, LFC, NANO and SWC), Technical Service Bulletin, (2010).

2.3 Membrane filtration system

A bench-scale cross flow membrane filtration system was used (Figure 3.1). Specification of the bench-scale filtration system is described in Chapter 3, Section 4.1.

2.4 Simulated chemical cleaning protocols

Chemical cleaning was simulated by immersing a membrane sample in a glass container containing a cleaning chemical solution. The flat sheet membrane samples were first rinsed with Milli-Q water to remove any preservative materials from the membrane

surface. In addition to these cleaning chemical solutions, Milli-Q water was also used for cleaning to obtain control membrane samples, and these control samples are designated as virgin membrane in this study. The containers were submerged in a temperature-controlled water bath (SWB1, Stuart[®], Staffordshire, UK) and the temperature was maintained at 30 ± 0.5 °C according to the membrane manufacturer's recommendation (Table 6.2). The simulated cleaning was carried out for 25 h. This cleaning simulation over 25 hours corresponds to the cumulative chemical cleaning period of typical three-year operation comprising six months of chemical cleaning frequency and approximately 4 h of each cleaning. After the chemical cleaning procedure, the membrane samples were rinsed with a copious amount of Milli-Q water and stored (in Milli-Q water) at 4 °C in the dark until they were used for further experiments. To evaluate the impact of a two-step cleaning procedure, the membrane sample was first immersed into a NaOH solution for 25 h followed by a CA solution for 25 h. For the evaluation of effects of each cleaning solution, two membrane samples were prepared.

A general chemical cleaning procedure in full-scale RO plants is based on a sequential cycle of the first recirculation of chemical solution, 1-8 h soaking, second recirculation of chemical solution at an elevated temperature (e.g. 30 – 35 °C), rinsing with clean water and flushing with feed water (Table 6.2). Although the first recirculation using chemical solution is effective to remove fouling layer from the membrane surface, the membrane surface might still be partially covered by a fouling layer compromising direct exposure of the top skin layer of the membrane to chemical cleaning solution. Moreover, the effectiveness of chemical cleaning in full-scale RO plants is generally enhanced by higher cross-flow velocities [154]. Despite the difference in the impact of chemical cleaning from full-scale RO plants, the simulated chemical cleaning procedure used in this study enables a systematic investigation for the impact of each chemical cleaning solution on the separation performance of RO membranes. In fact, similar experimental protocols on chemical cleaning were previously reported in the literature [121, 155, 156].

2.5 Filtration experiments

Prior to each filtration experiment, the membrane was compacted at 1,800 kPa using Milli-Q as the feed until the permeate flux stabilised. Following the compaction stage, the permeability of each membrane sample was measured at feed pressure of 1,000 kPa. The Milli-Q water in the feed was then conditioned at 20 mM NaCl, 1 mM CaCl₂ and 1 mM NaHCO₃ to simulate the background electrolyte composition typically found in secondary or tertiary treated effluent. The stock solution of N-nitrosamines was also spiked into the feed to make up 250 ng/L of each target compound. The permeate flux was then adjusted to 20 L/m²h, and the system was operated for at the least 2 h before the first samples of the feed and permeate were taken for analysis. A previous study revealed no significant changes in the rejection of almost all N-nitrosamines after 1 h filtration [150]. The cross flow velocity and feed temperature during tests were kept at 0.42 m/s and 20±0.1°C, respectively.

2.6 Analytical methods

2.6.1 *N-nitrosamine analytical technique*

N-nitrosamine concentrations were analysed using an analytical method described in Chapter 3, Section 5.1.

2.6.2 *Zeta potential measurement*

Details of zeta potential analysis are described in Chapter 3, Section 6.2.

2.6.3 *Surface chemistry*

Functional groups of RO membranes were analysed obtaining fourier transform infrared spectroscopy (FTIR) spectra described in Chapter 3, Section 6.3.

3 Results and discussion

3.1 Effects of membrane cleaning on membrane characteristics

Caustic chemical cleaning caused a significant increase in membrane permeability for both the TFC-HR and ESPA2 membranes (Figure 6.1). In comparison to caustic cleaning, the impact of acidic chemical cleaning on the membrane permeability was

much less discernible (Figure 6.1). Changes in the membrane permeability could occur via several mechanisms. A previous study by Kim et al. [157] suggested that under extreme conditions, the polyamide active skin layer can be hydrolysed to carboxylic acid derivatives, resulting in an increase in water permeability and surface hydrophilicity. Both acidic and caustic cleaning resulted in some variation in the membrane hydrophilicity and impact was specific to each membrane and the individual cleaning reagent (Figure 6.2). There was no evidence to suggest that the membrane was hydrolysed under the experimental conditions of this study. The increase in permeability can also be attributed to some extent to adsorption of cleaning additives such as chelating reagents and surfactants in the proprietary cleaning formulations on the membrane surface. A previous study by Ang et al. [154] suggested that a small amount of residual chemical reagent (e.g. EDTA) on the membrane surface makes the active skin layer more hydrophilic, leading to more water passage through the membrane. Indeed, the proprietary cleaning formulations MC11 (pH 11) and PC98 (pH 10.7) resulted in a similar increase in permeability of the TFC-HR membrane in comparison to the NaOH (pH 12) solution (Figure 6.1a).

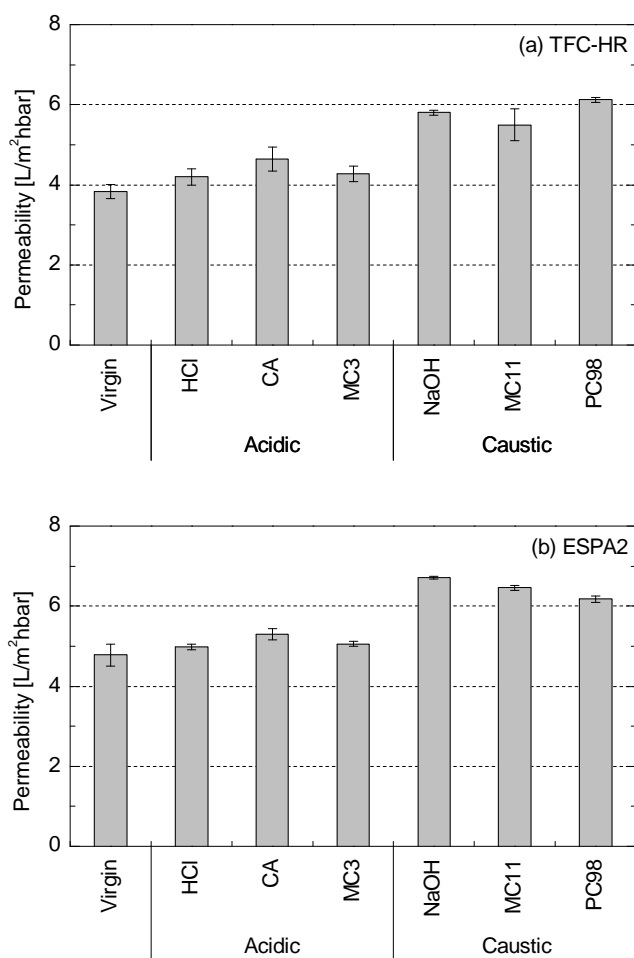


Figure 6.1: Changes in membrane permeability by the (a) TFC-HR and (b) ESPA2 membranes before and after being exposed to chemical solutions for 25 h at 30 °C. Membrane permeability was determined with Milli-Q water at 1,000 kPa and 20 °C feed temperature. Values reported here are the average and ranges of duplicate results.

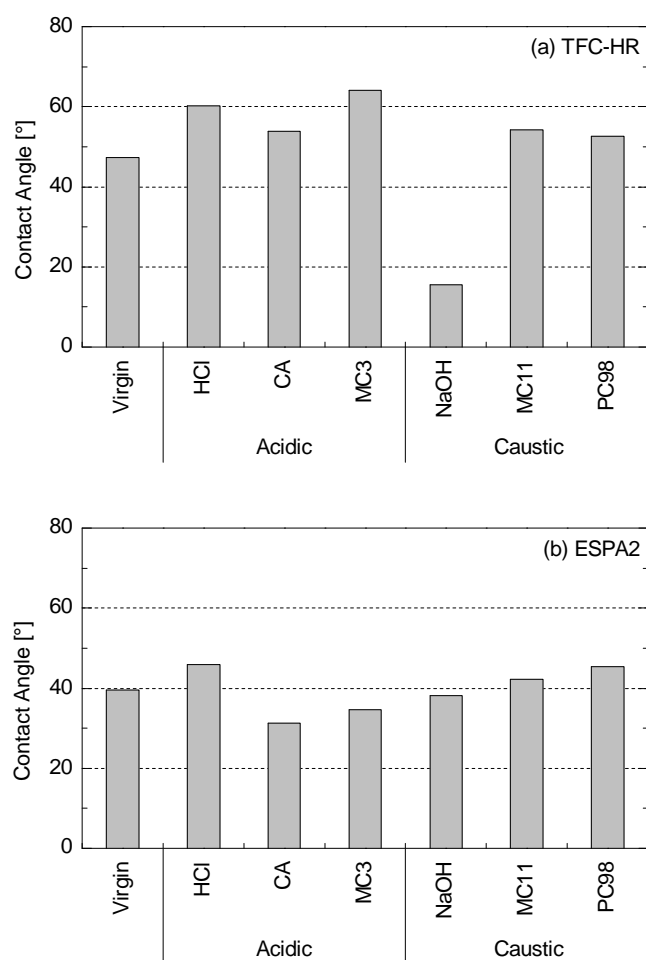


Figure 6.2: Hydrophobicity of the (a) TFC-HR and (b) ESPA2 membranes before and after being exposed to permeability of TFC-HR membrane before and after being exposed to cleaning solutions for 25 hours at 30 °C.

FTIR spectra of the virgin and several cleaned membranes in the range of 1750-750 cm^{-1} revealed the bonding structure of the polyamide active skin layer and the polysulfone supporting layer (Figure 6.3). The polyamide active skin layer exhibit peaks at 1663, 1609 and 1541 cm^{-1} , which represent C-O and C-N stretching and C-C-N deformation vibration (amide I), N-H deformation vibration and C=C ring stretching vibration of aromatic amide, and N-H in-plane bending and N-C stretching vibration of a -CO-NH-group (amide II), respectively [158, 159]. Details of the other peaks associated with polysulfone supporting layer can be found elsewhere [158]. The FTIR spectra exhibited no discernible variations in these peaks (i.e. 1663, 1609 and 1541 cm^{-1}) after exposing the membranes to chemical cleaning reagents (Figure 6.3). These results suggest that

hydrolysis of the polyamide skin layer did not occur and that other mechanisms are responsible for the increase in permeability after caustic chemical cleaning.

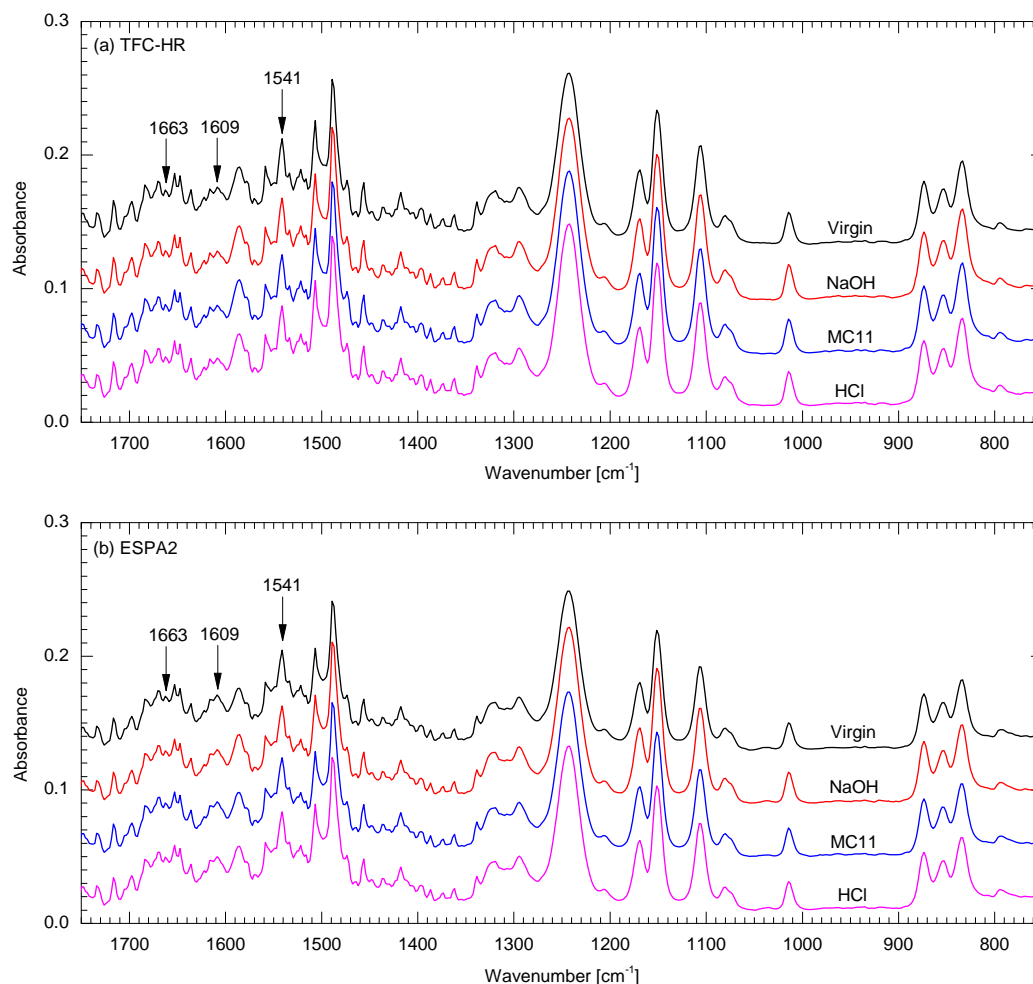


Figure 6.3: FTIR spectra of the (a) TFC-HR and (b) ESPA2 membranes before and after being exposed to the cleaning solutions NaOH, MC11 and HCl for 25 h at 30 °C.

Several previous studies have reported that changes in the membrane charge density can lead to conformational changes in the polymeric matrix due to a reduced electrostatic repulsion amongst charged functional group, which can result in a variation in the membrane pore and thus permeability [100, 160]. In this study, zeta potential of the virgin and chemically cleaned RO membranes was measured to substantiate any impact on permeability that may be caused by the changes in the membrane surface charge. The results reveal that acidic chemical cleaning (i.e., using HCl, CA and MC3 solutions) did not result in any discernible impact on zeta potential of the polyamide RO

membranes (Figure 6.4a and c). Although caustic chemical cleaning (i.e., using NaOH, MC11 and PC98 solutions) could slightly alter the membrane zeta potential (Figure 6.4b and d), such changes did not cause any discernible influence on the membrane permeability (Figure 6.5). Thus, changes in membrane surface charge are not likely to be a cause of changes in membrane permeability.

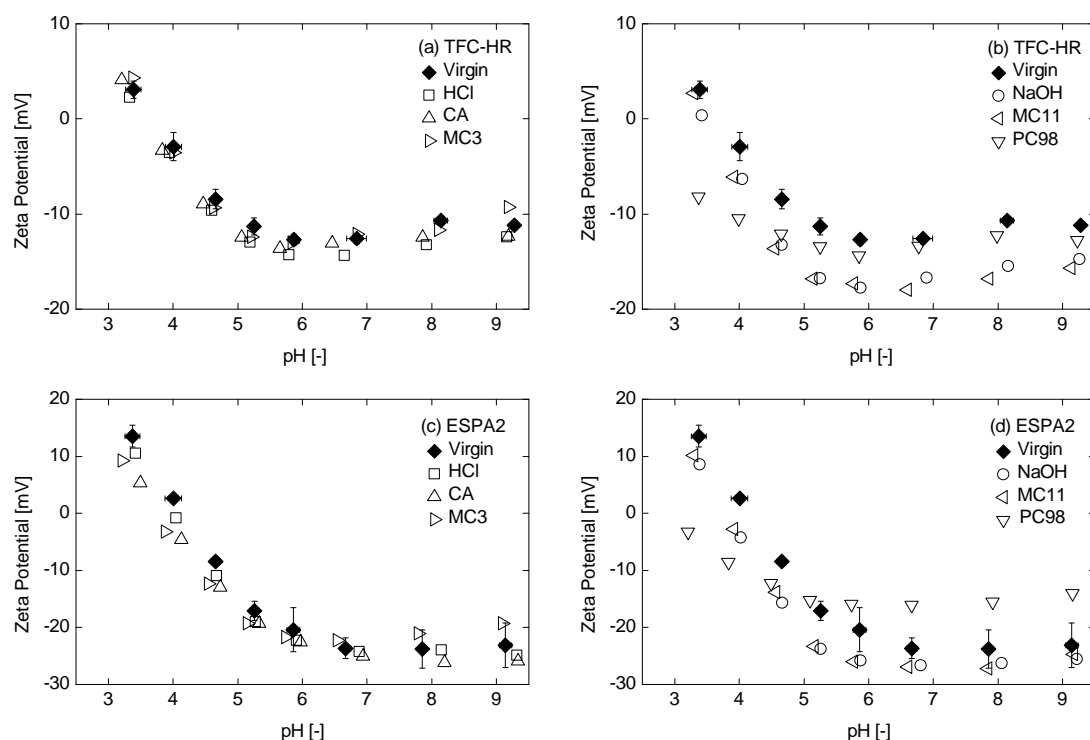


Figure 6.4: Changes in zeta potential of the (a) and (b) TFC-HR, (c) and (d) ESPA2 membranes before and after being exposed to chemical solutions for 25 h at 30 °C. The analysis of zeta potential was carried out in 1 mM KCl solution. Values reported here are the average and ranges of duplicate results.

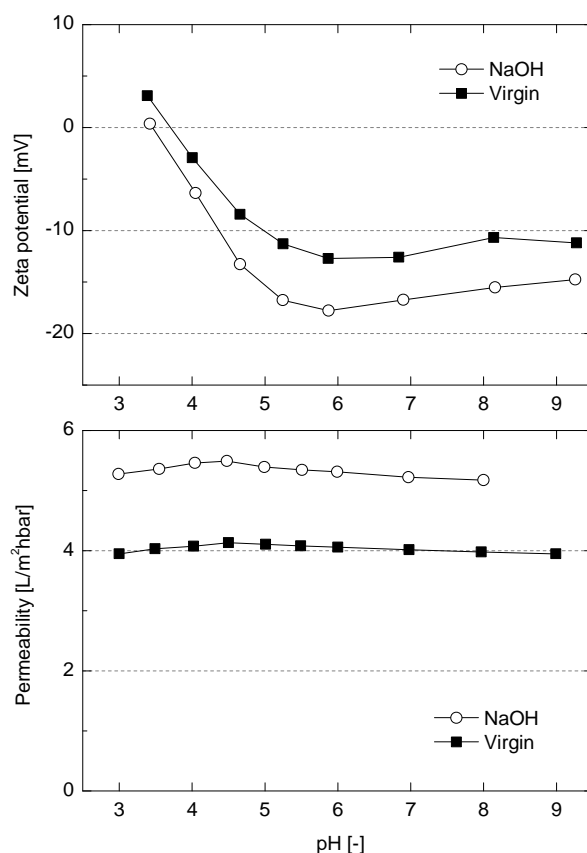


Figure 6.5: (a) Zeta potential and (b) permeability of TFC-HR membrane before and after being exposed to NaOH (pH 12) solution for 25 hours at 30 °C. The analysis of zeta potential was carried out in 1mM KCl solution. Pure water permeability was determined with Milli-Q water at 1,000 kPa and 20°C feed temperature.

3.2 Effects of chemical cleaning on rejection performance of RO membranes

Caustic chemical cleaning resulted in a notable decrease in the rejection of N-nitrosamines by the TFC-HR and ESPA2 membranes while impact of acidic cleaning was not significant (Figure 6.6). The impact of chemical cleaning was more apparent for low molecular weight N-nitrosamines (i.e., NDMA and NMEA). Negligible impact was observed for high molecular weight N-nitrosamines (i.e., NDPA and NDBA).

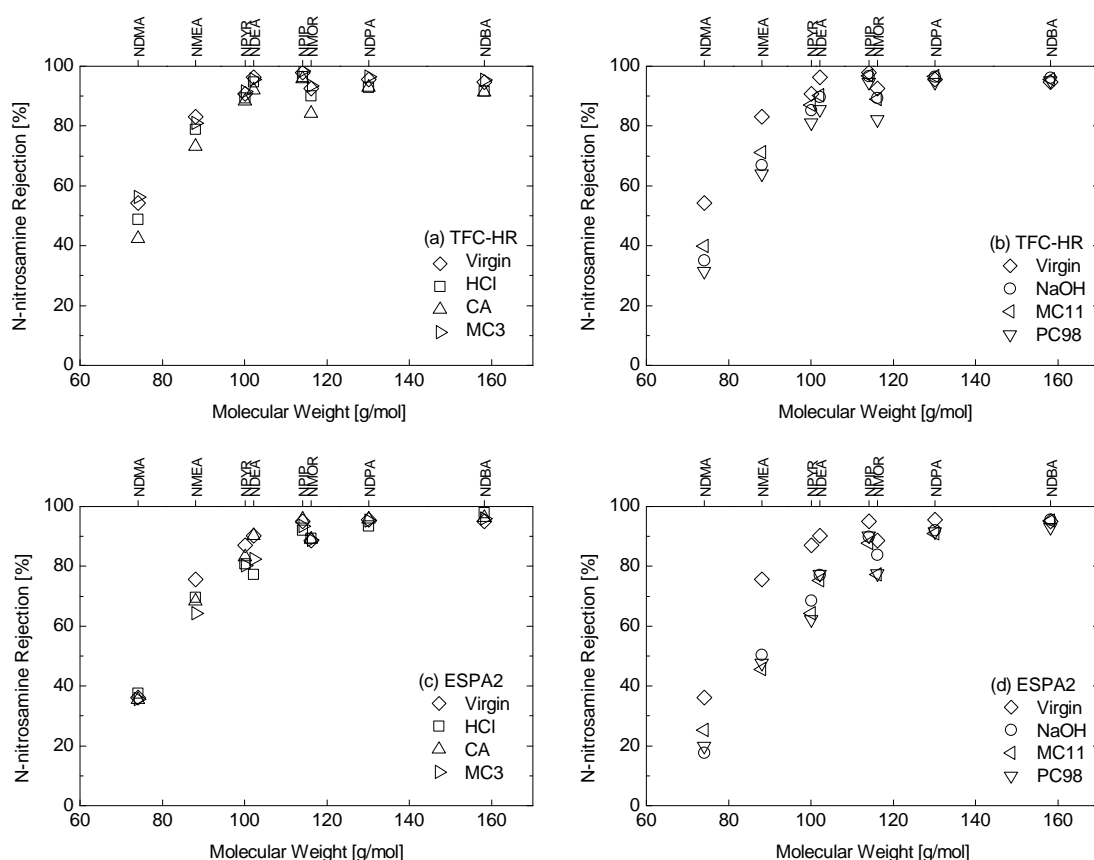


Figure 6.6: N-nitrosamine rejection of the virgin and chemical cleaned (a) and (b) TFC-HR, and (c) and (d) ESPA2 membranes (20 mM NaCl, 1 mM NaHCO₃, 1 mM CaCl₂, permeate flux 20 L/m²h, cross flow velocity 40.2 cm/s, feed pH 8.0 ± 0.1, feed temperature 20.0 ± 0.1 °C). Values reported here are the averages of duplicate results.

Results reported here are in agreement with the changes in the membrane permeability due to chemical cleaning reported in section 3.1. A correlation was observed between permeability and the rejection of NDMA ($R^2 = 0.86$ and 0.87) and NMEA ($R^2 = 0.93$ and 0.86) for the TFC-HR and ESPA2 membranes, respectively (Figure 6.7). These results indicate that the rejection of low molecular weight N-nitrosamines (i.e., NDMA and NMEA) by RO membranes decrease significantly in accordance with the degree of the permeability increase caused by chemical cleaning, while the rejection of high molecular weight N-nitrosamines is not affected by chemical cleaning. Water permeability and solute passage increase when the void volume within the active skin layer increases and effective thickness of the active skin layer decreases [92]. Al-Amoudi [161] recently used the positron annihilation spectroscopy technique to measure the change in membrane pore volume due to chemical cleaning and reported

that the pore volume increased slightly after chemical cleaning. Simon et al. [162] hypothesized that the enlargement of the membrane pore size immediately after caustic cleaning can be attributed to the increased electrostatic interactions at high pH among the deprotonated carboxylic functional groups of the polyamide active skin layer. Due to the hysteresis effect, the membrane pore size can only return to the normal condition after a sufficient period.

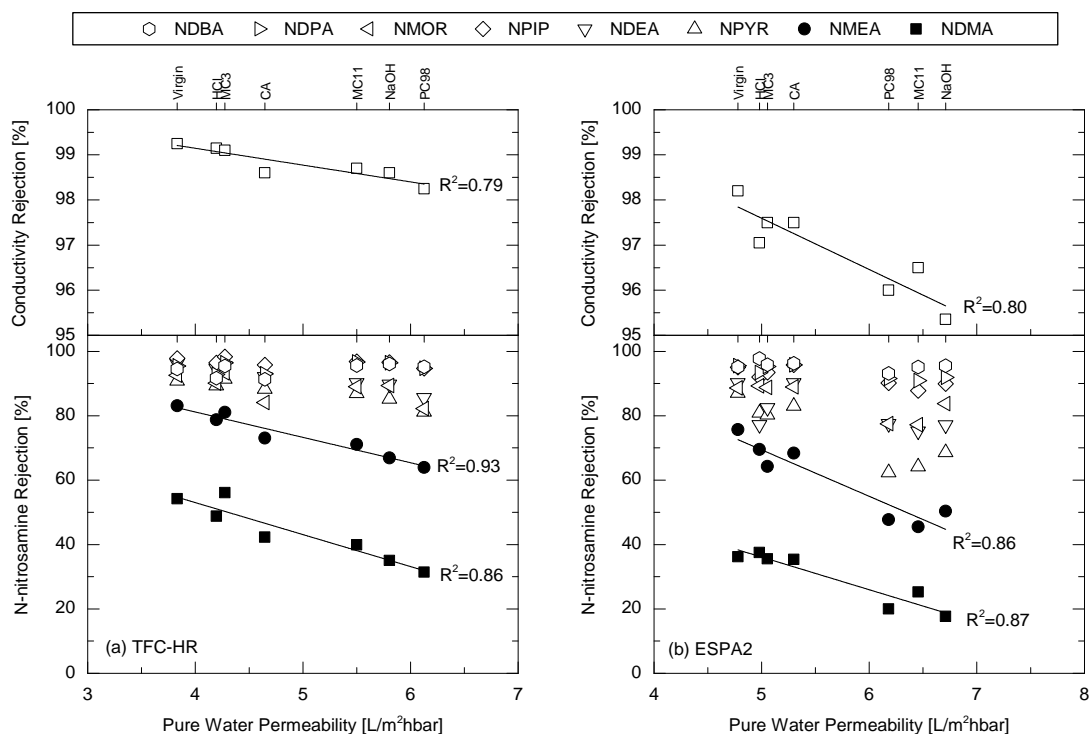


Figure 6.7: Rejection of N-nitrosamines by the virgin and chemical cleaned (a) TFC-HR and (b) ESPA2 membranes as a function of membrane permeability after being exposed to chemical solutions for 25 h at 30 °C.

It is also notable that in addition to N-nitrosamines rejection, a correlation ($R^2 = 0.79$ and 0.80 for the TFC-HR and ESPA2 membranes, respectively) between permeability and conductivity rejection was also observed (Figure 6.7). These results also suggest that changes in conductivity rejection, which is monitored online in full-scale plants, also correspond to some extent to variations in the rejection of low molecular weight N-nitrosamines.

3.3 Sequential cleaning

A sequential cleaning procedure using caustic followed by acidic chemicals are also used at water reclamation plants. This two-step cleaning procedure is particularly common for the third stage of an RO plant where both organic and inorganic fouling occurs [116]. In this study, permeability measured after a sequential cleaning (NaOH solution at pH 12 followed by CA solution at pH 2.1) was lower than that measured after a single cleaning using NaOH solution only (Figure 6.8). Likewise, the sequential cleaning also mitigated the impact of a single NaOH cleaning on NDMA and NMEA rejection, and the rejections of sequentially cleaned membranes were similar to those of CA cleaned membranes (Figure 6.9). The results reported here confirm the hypothesis proposed by Simon et al. [162] indicating that the interactions between membrane matrix and cleaning chemicals are reversible. Thus, the impact of caustic chemical cleaning on membrane separation performance could be alleviated by a sequence of caustic cleaning followed by acidic cleaning.

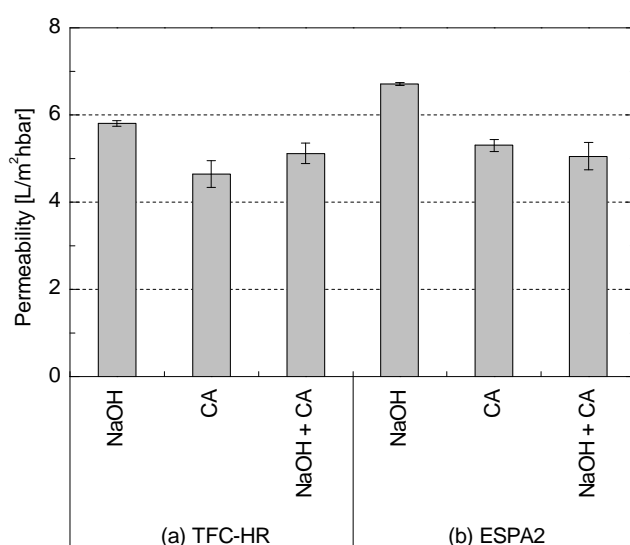


Figure 6.8: Permeability of the (a) TFC-HR and (b) ESPA2 membranes after being exposed to the NaOH solution or CA solution for 25 h at 30 °C, and NaOH solution for 25 h at 30 °C followed by CA solution for 25 h at 30 °C. Membrane permeability was determined with Milli-Q water at 1,000 kPa and 20 °C feed temperature. Values reported here are the average and ranges of duplicate results.

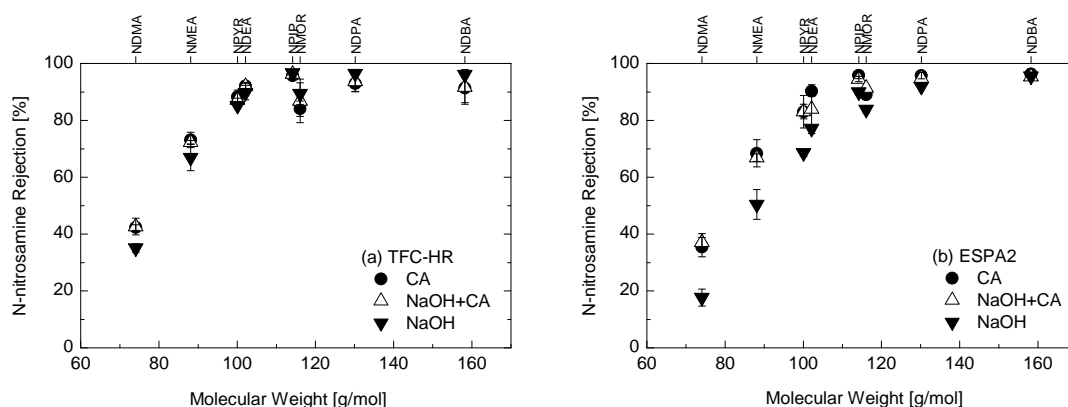


Figure 6.9: N-nitrosamine rejection of the virgin and chemical cleaned (a) TFC-HR and (b) ESPA2 membranes (20 mM NaCl, 1 mM NaHCO₃, 1 mM CaCl₂, permeate flux 20 L/m²h, cross flow velocity 40.2 cm/s, feed pH 8.0 ± 0.1, feed temperature 20.0 ± 0.1 °C). Values reported here are the average and ranges of duplicate results.

4 Conclusions

The effect of chemical cleaning on the rejection of N-nitrosamines by two RO membranes was investigated at bench-scale using six different caustic and acidic cleaning chemicals. Caustic chemical cleaning resulted in a considerable increase in the membrane permeability and the impact was much more significant than that of acidic cleaning. After exposure to caustic cleaning reagents, notable decrease in the rejection of low molecular weight N-nitrosamines (i.e., NDMA and NMEA) was observed. The rejection of larger molecular weight N-nitrosamines exhibited no discernible changes after chemical cleaning. The sequence of caustic followed by acidic cleaning could alleviate the impact of caustic chemical cleaning on permeability and N-nitrosamine rejection despite the fact that the additional cleaning leads to an increase in operational cost. This suggests that the impact of caustic cleaning on water permeation and transport of small molecular weight solutes is reversible and is not permanent. Indeed, FTIR analysis of the membrane surface before and after exposure to various chemical cleaning reagents did not show any discernible changes in the bonding structure of the polyamide skin layer.

Chapter 7

Effects of membrane characteristics

This chapter has been published as:

T. Fujioka, S.J. Khan, J.A. McDonald, A. Roux, Y. Poussade, J.E. Drewes, L.D. Nghiem, *N-nitrosamine rejection by nanofiltration and reverse osmosis membranes: The importance of membrane characteristics, **Desalination**, 316 (2013) 67-75.*

1 Introduction

Although most LPRO membranes available to date are able to achieve NaCl rejection of more than 99% under similar recovery and flux conditions [17], there are no specific criteria for selecting LPRO membranes in terms of the rejection of trace organic chemicals including N-nitrosamines. Several laboratory-scale studies have investigated the rejection of N-nitrosamines by several LPRO membranes in pure water matrices and reported NDMA rejections to be in the range of 45 – 70% and the rejection of the other N-nitrosamines to be over 75% [38, 82, 150]. On the other hand, a recent laboratory-scale study carried out by Fujioka et al. [163] demonstrated that LPRO membranes specifically designed for boron removal (such as the ESPAB) may achieve as high as 80% NDMA rejection. These studies suggest that a considerable variation in the rejection of N-nitrosamines exists amongst the LPRO membranes. Operating conditions (such as feed pH, feed salt concentration, feed temperature and permeate flux) can significantly influence the rejection of low molecular weight N-nitrosamines including NDMA [38, 150]. Because the reported rejection values currently available in the literature were obtained under different filtration conditions, it is unclear whether the significant variation in the rejection of NDMA by LPRO membranes can also be attributed to intrinsic differences in separation efficiency among the membranes.

The aim of this study was to evaluate the impact of membrane characteristics on N-nitrosamine rejection. This investigation was carried out with eight NF and RO

membranes, with a specific focus on LPRO membranes used for water reclamation applications. The rejection of N-nitrosamines was further examined under various permeate flux and feed temperatures to elucidate the impact of operating conditions on the rejection of N-nitrosamines and the underlying rejection mechanisms.

2 Materials and methods

2.1 RO membranes

Properties of eight membranes are summarized in Table 3.1 (Chapter 3).

2.2 Chemicals

Eight N-nitrosamines with molecular weight in the range from 74 to 158 g/mol were used in this study. Properties of these N-nitrosamines are summarized in Table 3.2 (Chapter 3).

2.3 Membrane filtration system

A laboratory-scale cross flow membrane filtration system was used (Figure 3.1). Specification of the bench-scale filtration system is described in Chapter 3, Section 4.1.

2.4 Filtration experiments

Prior to the experiment, each membrane sample was rinsed with a few litres of Milli-Q water to remove any water soluble preservatives on surface. Each filtration experiment started with a compaction step where the membrane was compacted at 1,800 kPa for at least 1 h using Milli-Q water feed. The cross-flow velocity was maintained at 0.42 m/s during the experiment. Unless otherwise stated, the feed temperature was maintained at 20 ± 0.1 °C. After the permeate flux stabilised, the feed pressure was adjusted to 1,000 kPa and pure water permeability was measured using the feed pressure. The feed solution was then conditioned at 20 mM NaCl, 1mM CaCl₂ and 1 mM NaHCO₃ by adding the stock solution of background electrolytes. A similar composition of background electrolytes simulating treated wastewater effluent has been reported in previous studies [38, 127]. The stock solution of N-nitrosamines was spiked into the feed to make up an initial concentration of 250 ng/L of each target compound. The system was then operated at 20 L/m²h permeate flux, which is typically used for water

reclamation applications [122]. Following at least 1 h of operation, 200 mL of feed and permeate samples were taken for analysis. Immediately following each sampling, the surrogate stock solution was dosed into each feed and permeate sample to make up 50 ng/L of each N-nitrosamine surrogate. For the experiments using variable permeate flux, the permeate fluxes was first set at 40 or 60 L/m²h and was stepwise decreased down to 5 L/m²h. Experiments with variable feed temperature started with low temperature (10 or 14 °C) and the feed temperature was stepwise increased up to 40 °C. In each experiment, the filtration system was operated for at least 1 h prior to any samplings to stabilise N-nitrosamine rejections. Conductivity and pH were both measured using an Orion 4-Star Plus pH/conductivity meter (Thermo scientific, USA).

2.5 N-nitrosamine analytical methods

N-nitrosamine concentrations were analysed using an analytical method described in Chapter 3, Section 5.1.

2.6 Transport model description

A numerous number of previous studies reported in the literature have been carried out based on the irreversible thermodynamics model [164]. Kedem and Katchalsky described water (J_v) and solute (J_s) flux through an NF/RO membrane with the following equations [129]:

$$J_v = L_p (\Delta P - \sigma \Delta \pi) \quad (1)$$

$$J_s = P_s \Delta x \frac{d}{dx} C + (1 - \sigma) C J_v \quad (2)$$

where L_p is pure water permeability; ΔP is pressure difference between the feed and permeate sides; σ is reflection coefficient; $\Delta \pi$ is osmotic pressure difference between the feed and permeate sides; P_s is solute permeability coefficient; Δx is membrane thickness; x is position in a pore from inlet; and C is solute concentration. The reflection coefficient (σ) represents the fraction of solute reflected by the membrane in convective flow [130]. Equation 2 is integrated with boundary limits ($x = 0, C = C_p$ and $x = \Delta x, C = C_m$) and is described with the following Spiegler-Kedem equations [131]:

$$R_{real} = 1 - \frac{C_p}{C_m} = \frac{\sigma(1-F)}{(1-\sigma F)} \quad (3)$$

$$F = \exp\left(-\frac{(1-\sigma)}{P_s} J_v\right) \quad (4)$$

where C_p and C_m are permeate and membrane concentration, respectively. Because solute concentration in the feed (C_b) can be obtained from experiments, the real rejection (R_{real}) is calculated using the observed rejection ($R_{obs}=1-C_p/C_b$) as follows [132]:

$$R_{real} = \frac{R_{obs} \exp\left(\frac{J_v}{k}\right)}{1 + R_{obs} \left[\exp\left(\frac{J_v}{k}\right) - 1 \right]} \quad (5)$$

where k is mass transfer coefficient. The value of k is calculated by the Sherwood number (Sh) using the following Grover equation [133]:

$$Sh = \frac{d_h k}{D} = 0.664 Re^{0.5} Sc^{0.33} \left(\frac{d_h}{L}\right)^{0.33} \quad (6)$$

where Reynolds number (Re) = $(d_h u / \nu)$, Schmidt number (Sc) = (ν / D) , d_h = hydraulic diameter, u = feed velocity, ν = kinetic viscosity and D = diffusion coefficient. Further details of the calculation are also available elsewhere [150].

3 Results and discussion

3.1 N-nitrosamine rejection by NF/RO membranes

3.1.1 N-nitrosamine rejection

The rejection of low molecular weight N-nitrosamines (i.e. NDMA and NMEA) by the eight NF/RO membranes used in this study varied significantly in the range from 8 – 82% and 23 – 94%, respectively (Figure 7.1). The type of membrane was less significant for other N-nitrosamines with higher molecular weights. NDPA and NDBA, which are the two largest N-nitrosamines selected in this study, were rejected by

approximately 70% by the NF90 and over 90% by any of the RO membranes. A small variation in the rejection of N-nitrosamines was observed among the four LPRO membranes (i.e. ESPA2, LFC3, TFC-HR and 70LW) which have been widely used for water reclamation applications. For example, NDMA rejection by these membranes ranged from 37% to 52%. The variation was less apparent for NMEA (69-82%) followed by NPYR (84-94%) and NDEA (86-95%), and was negligible for all the other N-nitrosamines. The results reported here suggest that the rejections of N-nitrosamines by LPRO membranes commonly used for water recycling applications under an identical filtration condition may differ from one another by about 15% despite the similarity in their nominal NaCl rejection values (Table 3.1). In other words, the nominal salt rejection value specified by the manufacturers may be not an appropriate criterion to accurately predict the rejection of low molecular weight N-nitrosamines by LPRO membranes. It is noteworthy that a model aquatic solution was used in this study. The presence of effluent organic matter in treated effluent can lead to membrane fouling, which may exert a small influence on the rejection of N-nitrosamines and inorganic salts by NF/RO membranes [163].

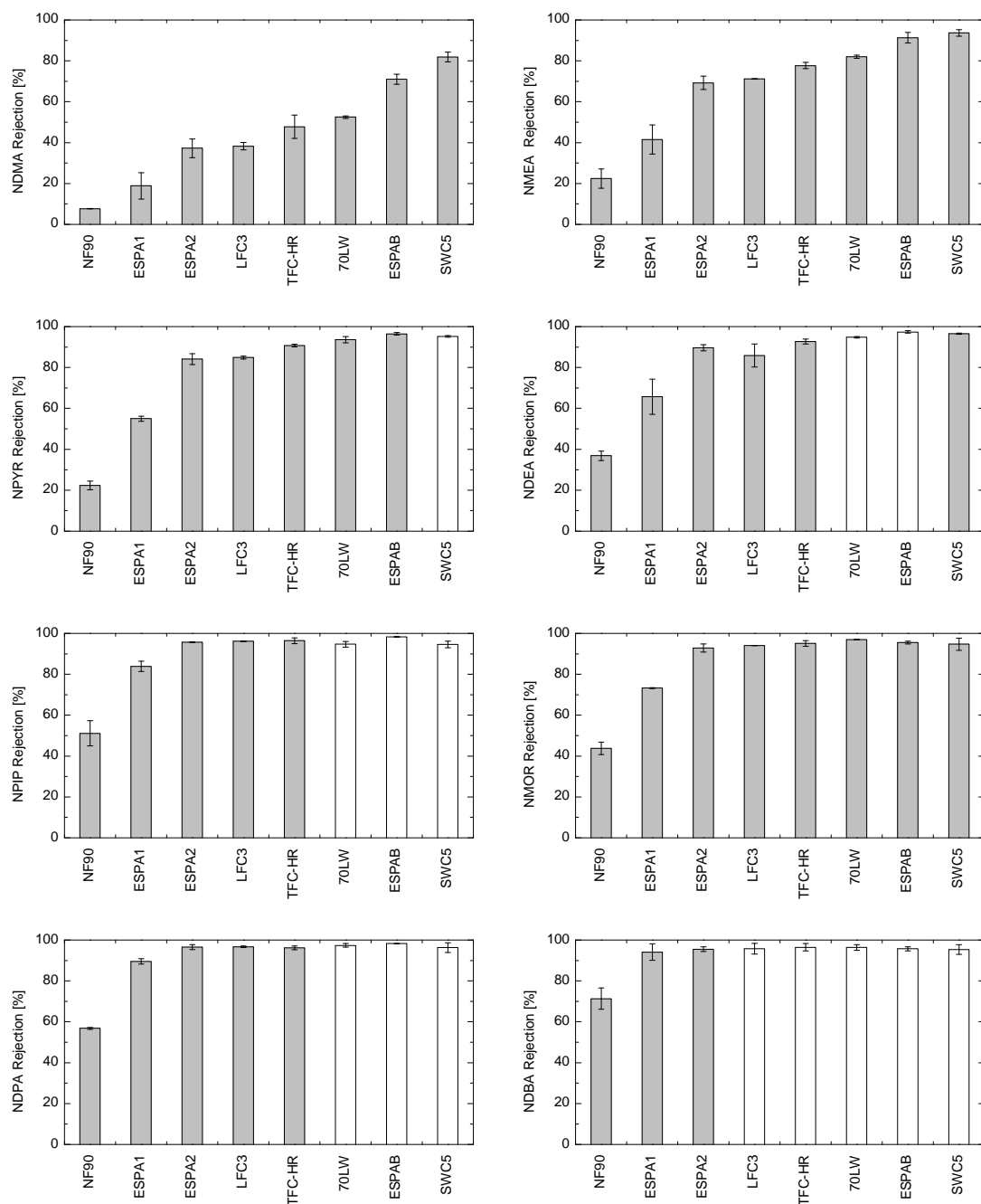


Figure 7.1: N-nitrosamine rejection by NF/RO membranes (20 mM NaCl, 1 mM NaHCO₃, 1 mM CaCl₂, permeate flux 20 L/m²h, cross flow velocity 40.2 cm/s, feed pH 8.0 ± 0.1, feed temperature 20.0 ± 0.1 °C). Open bar indicates that the permeate concentration was below the instrumental detection limit. Error bars show the standard deviation of two replicate experiments.

In general, the rejection of N-nitrosamines by a given membrane increased in the increasing order of their molecular weight (Figure 7.1). In addition to molecular weight, other solute properties such as charge, hydrophobicity and dipole moment can be also important factors determining solute rejections [165-168]. Van der Bruggen et al. [165] investigated the rejection of various organic compounds using NF membranes and reported that, for compounds with similar molecular weights, charged and hydrophilic compounds could be better rejected than hydrophobic compounds. This is because the apparent size of charged and hydrophilic compounds becomes larger due to hydration once they are in an aqueous solution. On the other hand, adsorption followed by diffusion could be a considerable transport mechanism for hydrophobic compounds to permeate NF/RO membranes [165, 167]. It has also been reported that compounds with higher dipole moments could have a lower rejection in comparison to another compound of similar molecular size but with a lower dipole moment [166, 168]. Nevertheless, the eight N-nitrosamines investigated here are neutral, quite hydrophilic and have very similar dipole moment (Table 3.2) and thus molecule weight (rather than charge, hydrophobicity, and dipole moment) appears to be the most important parameter when evaluating the rejection of N-nitrosamines by NF/RO membranes.

3.1.2 *Impact of membrane permeability*

The separation performance of NF/RO membranes can be evaluated by pure water permeability and solute rejection. A comparison between these parameters revealed that the rejection of NDMA and NMEA was inversely proportional to membrane permeability (Figure 7.2). For example, the SWC5 membrane revealed a high NDMA rejection (82%) but low permeability (1.9 L/m²hbar), while the NF90 membrane revealed a high permeability (13 L/m²hbar) but negligible rejection (8%). Permeability and N-nitrosamine rejection values obtained using the LPRO membranes were both within these limits of the SWC5 and NF90 membranes. Importantly, among the LPRO membranes the ESPAB membrane revealed a remarkably higher rejection of NDMA (71%) and NMEA (91%) despite of its relatively high permeability (4.3 L/m²hbar). In fact, the exclusion of the ESPAB membrane data improved the correlation of the rejections and permeability significantly, changing the coefficient of determination (R^2) of the linear regression between NDMA or NMEA rejection and the membrane

permeability from 0.61 to 0.70 and from 0.86 to 0.95, respectively. The underlying reason for this notably better performance of the ESPAB with respect to NDMA and NMEA rejection observed here is currently unknown and is the subject for a future study.

In the surface force-pore flow model, membrane permeability (L_p) increases with increasing membrane pore size (r_p) and with decreasing the thickness of the membrane active layer (Δx) as described with the Hagen-Poiseuille equation [92, 169].

$$L_p = \frac{r_p^2 A_k}{8\mu\Delta x} \quad (7)$$

where A_k is membrane porosity; and μ is viscosity of water. Because the changes in membrane pore size and the thickness of the membrane active layer also affect solute rejection [92], it can be hypothesized that the variation in NDMA and NMEA rejection by these NF/RO membranes is associated with the difference in the properties (i.e. r_p and Δx) of these membranes.

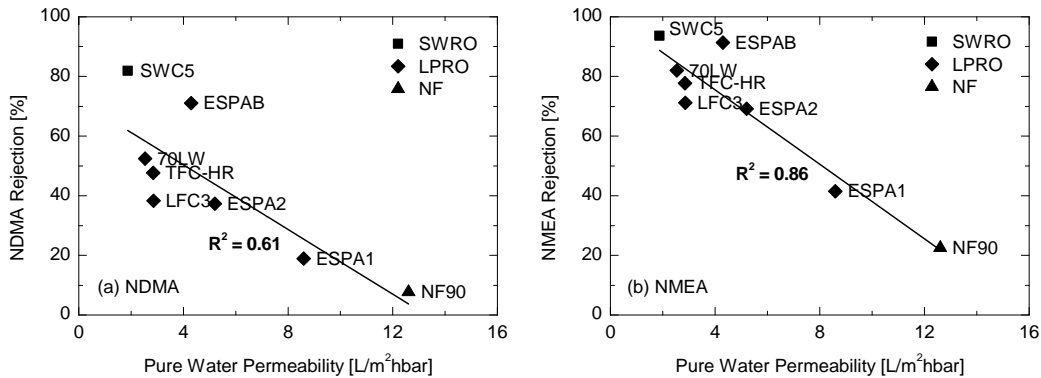


Figure 7.2: Rejection of NDMA and NMEA by NF/RO membranes as a function of pure water permeability. Experimental conditions are as described in Figure 7.1.

3.2 Effects of filtration conditions

3.2.1 Permeate flux

In general, solute rejection increases when water permeate flux increases, because water flux increases with applied feed pressure while the applied pressure has only a negligible impact on solute flux [96]. As expected, an increase in permeate flux led to

the increased rejection of conductivity and N-nitrosamines (Figure 7.3). For the 70LW membrane, permeate flux of 60 L/m²h was excluded from the experiment due to the feed pressure limitation of the filtration setup. For both membranes, the impact of the changes in permeate flux on N-nitrosamine rejection was stronger in lower ranges (e.g. 5-10 L/m²h). In addition, the rejection of low molecular weight N-nitrosamines was significantly affected by the changes in permeate flux. For instance, NDMA rejection by the ESPA2 dropped from 53 to 36% when permeate flux decreased from 42 to 10 L/m²h. The rejection trends observed in this investigation are consistent with a previous study using the LPRO TFC-HR membrane [150]. In addition, the difference in N-nitrosamine rejection value between the ESPA2 and 70LW membranes was observed to be small (<11%) when compared at both 10 and 42 L/m²h permeate flux (Figure 7.4).

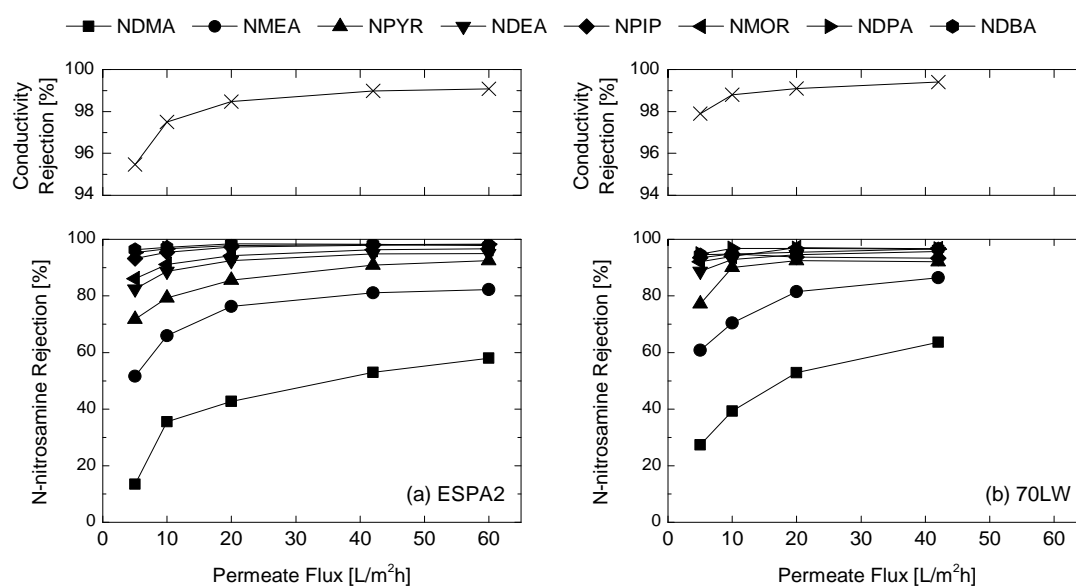


Figure 7.3: Rejection of conductivity and N-nitrosamines by (a) ESPA2 and (b) 70LW membranes as a function of permeate flux (20 mM NaCl, 1 mM NaHCO₃, 1 mM CaCl₂, cross flow velocity 40.2 cm/s, feed pH 8.0 ± 0.1, feed temperature 20.0 ± 0.1 °C).

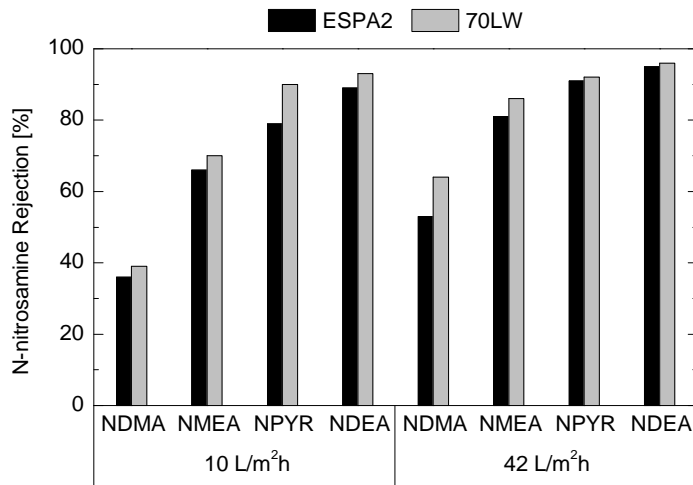


Figure 7.4: Rejection of NDMA, NMEA, NPYR and NDEA by the ESPA2 and 70LW membranes at permeate flux of 10 and 42 L/m²h. Experimental conditions are as described in Figure 7.3.

The real rejection of N-nitrosamines by the ESPA2 and 70LW membranes was well described by the irreversible thermodynamic model (Figure 7.5). For the 70LW membrane, NPYR, NPIP, NMOR, NDPA and NDBA were excluded from the modelling because some of their permeate concentrations were below their analytical detection limits. The reflection coefficient (σ) of all N-nitrosamines was generally high (>0.9) (Table 7.1) which is consistent with a previous study using the TFC-HR membrane [150]. These observations suggest that these LPRO membranes may be comparable in terms of N-nitrosamine rejection even in different permeate flux conditions.

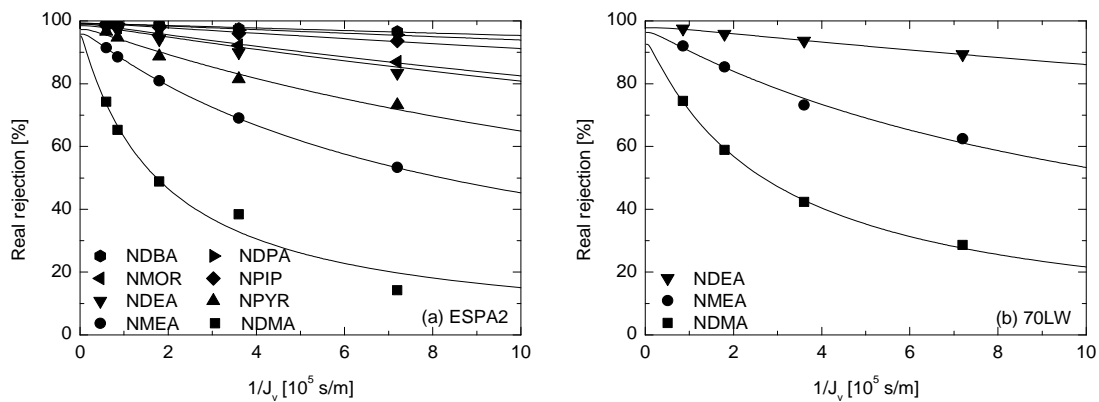


Figure 7.5: Real rejection of N-nitrosamines by (a) ESPA2 and (b) 70LW membranes as a function of reciprocal permeate flux. Experimental conditions are as described in Figure 7.3.

Table 7.1: Transport parameters of N-nitrosamines through the ESPA2, 70LW and TFC-HR [150] membranes.

N-nitrosamine	k [m/s]	σ [-]			P [m/s]		
		ESPA2	70LW	TFC-HR	ESPA2	70LW	TFC-HR
NDMA	2.26×10^{-5}	0.953	0.926	0.949	5.35×10^{-6}	3.32×10^{-6}	4.15×10^{-6}
NMEA	1.99×10^{-5}	0.958	0.963	0.968	1.14×10^{-6}	8.24×10^{-7}	1.07×10^{-6}
NPYR	1.99×10^{-5}	0.973	-	0.989	5.12×10^{-7}	-	6.74×10^{-7}
NDEA	1.99×10^{-5}	0.985	0.978	0.998	2.26×10^{-7}	1.47×10^{-7}	2.49×10^{-7}
NPIP	2.09×10^{-5}	0.993	-	-	9.25×10^{-8}	-	-
NMOR	2.18×10^{-5}	0.991	-	0.988	2.06×10^{-7}	-	1.99×10^{-7}
NDPA	2.02×10^{-5}	0.992	-	-	6.02×10^{-8}	-	-
NDBA	1.99×10^{-5}	0.990	-	0.983	4.33×10^{-8}	-	1.01×10^{-7}

3.2.2 Feed temperature

An increase in feed temperature resulted in the decreased rejection of conductivity and N-nitrosamines (Figure 7.6). For example, an increase in the feed temperature from 20 to 40 °C led to a decrease in NDMA rejection by the ESPA2 and 70LW membrane from 41 to 15% and from 52 to 22%, respectively. In response to the feed temperature increase, NMEA and NPYR rejections also dropped significantly. The impact of feed temperature was less pronounced with increasing their molecular weight, and the rejection of high molecular weight N-nitrosamines (i.e. NDPA and NDBA) equally remained almost constant and high (>94%) within the ranges of feed temperature tested here (Figure 7.6). When feed temperature increases, the pore size within an active skin layer of membranes can enlarge slightly [111] and the permeability coefficient of solutes also increases [130, 132], both of which cause more solute passage through membranes. Thus, these combination effects may have decreased the rejection of N-nitrosamines against the increase in feed temperature. Between the two LPRO membranes, the difference in the rejection values of NDMA, NMEA, NPYR and NDEA was always less than 13% at the feed temperature of both 20 and 40 °C (Figure 7.7). The observations reported here indicate that the impact of feed temperature on the rejection of N-nitrosamines is similar among the LPRO membranes tested.

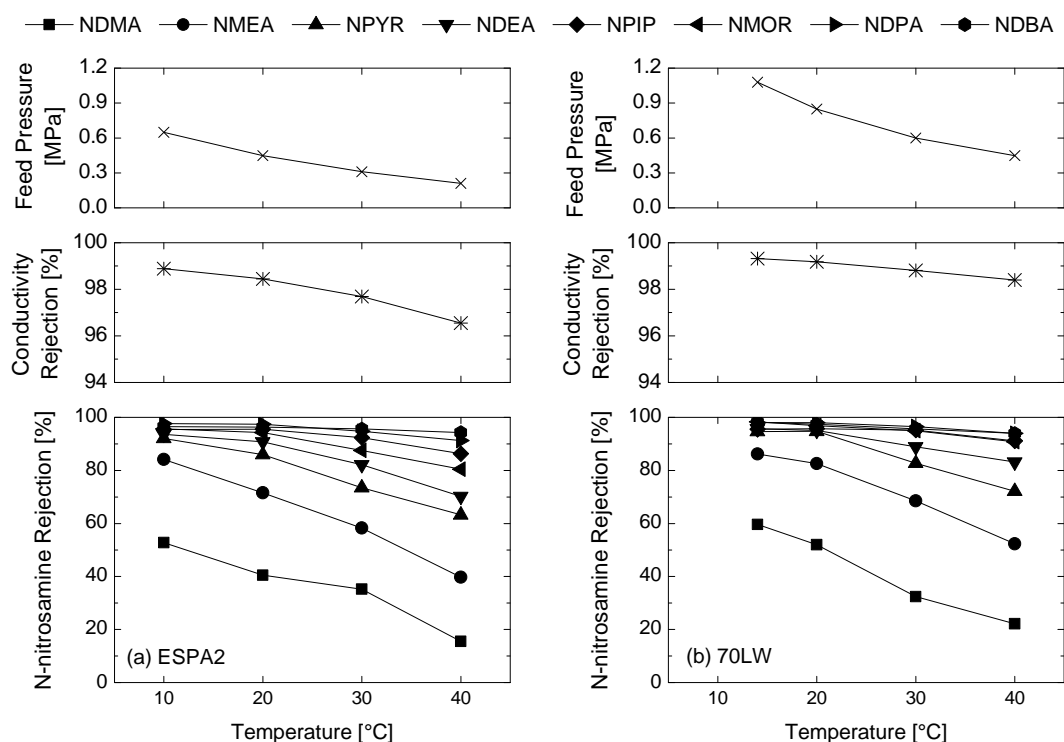


Figure 7.6: Effects of feed temperature on the feed pressure and the rejection of conductivity and N-nitrosamines by (a) ESPA2 and (b) 70LW membranes (20 mM NaCl, 1 mM NaHCO₃, 1 mM CaCl₂, permeate flux 20 L/m²h, cross flow velocity 40.2 cm/s, feed pH 8.0 ± 0.1, feed temperature 20.0 ± 0.1 °C).

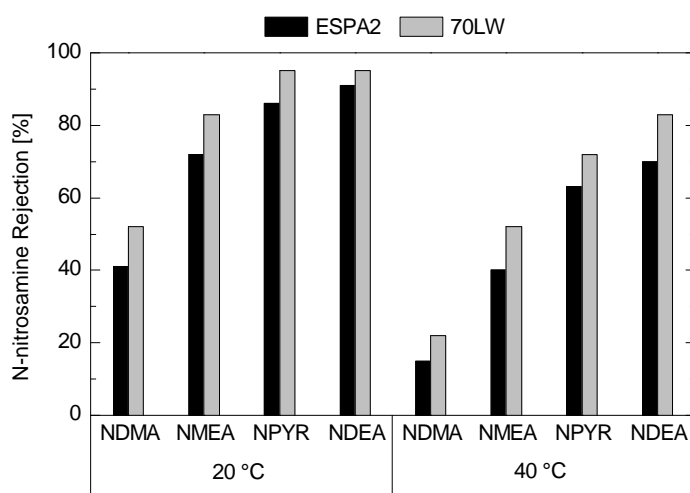


Figure 7.7: Rejection of NDMA, NMEA, NPYR and NDEA by the ESPA2 and 70LW membranes at feed temperature of 20 and 40 °C. Experimental conditions are as described in Figure 7.6.

4 Conclusions

The rejection of NDMA by NF/RO membranes varied significantly in the range of 8-82% depending on the membrane and operating conditions. The impact of membrane characteristics was less apparent for higher molecular weight N-nitrosamines and the rejection of NPYR, NMOR, NDPA and NDBA were over 90% by any of the tested RO membranes. Using these NF/RO membranes, a correlation was found between membrane permeability and the rejection of low molecular weight N-nitrosamines (i.e. NDMA and NMEA). The variation in NDMA and NMEA rejections among the LPRO membranes frequently used for water reclamation applications (i.e. ESPA2, LFC3, TFC-HR and 70LW) was relatively small, at 37-52% and 69-82%, respectively. However, a high rejection of NDMA (71%) and NMEA (91%) was obtained with the ESPAB membrane which is also an LPRO membrane but is specifically designed for the removal of boron. Results reported here suggest the potential of using boron removal LPRO membranes (i.e. ESPAB) for wastewater recycling applications where NDMA concentration in the final water is a critical parameter under water quality regulations. Similar rejection behaviours of N-nitrosamines were obtained with two different LPRO membranes (i.e. ESPA2 and 70LW) when compared with variable permeate flux and feed temperature conditions. In particular, the rejection of low molecular weight N-nitrosamines such as NDMA and NMEA decreased significantly when the permeate flux decreased or the feed temperature increased. In practice, some variations in permeate flux and temperature are inevitable. Thus, the impact of permeate flux and solute temperature on the rejection of N-nitrosamines reported here has an important implication to full-scale operation of NF/RO systems for water reclamation applications. Results reported here also suggest that membrane properties associated with membrane permeability such as the pore size and thickness of the active skin layer might determine N-nitrosamine rejection.

Chapter 8

Role of free-volume hole-space of RO membranes

This chapter has been published as:

T. Fujioka, N. Oshima, R. Suzuki, S.J. Khan, J.A. McDonald, A. Roux, Y. Poussade, J.E. Drewes, L.D. Nghiem, Rejection of small and uncharged chemicals of emerging concern by reverse osmosis membranes: The role of free volume space within the active skin layer, *Separation Purification Technology*, 116 (2013) 426-432..

1 Introduction

The rejection of solutes through the active skin layer of RO thin-film composite membranes is usually described using indirect molecular transport measures such as salt rejections [3]. This simplification is due to the unavailability of any techniques for directly analysing the free-volume distribution of these membranes in the past. Recently, positron annihilation lifetime spectroscopy (PALS) has been successfully applied to quantify free-volume hole-radii within the active skin layers of NF/RO membranes [94, 95, 170-174]. In a pioneering study, Kim et al. [95] applied the PALS technique to several surface-modified RO membranes and reported that permeability increased with increasing free-volume hole-radius of the active skin layer. Another recent PALS study by Chen et al. [94] also revealed that the rejection of several uncharged compounds (i.e., urea, ethylene glycol, and 1- or 2-propanol) by NF/RO membranes increased with decreasing free-volume hole-radii. To the best of our knowledge, to date, no studies have applied PALS to examine the impact of free-volume hole-size on the rejection of water contaminants of significant health and environmental concern such as N-nitrosamines and boron.

The aim of this study was to provide an understanding of uncharged solute transport through nanoscale free-volume structure within RO membranes. A PALS technique with a slow positron beam was used to analyse the free-volume hole-radii within the

active skin layers of commercial RO membranes. The relationship between the free-volume hole-radius of the active skin layer of three different RO membranes and the transport of boric acid and N-nitrosamines was examined.

2 Materials and methods

2.1 RO membranes

Specimens of three RO membranes – namely SWC5, ESPAB, and ESPA2 – were used in this study. Properties of these membranes are summarized in Table 3.1 (Chapter 3).

2.2 Chemicals

Eight N-nitrosamines were selected for this investigation. Properties of these N-nitrosamines are summarized in Table 3.2 (Chapter 3). Key physicochemical properties of boric acid are summarised in Table 8.1.

Table 8.1: Physicochemical characteristics of the selected N-nitrosamines and boric acid.

Name	Molecular weight [g/mol]	Log K_{ow} ^a	Molecular volume V_m ^b [nm ³ /molecule]
B (Boric acid)	61.83	-0.62	0.071
NDMA	74.05	-0.50	0.124
NMEA	88.06	0.01	0.151
NPYR	100.06	-0.09	0.134
NDEA	102.08	0.52	0.178
NPIP	114.08	0.44	0.161
NMOR	116.06	-0.81	0.145
NDPA	130.11	1.54	0.232
NDBA	158.14	2.56	0.286

^a ACD/PhysChem Suite software (Advanced Chemistry Development, Inc., Ontario, Canada)

^b The molecular volume of each molecule was estimated with the equation ($V_m = \text{Molecular volume [nm}^3/\text{mol}]/N_A$) where Avogadro constant (N_A) is 6.022×10^{23} 1/mol. The molecular volume of each molar was obtained from ACD/PhysChem Suite software.

2.3 Membrane filtration system

A laboratory-scale cross flow membrane filtration system was used (Figure 3.1). Specification of the bench-scale filtration system is described in Chapter 3, Section 4.1.

2.4 Experimental protocols

Prior to each filtration experiment, the membrane sample was compacted at 1,800 kPa using Milli-Q water until permeate flux has been stabilised. The cross flow velocity and solution temperature were 0.42 m/s and 20 ± 0.1 °C, respectively. Following the compaction step, the feed water solution was conditioned at 20 mM NaCl, 1mM CaCl₂ and 1 mM NaHCO₃ by adding appropriate volumes of the stock solutions of each background electrolyte. The stock solutions of N-nitrosamines and boric acid were also introduced into the feed to obtain approximately 250 ng/L of each N-nitrosamine and 1.0 mg/L of boron. Thereafter, the permeate flux was adjusted with 20 L/m²h. The system was continuously operated for 2 h before the first permeate and concentrate samples were taken for analysis.

2.5 Analytical technique

2.5.1 PALS

The free-volume hole-radii of the RO membranes were analysed using a PALS technique with a pulsed slow positron beam at the National Institute of Advanced Industrial Science and Technology (AIST) in Tsukuba, Japan [175]. Details of this PALS analysis are available elsewhere [94, 176, 177]. In brief, the PALS technique with a slow positron beam is capable of measuring free-volume hole-radius within a sub-nanometer range within the membrane active skin layer [94]. In principal, when positrons are injected into a solid sample, the positrons annihilate with electrons of the solid sample and emit gamma-rays. Application of PALS relies on the fact that some positrons combine with an electron to form the hydrogen-like bound state, positronium (Ps). The intrinsic lifetimes of spin-antiparallel *para*-positronium (*p*-Ps) and spin-parallel *ortho*-positronium (*o*-Ps) in vacuum are 0.125 ns and 142 ns, respectively. In a polymer sample, a typical positron lifetime spectrum of a polymer contains three exponentially decaying components, due to the intrinsic *p*-Ps, free positron (non-Ps) and *o*-Ps annihilation. Although *o*-Ps annihilates with a lifetime much shorter than 142 ns in a polymer sample, *o*-Ps still survives far longer than the *p*-Ps and free positrons which indicates that *o*-Ps is the longest lifetime component.

Lifetime of o -Ps (τ_{o-Ps}) is affected by the free volume size in insulating materials including polymer and their relationship is given by the Tao-Eldrup model as follows [178, 179]

$$\tau_{o-Ps} = 0.5 \left[1 - \frac{r}{r + 0.166} + \frac{1}{2\pi} \sin\left(\frac{2\pi r}{r + 0.166}\right) \right]^{-1} \quad (1)$$

where r (≤ 1 nm) is the radius of the free volume hole approximated as a spherical shape. Consequently, the free-volume hole-space (V_f) can be calculated with the following formula.

$$V_f = \frac{4}{3} \pi r^3 \quad (2)$$

It should be noted that the evaluated r (calculated by Eq. 1) represents the mean radius of free-volume holes which were probed by o -Ps. Although this indicates that the PALS technique is expected to have a limited range for evaluating the size of free-volume hole [176, 177], the mean free-volume hole-radius based on the PALS technique was referred simply as “mean free-volume hole-radius” in this study.

Positron lifetime was measured as the time difference between the pulsing trigger from the beam pulsing system and the detection timing of annihilation gamma-ray detected by a BaF₂ scintillation detector [175] (Figure 8.1). The analysis was carried out under vacuum at 10^{-5} Pa. The mean implantation depth of positrons was adjusted by changing positron incident energy of the slow positron beam. During the PALS analysis in this study, positron incident energy was set at 1.0 keV which corresponds to a mean depth of around 40 nm. This energy (1 keV) and corresponding implantation depth (~ 40 nm) of slow positron was decided reasonably for our sample evaluation based on previous investigations. For example, previous studies investigated the mean free-volume hole-radius in variable implantation depths using composite polyamide RO membranes and reported that smallest mean free-volume hole-radii were found at mean implantation depth of 40-100 nm [94, 180] where the active skin layer is expected to exist. In fact, for LPRO and SWRO membranes the total thickness of about 200 nm active skin layers has been estimated with transmission electron microscopy by Freger et al. [181].

Approximate 2×10^6 events of positron annihilation were collected to obtain one positron lifetime spectrum for each sample. The positron lifetime spectra were analysed assuming three exponential components to deduce the lifetime, τ_{o-Ps} , using a non-linear least-squares fitting program. The relative measurement uncertainty of τ_{o-Ps} was evaluated not more than 5%.

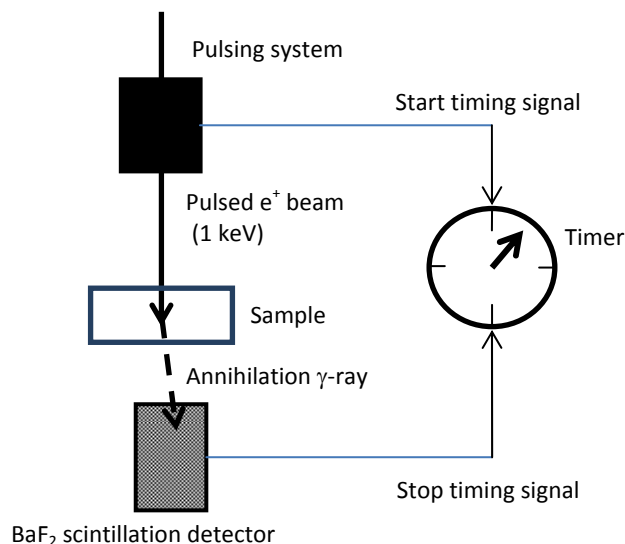


Figure 8.1: Schematic diagram of the PALS analysis.

2.5.2 *N-nitrosamine analysis*

N-nitrosamine concentrations were analysed using an analytical method described in Chapter 3, Section 5.1.

2.5.3 *General analytical techniques*

Basic analytical techniques are described in Chapter 3, Section 5.2.

3 *Results and discussion*

3.1 *PALS analysis*

The *o-P_s* lifetime (τ_{o-Ps}) of the LPRO membranes (i.e. ESPA2 and ESPAB) obtained here were almost identical ($\tau_{o-Ps} = 2.07$ ns) and, as a result, these two membranes were determined to have the same mean free-volume hole-radii (r) of 0.289 nm (Table 8.2). The *o-P_s* lifetime (τ_{o-Ps}) of the SWC5 membrane was 1.75 ns and the corresponding mean free-volume hole-radius (r) was determined to be 0.259 nm. In good agreement

with our results, Lee et al. [174] used the PALS technique and obtained a mean free-volume hole-radius of 0.278 nm for the SW30 which is commonly used as seawater RO membrane. Pure water permeability was generally membrane dependent and increased in the order of the SWC5, ESPAB and ESPA2 membranes and sodium ion rejection decreased following the same order (Table 8.2).

Although the mean free-volume hole-radii of the ESPA2 and ESPAB probed by *o*-Ps are both 0.289 nm, a notable variation was found for their pure water permeability and sodium ion rejections (Table 8.2). In general, pure water permeability of RO membranes increases and solute rejection decreases with increasing mean free-volume hole-radius (r) and with decreasing the effective thickness of the membrane active skin layer [92], thus these two parameters (i.e, mean hole-radius and effective thickness) are likely to be key factors differentiating permeability and solute rejections among these membranes. Although not reported in this study, it is noteworthy that the distribution of the free-volume hole-radii may also play a role in permeability and solute rejection. Freger [181] measured the membrane thickness of LPRO and SWRO membranes by transmission electron microscopy and reported that the LPRO membrane have thinner active skin layer than the SWRO membrane, which is consistent with the fact that it is an SWRO membrane with lower permeability and higher sodium ion rejection than the ESPA2 and ESPAB membranes (Table 8.2). In addition, Prakash et al. [182] reported a strong correlation between the effective thickness of active skin layer and pure water permeability of RO membranes. It is also noteworthy that the ESPAB is likely to be a modified version of the ESPA2 (which may explain the same calculated free-volume hole-radii of these two membranes). The details of this modification are proprietary information of the manufacturer. However, it can be speculated that the lower pure water permeability and higher sodium ion rejection of the ESPAB compared to the ESPA2 is attributed to a thicker active layer thickness and different free-volume hole-radius distribution of the ESPAB. Although it is beyond the scope of this study, measurement of the active layer thickness and distribution of free-volume hole-radius within the active skin layer would be useful to substantiate this hypothesis.

Table 8.2: Mean free-volume hole-size and hole-space, pure water permeability and sodium ion rejection of the RO membranes.

Membrane	τ_{o-Ps} [ns]	Mean free- volume hole-radius, r [nm]	Mean free- volume hole-space, V_f [nm ³]	Pure water permeability ^a [L/m ² hbar]	Na ⁺ rejection ^b [%]
ESPA2	2.07	0.289	0.101	5.9 ± 0.3	97.1 ± 1.4
ESPAB	2.07	0.289	0.101	4.6 ± 0.1	99.0 ± 0.1
SWC5	1.75	0.259	0.073	2.6 ± 0.1	99.2 ± 0.4

^a Determined with Milli-Q water at 1,000 kPa and 20 °C feed temperature. Values reported here are average and ranges of duplicate results.

^b Analysed with feed solution contained 20 mM NaCl, 1 mM NaHCO₃, 1 mM CaCl₂ at permeate flux 20 L/m²h, cross flow velocity 40.2 cm/s, feed pH 8.0 ± 0.1 and feed temperature 20.0 ± 0.1 °C. Values reported here are average and ranges of duplicate results.

3.2 Rejection of boric acid and N-nitrosamines

The rejection of boric acid and N-nitrosamines by the three RO membranes used in this study generally increased in the increasing order of their molecular volume (Figure 8.2). Significant differentiation in solute rejection by the three membranes was observed for those smaller than 0.13 nm³/molecule. The ESPAB and SWC5 membranes exhibited similar rejection values for any given solute with boric acid and NDMA being the only notable exceptions (Figure 8.2) despite the fact that their mean free-volume hole-radii differ by 0.03 nm (Table 8.2). Likewise, although the mean free-volume hole-radii of the ESPAB and ESPA2 were both 0.289 nm, the rejection values of small molecular volume solutes by these membranes were distinctly different.

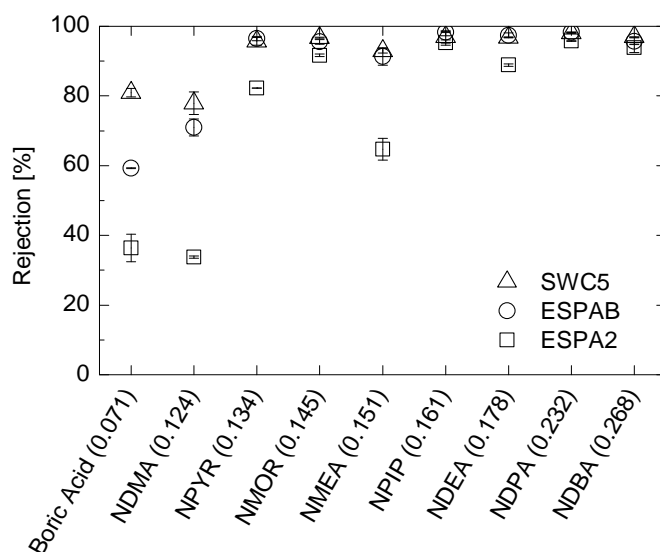


Figure 8.2: Rejection of boric acid and N-nitrosamines (20 mM NaCl, 1 mM NaHCO₃, 1 mM CaCl₂, permeate flux 20 L/m²h, cross flow velocity 40.2 cm/s, feed pH 8.0 ± 0.1, feed temperature 20.0 ± 0.1°C). The molecular volume (nm³/molecule) is shown in the parentheses. Values reported here are the average and ranges of duplicate results.

3.3 Rejection mechanisms

The rejection of boric acid, NDMA and sodium ion by the RO membranes was inversely correlated with their pure water permeability (Figure 8.3). The rejection of sodium ion was significantly higher than that of boric acid and NDMA (Figure 8.3) because sodium ion is strongly hydrated (Na⁺-6H₂O) at the tested pH and the charged sodium ion is rejected by both steric and electrostatic interactions [3]. For the case of the ESPA2 and ESPAB membranes both of which have 0.289 nm mean free-volume hole-radii, as described in a previous section the thicker active skin layer and different free-volume hole-radius distribution of the ESPAB membrane may be the reason why the rejection of small molecular volume solutes (i.e. boric acid, NDMA and sodium ion) by the ESPAB was higher than the ESPA2 membrane. On the other hand, the SWC5, being a SWRO membrane, is expected to have a thicker active skin layer than LPRO membranes [181]. Because the PALS analysis showed that the SWC5 membrane has a smaller mean free-volume hole-radius than the LPRO membranes, two parameters (i.e. mean free-volume hole-radius and/or its distribution and active skin layer thickness) can be expected to contribute to the higher rejection of uncharged solutes by the SWC5 compared to the ESPA2 and ESPAB.

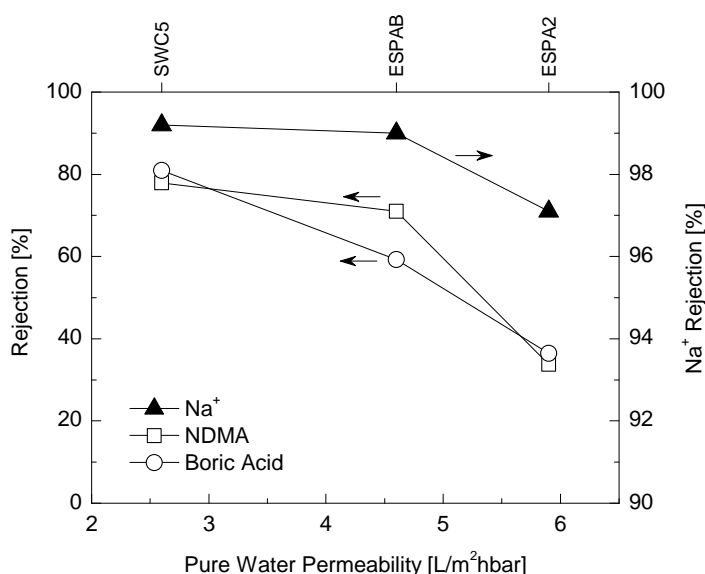


Figure 8.3: Rejection of boric acid, NDMA and sodium ion as a function of pure water permeability. Experimental conditions are as described in Figure 8.2.

The effect of the size relationship between mean free-volume hole-space and solute volume on the rejection of the uncharged solutes was evaluated using the ratio of molecular volume (V_m) to the mean free-volume hole-space (V_f) (Figure 8.4). As a result, rejection increased drastically around V_m/V_f ratio of one with an increasing V_m/V_f ratio and reached almost constant value of 95 % over V_m/V_f ratio of two. Such significant changes in rejections were also observed in the similar range of the V_m/V_f ratio (between one and three) in previous studies [94, 180].

A previous study by Chen et al. [94] revealed that a correlation between V_m/V_f and the rejection of uncharged solutes among one RO and two NF membranes was approximately linear (Figure 8.4). They reported that the rejection of uncharged solute is highly associated with the mean free-volume hole-space of the membranes and the correlation is valid for different solutes and membranes (Figure 8.4). While our experimental results showed that the correlation between rejection and V_m/V_f is not linear, rejection increased almost monotonically with increasing function of V_m/V_f for each membrane like the previous studies [94, 180]. These results indicate that the mean free-volume hole-space (V_f) is an important parameter determining uncharged solute rejection. It is also noteworthy that the rejections of solutes with molecular volume of less than $0.13 \text{ nm}^3/\text{molecule}$ by the three RO membranes differ considerably from one

to another although the mean free-volume hole-space (V_f) of these membranes were similar. Thus, in addition to the mean free-volume hole-space (or mean radius), other membrane characteristics such as the free-volume hole-radii distribution and active skin layer thickness could also be important parameters governing the rejection of small and uncharged solutes by RO membranes.

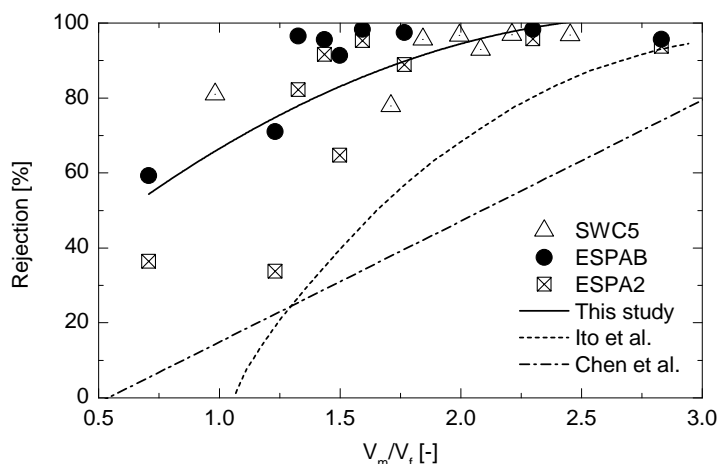


Figure 8.4: Correlation between the ratio of molecular volume (V_m) to the mean free-volume of the membranes (V_f) and the rejection of boric acid and N-nitrosamines. Experimental conditions are as described in Figure 8.2. The correlation data of this study was obtained from the rejection of boron and eight N-nitrosamines by the three RO membranes. The short dash line and the dash dotted line represent the correlation data reported by Ito et al. [180] and Chen et al. [94], respectively.

4 Conclusions

PALS analysis with 1 keV slow positron beam revealed that the seawater RO (SWC5) membrane has the smallest mean free-volume hole-radius followed by the two low pressure RO membranes (ESPA2 and ESPAB). The SWC5 membrane also exhibited the highest rejection of uncharged solutes (i.e. boric acid and N-nitrosamines) and sodium ions. The ESPAB membrane revealed a lower pure water permeability and higher rejection of uncharged solutes and sodium ions than the ESPA2 membrane, despite their identical mean free-volume hole-radii. The comparison between solute volume (V_m) and mean free-volume hole-space (V_f) evaluated by PALS by exhibited a monotonically increasing factor of V_m/V_f , indicating the mean free-volume hole-space (or referred as hole-radii) is indeed an important factor determining uncharged solute

rejection. Nevertheless, because the rejection of small and uncharged solutes by the three RO membranes differ considerably from one to another, other membrane parameters and properties such as the distribution of free-volume hole-radius and thickness of the active skin layer are also likely to play a role in governing the passage of solutes with small molecular volume.

Chapter 9

Full-scale monitoring

This chapter has been published as:

T. Fujioka, S.J. Khan, J.A. McDonald, A. Roux, Y. Poussade, J.E. Drewes, L.D. Nghiem, N-nitrosamine rejection by reverse osmosis membranes: A full-scale study, **Water Res.**, 47 (2013) 6141-6148.

1 Introduction

The rejection of N-nitrosamines by RO membranes has been extensively investigated at the laboratory scale [38, 82, 83, 150]. However, full-scale monitoring data to reaffirm findings from laboratory-scale experiments and to assess the impact of realistic operating conditions on the rejection of N-nitrosamines have rarely been reported in the peer review literature. Plumlee et al. [18] studied the removal of NDMA by different treatment processes (including RO) at the Interim Water Purification Facility (Orange County, California, USA). NDMA removal by the RO process varied from 24 to 56%. The authors suggested that the variation in NDMA rejection observed in their study might be associated with changing feed conditions and membrane fouling. However, the authors did not monitor the feed and membrane fouling conditions. Farré et al. [12] reported the fate of NDMA after each treatment process of the Bundamba Water Recycling plant in Queensland, Australia. Because Farré et al. [12] did not focus on the RO process, only one overall rejection value of NDMA by the RO system can be inferred from their study. Some information about the rejection of NDMA and NMOR by a full-scale RO plant can also be inferred from a study by Krauss et al. [8], who investigated the fate of N-nitrosamine precursors at the Wulpen/Torreele Water Recycling plant in Belgium. In comparison to NDMA, very little is known about the fate and removal of other N-nitrosamines during RO filtration at full scale. The scarcity of full-scale monitoring and the lack of information regarding operating conditions (e.g. permeate flux and recovery) and feed water characteristics (e.g. temperature, ionic

composition) significantly hinder any meaningful data analysis. RO systems for wastewater recycling are typically designed using three stages to achieve recovery around 85% [122]. Although the RO feed is further concentrated after each filtration stage, no studies available to date have examined rejection efficiencies for nitrosamines at subsequent stages.

The aim of this study was to assess the removal of eight N-nitrosamines in three full-scale RO plants. N-nitrosamine rejection values obtained at different stages were systematically related to the operating conditions and feed water characteristics. In addition, the difference in N-nitrosamine rejections between a cool and a warm weather period at one plant was also elucidated. Based on the obtained results, implications to water recycling practice were highlighted and discussed.

2 *Materials and methods*

2.1 RO systems

Samples were collected from three full-scale water recycling plants denoted as A, B and C located in Australia. In these plants, prior to RO filtration, secondary treated effluent is first pretreated by either microfiltration (MF) or ultrafiltration (UF). At plant A and B, ferric chloride is used as coagulant. In all three plants, pre-formed chloramines were added to the process prior to MF or UF filtration to mitigate biofouling on the RO membranes (Figure 9.1). The RO membranes used in these plants are from three different manufacturers. The membranes used in these three plants are thin film composite with a polyamide skin layer. They were characterized by similar salt (NaCl) rejection and water permeability [183]. The process flow diagrams of these RO systems are shown in Figure 9.1. Samples were collected from plant A during cool (A-1) and warm (A-2) weather periods. At plant A, chloramination is normally added downstream of the coagulation process, which was the configuration when sampling campaign A-1 was conducted (Figure 9.1). During an extended period of warm weather when it is necessary to control algal growth during the coagulation process, chloramination can be added upstream of the coagulation process. Plant A was operated in this configuration when the sampling campaign A-2 took place (Figure 9.1). Unlike plants B and C, plant A is equipped with a booster pump prior to the third stage to maintain the same average

flux at all three stages (Figure 9.1). All three systems produce reclaimed water for industrial and/or agriculture uses. Plants A and B were designed for a possible indirect potable water recycling application where high quality reclaimed water can be used to replenish an existing reservoir for drinking water supply. Thus, the UV-H₂O₂ process was also installed after the RO process at these systems for the destruction of residual NDMA in the RO permeate. Similar installation using the UV-H₂O₂ process specifically for the removal of residual NDMA in the RO permeate can also be found elsewhere [18, 20].

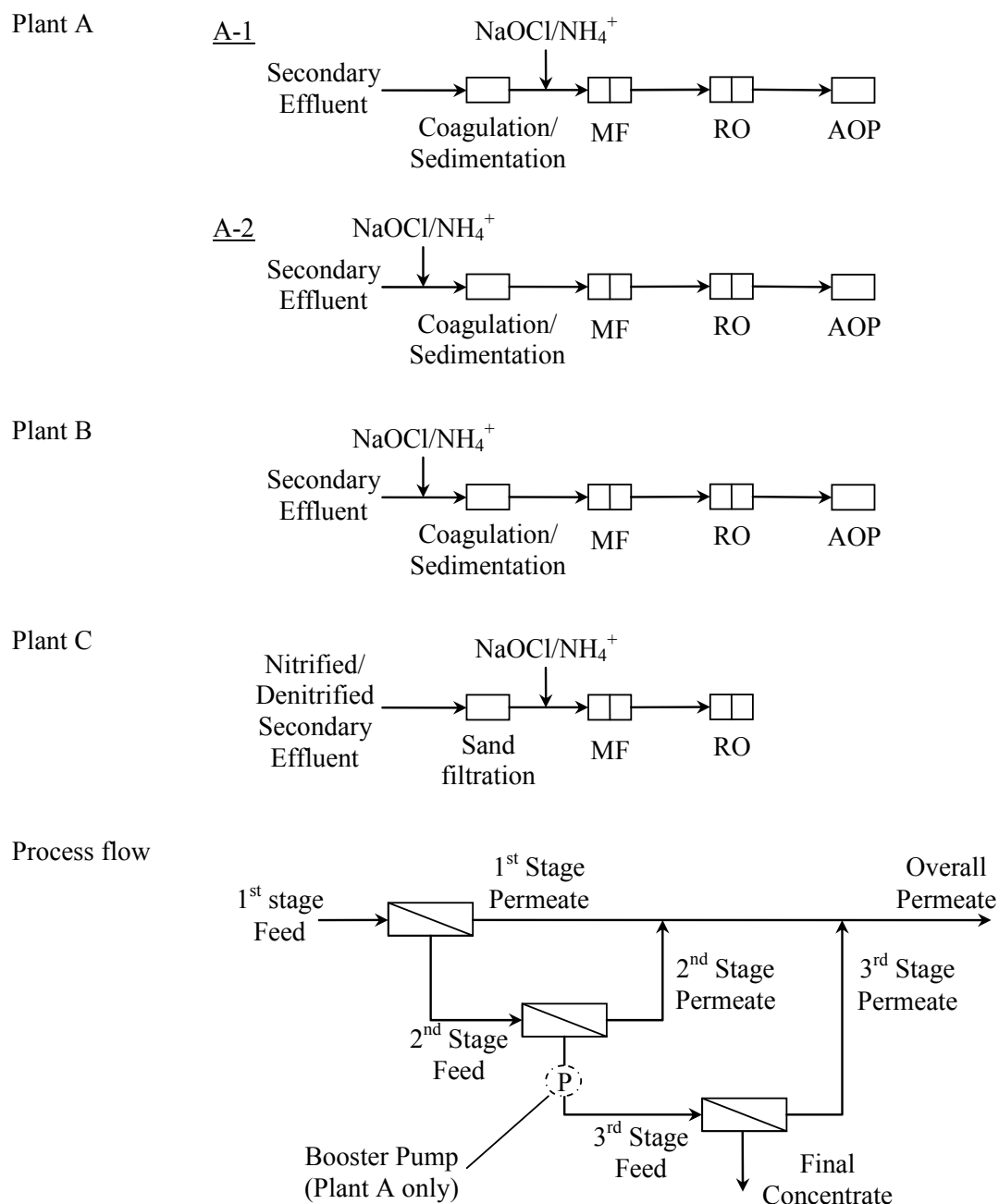


Figure 9.1: Treatment processes and process flow diagrams of the three RO plants.

2.2 Sampling protocol

RO feed and permeate samples were collected from each RO stage (Figure 9.1). From each sampling point, one sample was collected from plant C in May and December 2012 and duplicate samples were collected in all other sampling events for N-nitrosamine analysis. These samples (500 mL) were stored in amber glass bottles.

Deuterated N-nitrosamines corresponding to each target compound were used as isotope labelled surrogates. These deuterated N-nitrosamines were purchased from CDN Isotopes (Pointe-Claire, Quebec, Canada). A surrogate stock solution containing 100 µg/L of each deuterated N-nitrosamine was prepared in pure methanol. Immediately after sample collection, the surrogate stock solution was added to the sampling bottles to obtain 50 ng/L of each isotope labelled N-nitrosamine. Analytical grade sodium thiosulfate (100 mg/L) was also added to the sample as quenching reagent to prevent any further NDMA formation during transportation and sample processing. From each sampling point, 20 mL sample was collected in plastic bottles for the analysis of cations and boron and 100 mL sample was collected in amber glass bottle for the analysis of anions and total organic carbon. Operating conditions and feed temperature of the RO systems on the sampling day are summarised in Table 9.1. The difference in feed temperature between the entrance and exit of each RO unit was less than 1 °C.

Table 9.1: Operating conditions at each sampling event.

Sampling Tag	Plant A		Plant B		Plant C	
	A-1	A-2	B	C-1	C-2	C-3
Sampling date	Jun 2012	Dec 2012	Jun 2012	May 2012	Dec 2012	Feb 2013
Feed temperature [°C]	19.4	28.0	22.1	19.0	22.4	24.1
Average flux [L/m ² h]	Overall	17.7	17.7	18.1	17.5	17.5
	Stage 1	17.7	17.7	n.a.	n.a.	n.a.
	Stage 2	17.6	17.6	n.a.	n.a.	n.a.
	Stage 3	17.8	17.8	n.a.	n.a.	n.a.
Recovery [%]	Overall	85.0	85.0	85.0	85.0	85.0
	Stage 1	48.6	48.6	n.a.	n.a.	n.a.
	Stage 2	47.1	47.1	n.a.	n.a.	n.a.
	Stage 3	44.9	44.9	n.a.	n.a.	n.a.
Operating time since the last chemical cleaning [months]	2	4	3	7	13	15

n.a.: data not available

2.3 Analytical technique

N-nitrosamine concentrations were analysed using an analytical method described in Chapter 3, Section 5.1. Basic analytical techniques are described in Chapter 3, Section 5.2.

2.4 Calculation

The rejection of N-nitrosamines and other solutes in each RO stage and combined RO stages was calculated using the following equations.

$$\text{Each stage rejection } R_i [\%] = \left(1 - \frac{C_{pi}}{C_{fi}} \right) \times 100 \quad (1)$$

$$\text{Overall rejection } R_T [\%] = \left(1 - \frac{C_{pT}}{C_{f1}} \right) \times 100 \quad (2)$$

where i is the number of stage, C_{pi} is the solute concentration in the RO permeate of the stage i , C_{fi} is the solute concentration in the RO feed of the stage i , and C_{pT} is the solute concentration in the combined RO permeate.

3 Results and discussion

3.1 Organic and inorganic constituent removal

The feed waters to the three RO systems differed markedly in TOC concentration and salinity(). In particular, the feed water to plant A exhibited a relatively high conductivity (salinity) at approximately 2.5 mS/cm. The sewer catchment of plant A is predominantly in a low-lying coastal area and is subjected to seawater intrusion. In fact, due to seawater ingresses, boron concentration in the feed to plant A was also higher compared to plant B and C. Despite the high feed water salinity, the quality of RO permeate at plant A was comparable to that at the other two RO systems. Most common cations and anions in the feed water can be rejected well by the RO membranes. As a result, the permeate at all three RO systems was of high quality with respect to basic water quality parameters. In agreement with the 85% water recovery (Table 9.1) of these RO systems, TOC and conductivity concentrations in the final concentrates were approximately six times greater than those in the feed waters (Table 9.2).

The rejections of TOC, cations (sodium, magnesium, potassium and calcium), anions (chloride, nitrate and sulphate) and boric acid by all three RO systems are summarised in Figure 9.2. Divalent ions (i.e. magnesium, calcium and sulphate) were consistently

removed over 99%. On the other hand, in agreement with a previous study by Bellona and Drewes [184], nitrate rejection was slightly lower than that of all other ions. The rejection of boric acid was in the range of 15-30%, which is consistent with the fact that boric acid has a small molecular size and is uncharged at pH below 8 [185]. The difference between the charged and uncharged solutes observed here can be attributed to the electrostatic interaction and size exclusion rejection mechanisms. In addition to size exclusion, electrostatic repulsion can also play an important role in the rejection of charged solutes by NF/RO membranes [3].

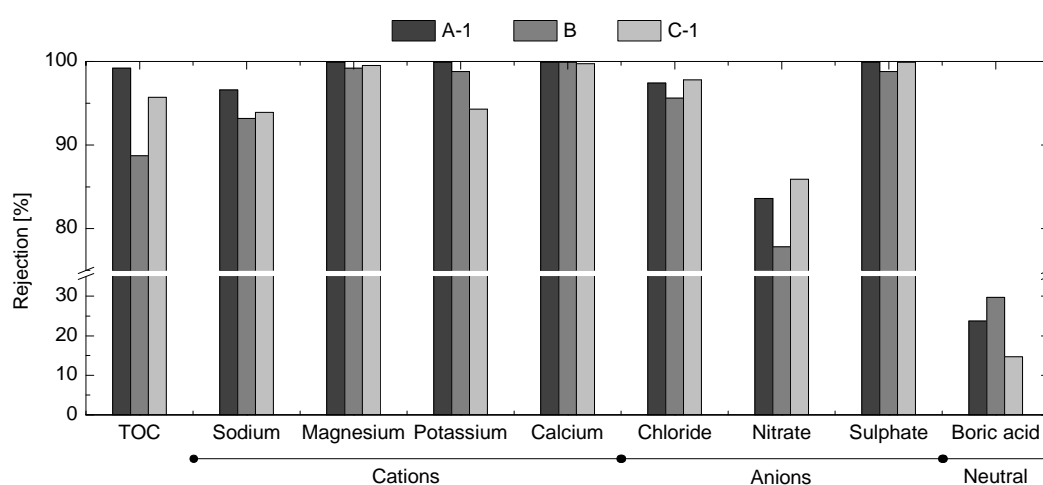


Figure 9.2: Overall rejection of TOC and inorganic constituents by RO membranes.

Table 9.2: Water quality of the RO feed, combined RO permeate and final RO concentrate.

Sampling Tag	RO feed						Combined RO permeate						Final RO concentrate					
	A-1	A-2	B	C-1	C-2	C-3	A-1	A-2	B	C-1	C-2	C-3	A-1	A-2	B	C-1	C-2	C-3
TOC [mg/L]	8.9	7.2	2.3	21	8.2	19.6	<0.5	<0.5	<0.5	0.7	<0.5	0.6	52	49	13	117	58	105
pH [-]	7.4	7.5	6.7	7.0	6.7	6.8	6.2	6.5	5.3	5.8	5.3	5.5	7.8	7.9	7.5	7.8	7.5	7.3
Conductivity [mS/cm]	2.34	2.59	1.26	0.95	0.92	0.85	0.07	0.13	0.07	0.04	0.03	44	13.2	14.3	7.2	5.5	5.4	4.8
Boron [mg/L]	0.14	n.a.	0.07	0.08	0.11	0.08	0.10	n.a.	0.05	0.07	0.11	0.06	0.35	n.a.	0.15	0.19	0.26	n.a.
Na ⁺ [mg/L]	313	496	144	93	118	119	11	48	10	6	6	5	2114	4033	952	592	875	998
Mg ²⁺ [mg/L]	35	n.a.	17	9	12	11	<1	n.a.	<1	<1	<1	<1	236	n.a.	121	63	94	90
K ⁺ [mg/L]	169	36	76	16	20	22	<1	6	<1	<1	3	<1	1245	370	542	105	149	177
Ca ²⁺ [mg/L]	71	n.a.	46	20	33	25	n.d.	n.a.	n.d.	n.d.	n.d.	n.d.	384	n.a.	337	134	253	195
Cl ⁻ [mg/L]	442	640	218	183	132	160	11	26	10	4	3	3	2895	4972	1347	1202	1150	1052
NO ₃ ⁻ [mg/L]	10	4	7	52	37	60	2	1	2	7	5	7	53	25	40	314	298	395
SO ₄ ²⁻ [mg/L]	63	118	46	38	25	42	n.d.	n.d.	0.6	n.d.	n.d.	n.d.	427	926	313	264	273	320

n.d.: not detectable. n.a.: not available.

3.2 N-nitrosamine removal

3.2.1 Occurrence of N-nitrosamines in the RO feed water

NDMA was detected in all RO feed water samples (Figure 9.3). NDMA concentrations (7-16 ng/L) detected in the RO feed solutions were below or only marginally higher than the value (i.e. 10 ng/L) in the final product water stipulated by the Australian Guidelines for Water Recycling, with samples from A-2 being the only exception. In A-2, chloramine was added upstream of the coagulation process and thus resulting in an increase in NDMA formation. Results in Figure 9.3 are consistent with those obtained from previous studies [12, 18, 27]. For typical water recycling plants where NDMA in raw water can be controlled to similar levels found in this study, reducing NDMA formation in the feed [27] and RO filtration can be implemented to meet the guideline value without relying on an additional subsequent treatment process such as AOP.

In addition to NDMA, several other N-nitrosamines (i.e. NPYR, NDEA, NPPI, NMOR and NDBA) were also detected in some but not all RO feed water samples (Figure 9.4). NMEA, which is the second lowest molecular weight compound among the N-nitrosamines investigated here, was not detected during any sampling campaign. Surprisingly, a comparatively high NMOR concentration (177-475 ng/L) was observed in the feed water at plant C. Compared to plant C, NMOR concentrations detected in the RO feed in plants A-2 and B configurations were low. It is noted that NMOR concentrations in A-1, B and C-1 were not reported due to unsatisfactory variation between duplicate samples and poor recovery of the isotopically labelled internal standard. In fact, a sampling program conducted in plant A from 2010 to 2012 revealed low NMOR concentrations (< 21 ng/L) in the RO feed (Figure 9.5) which indicates that a very high NMOR concentration like plant C has not been identified in plant A. Likewise, a sampling program conducted in plant B from 2009 to 2011 also showed a relatively low NMOR concentrations in the range from 9 to 57 ng/L in the RO feed (Figure 9.5). The results reported here suggest that high NMOR concentrations in RO feed may be site specific and could relate to certain industrial dischargers. Thus, further research is necessary to identify sources of NMOR within the catchment of plant C.

After each stage, concentrations of N-nitrosamines increased to quantifiable levels due to the concentration effect leading to higher feed concentrations in subsequent stages (Figure 9.3). As a result, the highest N-nitrosamine concentration was consistently observed in the final RO concentrate. For example, NDMA concentrations in the final RO concentrate were two to six times higher than those in the RO feed. Likewise, NMOR concentrations in the RO concentrate were approximately six times higher than those in the RO feed.

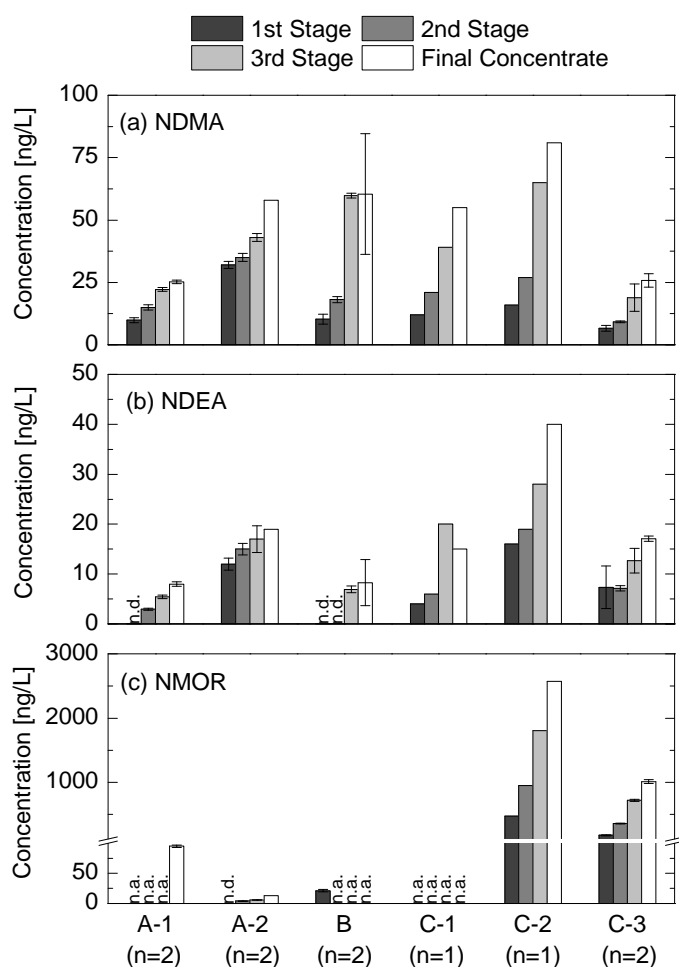


Figure 9.3: Concentrations of NDMA, NDEA and NMOR in the RO feed and RO concentrate in the three RO plants. (n.a.: data not available, and n.d.: not detectable in the feed). The number of replicate samples is shown in the parentheses. Values reported for A-1, A-2, B and C-3 are the average and range of duplicate measurements.

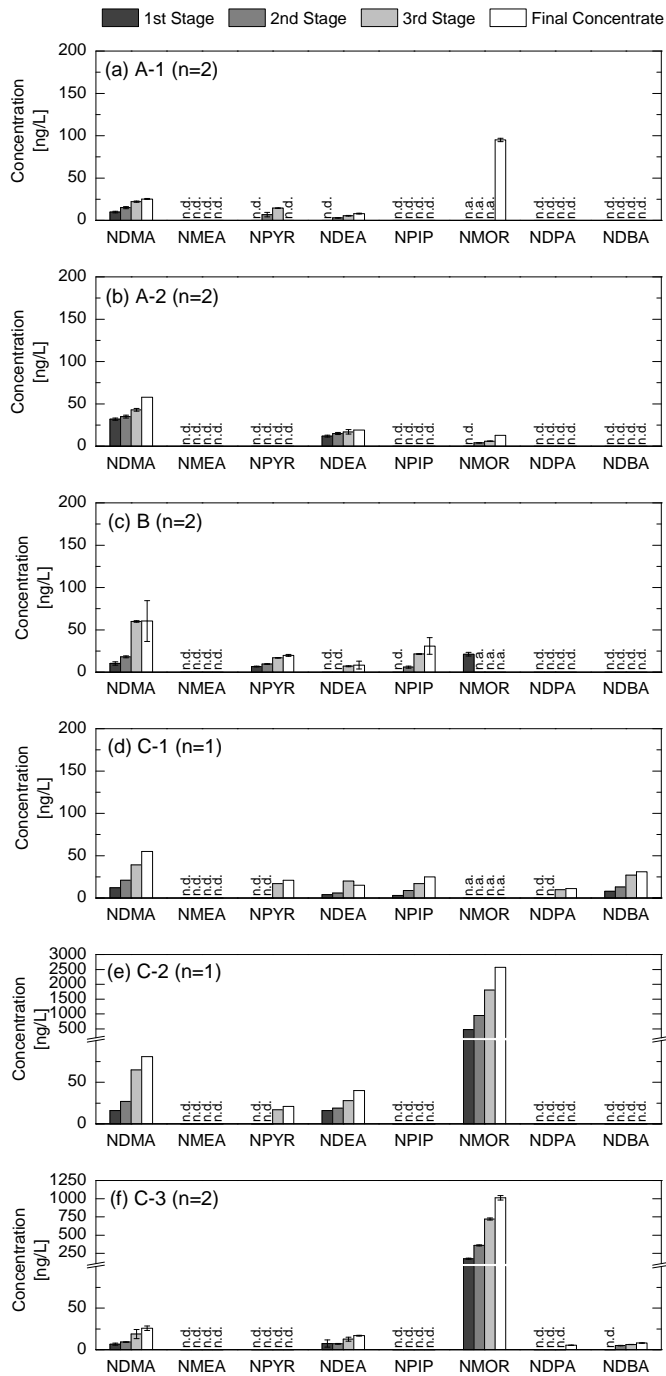


Figure 9.4: N-nitrosamine concentrations of the RO feed and RO concentrate in the three RO plants. n.a. represents that the data is not available and n.d. represents that the concentration was below their detection limits. The number of replicate samples is shown in the parentheses. Values reported for A-1, A-2, B and C-3 are the average and range of duplicate measurements.

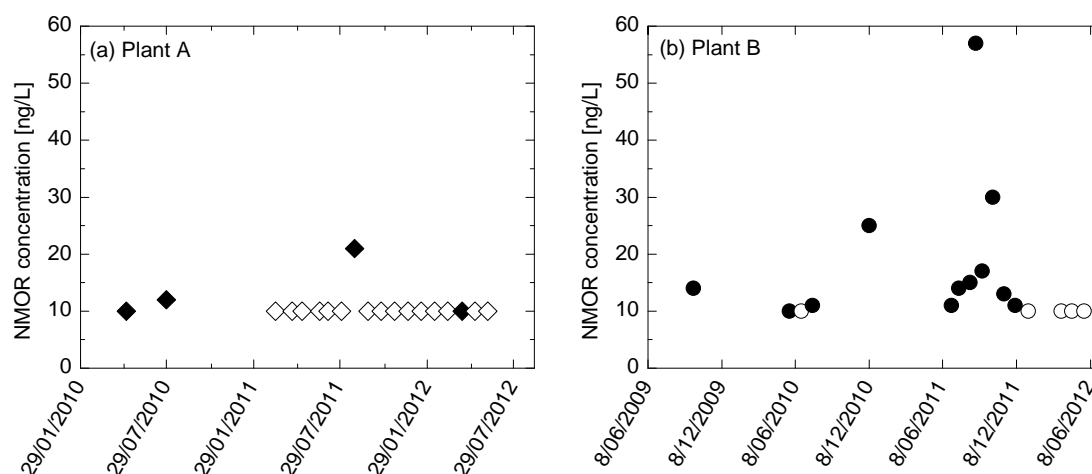


Figure 9.5: Historical record of NMOR concentrations in the RO feed in (a) plant A and (b) plant B. Open symbols indicate that NMOR concentration in the RO feed was below its detection limit (i.e. 10 ng/L).

3.2.2 *N-nitrosamine concentrations in the RO permeate*

NDMA concentrations in the RO permeate were detected above the detection limit (3 ng/L) at least once in samples from each plant (Figure 9.6). However, most of these detections did not exceed the guideline value of 10 ng/L, again with a sample collected from A-2 being the only exception. Of the seven remaining N-nitrosamines, only NDEA, NMOR and NDBA were detected in RO permeate samples (Figure 9.7). NMOR concentration in the overall RO permeate samples of plant C varied between 34 and 76 ng/L, which was comparatively higher than the other N-nitrosamines. This is because NMOR concentration in the RO feed of plant C was also higher than all other N-nitrosamines (Figure 9.3). Once again, NMOR concentrations in A-1, B and C-1 are noted as not available due to a large variation in analysed NMOR concentration between duplicate samples and poor recovery of the isotopically labelled internal standard.

In all cases, the concentration of N-nitrosamines in the RO permeate increased in later stages due to the increased concentration in the RO feed for each stage (Figure 9.6). As a result, N-nitrosamine concentrations in the overall RO permeate (i.e. the combined RO permeate of the first, second and third stages) were higher than those in the first stage. The results here indicate that rejection estimates obtained from laboratory-scale systems, which are operated at low water recovery, may result in an underestimation of

N-nitrosamine concentrations in the RO permeate. Although the permeation of NDMA through RO membranes can be managed by a subsequent UV-H₂O₂ based AOP, little is known about its removal efficiency for NMOR and other N-nitrosamines. The results reported here also suggest that, in addition to NDMA, it is necessary to monitor the concentration of several other N-nitrosamines particularly NMOR in secondary treated effluent and the corresponding RO permeate.

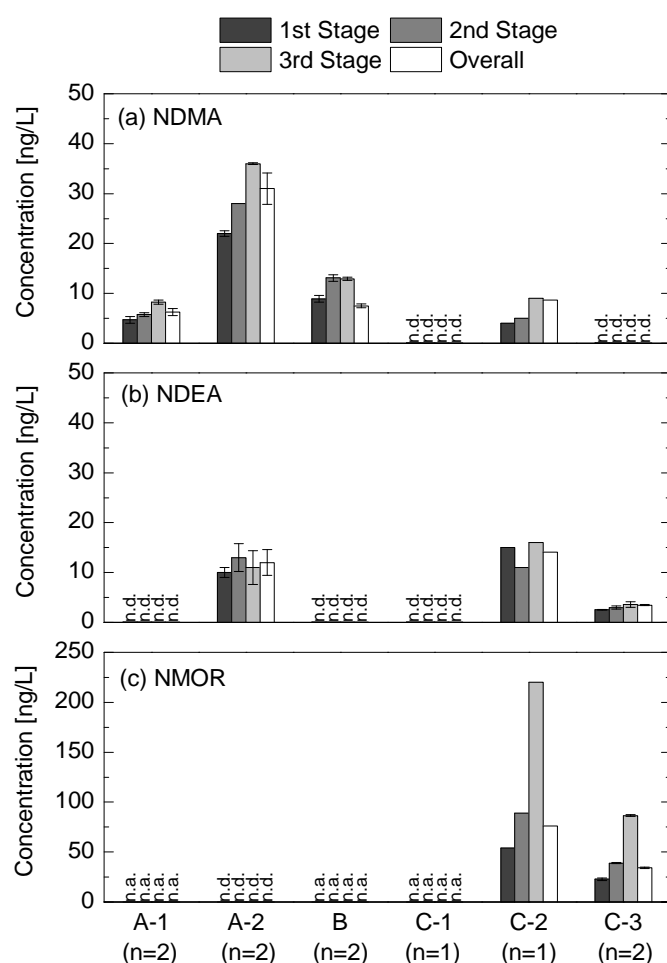


Figure 9.6: Concentrations of NDMA, NDEA and NMOR in the RO permeate in the three RO plants. n.a. represents that the data is not available and n.d. represents that the concentration was below their detection limits. The number of replicate samples is shown in the parentheses. Values reported for A-1, A-2, B and C-3 are the average and range of duplicate measurements.

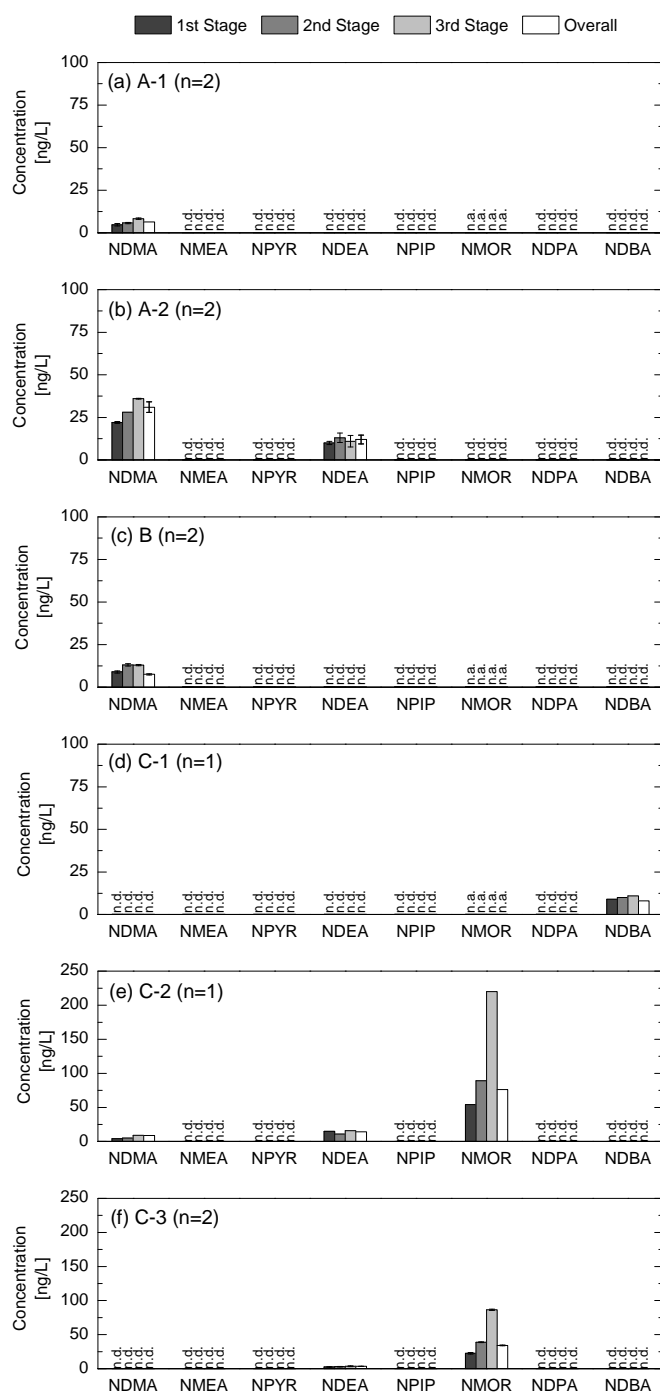


Figure 9.7: N-nitrosamine concentrations of the RO permeate in the three RO plants. n.a. represents that the data is not available and n.d. represents that the concentration was below their detection limits. The number of replicate samples is shown in the parentheses. Values reported for A-1, A-2, B and C-3 are the average and range of duplicate measurements.

3.3 Rejections by RO membranes

3.3.1 Overall rejection

Overall NDMA rejections varied significantly with a range of 4-47% among the three RO systems (Figure 9.8). In plant A, two distinct overall NDMA rejections (36 and 4%) were observed during different sampling occasions. Plant A was operated under the same operating conditions (e.g. recovery and permeate flux) during the two sampling events (i.e. A-1 and A-2), but their feed water temperature differed (19.4 and 28.0 °C) (Table 9.1). A previous laboratory-scale study revealed that an increase in feed temperature from 20 to 30 °C resulted in a reduction of NDMA rejection from 49 to 24% [150].

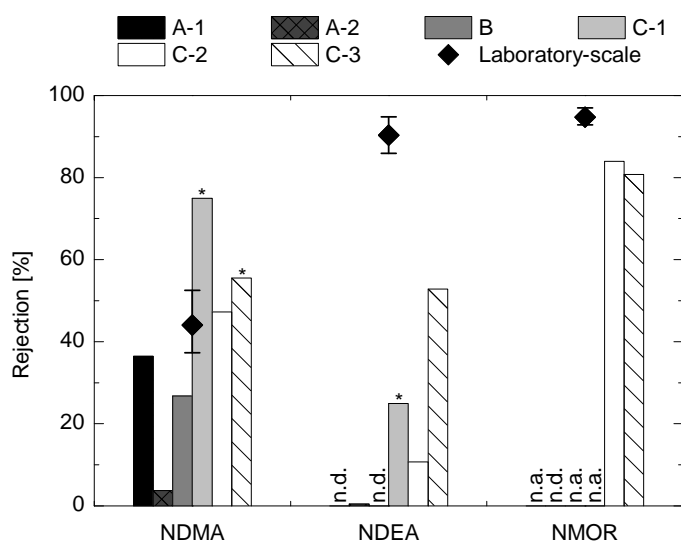


Figure 9.8: Rejection of NDMA, NDEA and NMOR for the present study and laboratory-scale study by Fujioka et al. (2013b). Solid diamond symbols represent the average of rejections by four RO membranes and error bars indicate the maximum and minimum rejections. Bar with asterisk (*) indicates that the rejection was calculated based on the detection limit of N-nitrosamine in permeate (n.a.: data not available, and n.d.: not detectable in the feed).

NDEA rejection at plant A and C varied between zero and 53% (Figure 9.8). This is considerably lower than the values (86-95%) reported in a recent laboratory-scale study using low pressure RO membranes and synthetic clean water solutions [150]. Although the mechanism underlining this phenomenon is still unknown, the results reported here

indicate that RO filtration in treated wastewater can result in a significant reduction in NDEA rejection. In fact, in a laboratory-scale study Fujioka et al. [163] reported a considerable deterioration in NDEA rejection using tertiary effluent as feed water. Overall, NMOR rejection was high and each stage exhibited rejection ranges of 87-91% (Figure 9.8) which is consistent with previous laboratory-scale studies [150, 163].

3.3.2 Rejection at each stage

In plant B, 16 inch membrane elements were used whereas 8 inch membrane elements were used in plants A and C. Thus, the hydraulic distribution of plant B can differ significantly from that of plant A and C. At plant B, a significant variation in NDMA rejection (14-78%) was observed among the three RO stages (Figure 9.9). Changes in the permeate flux after each filtration stage may contribute to this variation to some extent (Fujioka et al. 2012b). However, because permeate flux was not monitored in each individual stage at plant B, it was not possible to confirm this hypothesis. Rejection of N-nitrosamines was further investigated using the two sampling events at plant A, focusing on the difference in NDMA rejection among the three stages. As RO filtration progressed, feed pH increased slightly and feed conductivity increased significantly for both sampling events (Figure 9.10). During the first sampling event (A-1) an increase in NDMA rejection from the first stage to third stage was observed. In general, an increase in feed conductivity (or ionic strength) results in a decrease in N-nitrosamine rejection [150]. However, the current study revealed an opposite trend which indicates that another factor such as membrane fouling may have been developed more extensively in later stages and may have compensated the decreased trend of NDMA rejection. On the other hand, during the second sampling event (A-2), NDMA rejections decreased as RO filtration progressed to later stages (Figure 9.10). The results reported here indicate that NDMA rejections among three RO stages may vary significantly even when operating conditions (i.e. permeate flux and recovery) were maintained constant.

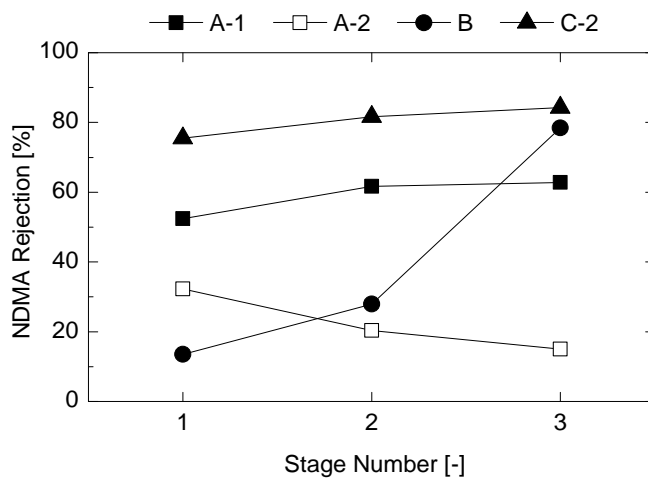


Figure 9.9: Rejection of NDMA at each stage of the three RO plants.

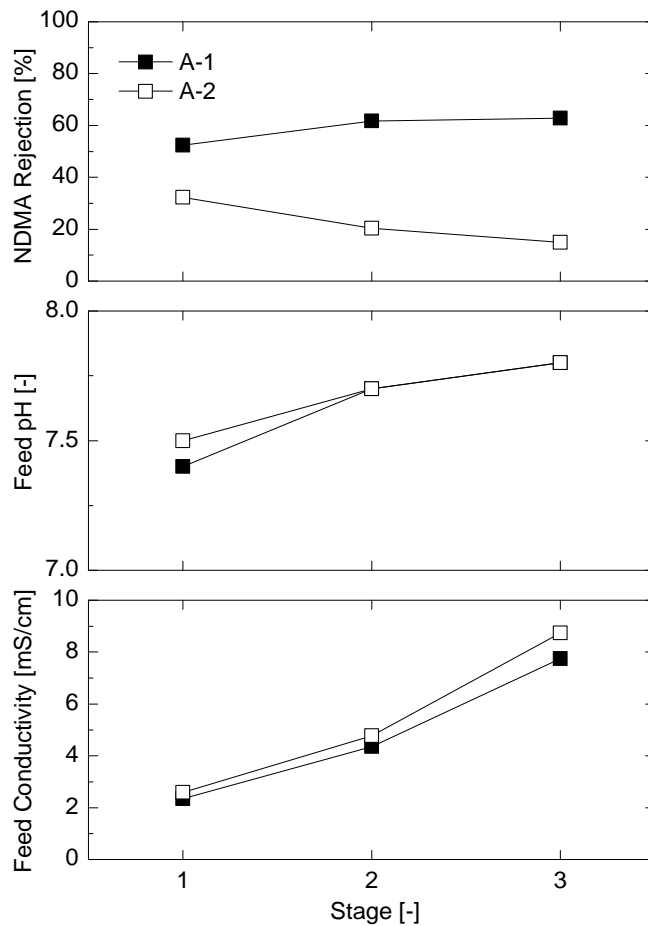


Figure 9.10: NDMA rejection, feed pH and feed conductivity at each stage of RO plant A.

4 Conclusions

NDMA was detected in all feed samples at the three full-scale RO trains investigated in this study. Although most other N-nitrosamines were not detected in the RO feed, several N-nitrosamines became detectable as the feed was further concentrated after each filtration stage. N-nitrosamine concentrations in the final RO concentrate were up to six times higher than those in the RO feed. As a notable exception, one of the three plants exhibited high NMOR concentrations (177-475 ng/L) in the feed, resulting in high NMOR concentrations (34-76 ng/L) in the permeate. In most cases, NDMA was detected below the Australian guideline value in the RO permeate. Overall rejection of NDMA and NDEA among the three RO systems varied significantly with a range of 4-47% and 0-53%, respectively. NDMA rejections among three RO stages also exhibited a significant variation in several cases. These rejection variations may have resulted from the difference in feed temperature and possibly membrane fouling. These findings suggest that N-nitrosamine rejection estimates derived from laboratory-scale flat-sheet membrane studies, which are operated at very low water recovery, may not be representative of full-scale operation. On the other hand, overall NMOR rejections were equally high with a range of 81-84%. The findings of this study provide insights for potential variations in N-nitrosamine rejection among different RO systems and RO stages.

Chapter 10

Mathematical model development and validation

This chapter has been published as:

T. Fujioka, S.J. Khan, J.A. McDonald, A. Roux, Y. Poussade, J.E. Drewes, L.D. Nghiem, *Modelling the rejection of N-nitrosamines by a Spiral-Wound Reverse Osmosis System: Mathematical model development and validation*, **J. Membr. Sci.**, **454** (2014) 212-219.

1 Introduction

Modelling the rejection of N-nitrosamines under various conditions is essential for the design of RO plants and compliance monitoring. NDMA and several other N-nitrosamines have been frequently detected in the feed water to RO treatment at concentration higher than the regulatory levels [122]. In addition, N-nitrosamine rejection by RO membranes is sensitive to operating conditions and feed solution characteristics [150]. Difficulties associated with analytical determination of N-nitrosamines in the permeate at regulatory concentrations (i.e. 1 to 10 ng/L) [18, 67, 73] also underscore the need for a model that can accurately describe the rejection of N-nitrosamines. N-nitrosamine concentrations in aqueous samples can be determined by chromatography (GC) or high pressure liquid chromatography (HPLC) with tandem mass spectrometry (MS/MS) detector. However, the number of commercial laboratories capable of trace level N-nitrosamine analysis is still limited and regular monitoring of N-nitrosamines remains difficult and expensive. Thus, a capacity to describe and predict the rejection of N-nitrosamines by the RO process is particularly useful for the management of these trace organic chemicals in water recycling applications.

The rejection of inorganic salts by multi-stage RO membrane systems can be simulated with a high level of accuracy using commercially available RO design software packages (e.g. IMSDesign, TorayDS/DS2, and ROSA provided by Hydranautics, Toray, and Dow/FilmTec, respectively). The development of mathematical models for

simulating specific trace organic and inorganic chemicals by spiral wound RO membrane systems has been reported in several recent studies. Kim and co-workers have successfully developed a model for predicting boron rejection by applying the irreversible thermodynamic principle and sub-dividing a spiral wound element into a number of small sub-sections [186-188]. Using a similar approach, Verliefde et al. [189] have also developed a full-scale rejection model for several pharmaceutically active compounds (PhACs) using nanofiltration (NF) membranes. These models significantly enhance our understanding of the permeation of boron and PhACs through RO membranes under realistic conditions. However, to date, there have yet been any software packages or mathematical models that can simulate the rejection of N-nitrosamines.

The aim of this study was to develop a mathematical model to predict the rejection of N-nitrosamines by RO systems under a range of operating conditions. The developed model was validated using experimental data obtained from a pilot RO system. The potential application of this model for predicting N-nitrosamine rejection at full-scale level was also discussed.

2 *Theoretical background*

2.1 Membrane element characteristics

A commercial spiral-wound element has one or several membrane leaves. Each leaf consists of two flat sheet membranes sealed on three sides with the forth side attached to a perforated tube called the permeate collector. The membrane leaf is wound around the permeate collector. As a result, each spiral-wound element can essentially be presented by a large flat sheet membrane. In this study, each element is geometrically described with the length (L), width (W) and feed channel height (h_b) (Figure 10.1). On the other hand, the irreversible thermodynamic principle can be used to model the rejection of N-nitrosamines by a small flat sheet membrane for a given hydrodynamic condition. Thus, the irreversible thermodynamic principle can also be used to model solute rejection by a spiral wound element. This can be done by sub-dividing the membrane area on each element smaller sections of the same size and using fluid mechanics to calculate and define the hydrodynamic condition for each sub-section. In this study, the membrane

area on one each element is divided into 20 sub-sections ($m = 20$) in a longitudinal direction where each sub-section length (Δx) is described as:

$$\Delta x = \frac{L}{m} \quad (1)$$

It is noteworthy that the length of each sub-section selected here is similar to that of the flat sheet membrane coupon used in the laboratory-scale study. The membrane surface area attached to the feed spacers is assumed to be 10% and this area is not utilised for filtration. Thus, the active surface area in each sub-section (ΔS) is defined as:

$$\Delta S = \frac{0.9S}{m} \quad (2)$$

The cross-section area of the feed channel (ΔS_c) is expressed as:

$$\Delta S_c = Wh_b \quad (3)$$

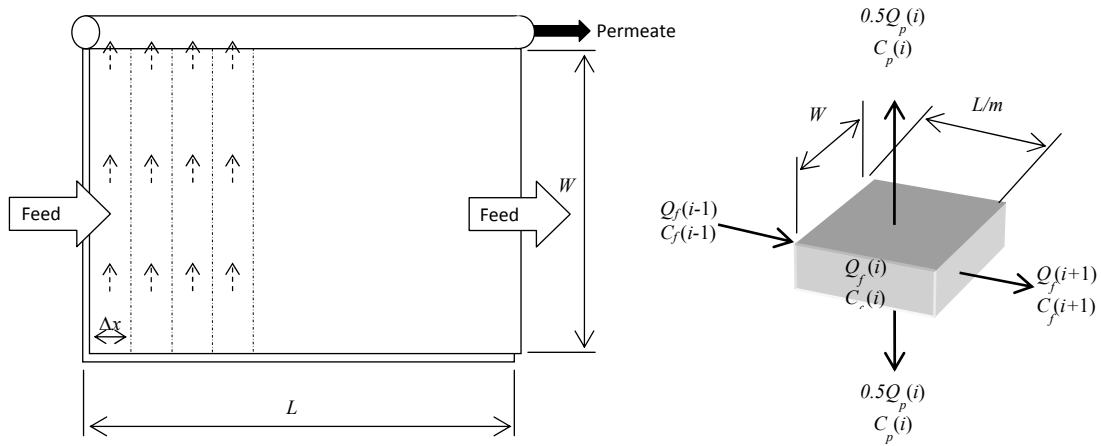


Figure 10.1: Representation of a spiral-wound RO element as flat sheet configuration including the mass balance of a flat sheet sub-section.

2.2 Hydrodynamics

The local permeate flux ($J_p(i)$), local permeate flow rate ($Q_p(i)$) and the overall permeate flow rate of a membrane element ($Q_{p,t}$) are calculated using equations 4 - 6.

$$J_p(i) = L_p \left(\{P_f(i) - P_p(i)\} - \Delta\pi(i) \right) \quad (4)$$

$$Q_p(i) = J_p(i) \times \Delta S \quad (5)$$

$$Q_{p,t} = \sum_{i=1}^m Q_p(i) \quad (6)$$

where L_p = pure water permeability which is obtained from bench-scale tests. Because permeate pressure (P_p) is negligible compared to feed pressure (P_f), local permeate pressure ($P_p(i)$) is assumed to be zero in this study. Local osmotic pressure ($\pi(i)$) shown in equation 4 is computed with feed solution temperature (T) and molar concentrations of ions ($m_{salt}(i)$).

$$\pi(i) = 1.19(T + 273) \sum_1^i m(i) \quad (7)$$

Concentration of the solute ($m_{salt}(i)$) increases in the feed in the subsequent sub-sections since the solute is retained by the membrane. Changes in solute concentration can be calculated using the following equation:

$$m_{salt}(i+1) = m_{salt}(i) \frac{Q_f(i) - (1 - R_{salt}) \times Q_p(i)}{Q_f(i+1)} \quad (8)$$

where $Q_f(i)$ = local feed flow rate and R_{salt} = salt rejection. In the model, overall feed flow rate measured in the pilot system is used as the feed flow rate of the first sub-section $Q_f(1)$. Local feed flow rate ($Q_f(i+1)$) is calculated from the feed and permeate flow rates of the previous sub-section ($Q_f(i)$):

$$Q_f(i+1) = Q_f(i) - Q_p(i) \quad (9)$$

Using the local feed flow rate ($Q_f(i)$), local bulk velocity of the feed within the feed channel ($U_b(i)$) is defined as:

$$U_b(i) = \frac{Q_f(i)}{\Delta S_c} \quad (10)$$

The pressure drop in the feed stream ($\Delta P_f(i)$) and overall pressure drop of an element in the feed stream ($\Delta P_{f,t}$) is calculated using the following formula [190, 191]:

$$\Delta P_f(i) = \frac{1}{2} f_{fb} \rho(i) U_b^2(i) \frac{\Delta x}{d_h} \quad (11)$$

$$\rho(i) = 498.4 M + \sqrt{248400 M^2 + 752.4 M \Sigma C_{salt}} \quad (12)$$

$$M = 1.0069 - 2.757 \times 10^{-4} T \quad (13)$$

$$\Delta P_{f,t} = \sum_{i=1}^m \Delta P_f(i) \quad (14)$$

where f_{fb} = feed friction parameter, $\rho(i)$ = local solution density [192], T = feed temperature and d_h = hydraulic diameter ($d_h = 2h_b$) [190]. Friction parameter (f_{fb}) is determined by an approach minimising the difference between the experimentally modelled and measured overall pressure drops. Feed pressure which is experimentally measured at the entrance of the first membrane element is used as the feed pressure of the first sub-section in the model. Then local feed pressure in the next sub-section ($P_f(i+1)$) is calculated from the feed pressure ($P_f(i)$) and the feed pressure loss ($\Delta P_f(i)$) of the previous section:

$$P_f(i+1) = P_f(i) - \Delta P_f(i) \quad (15)$$

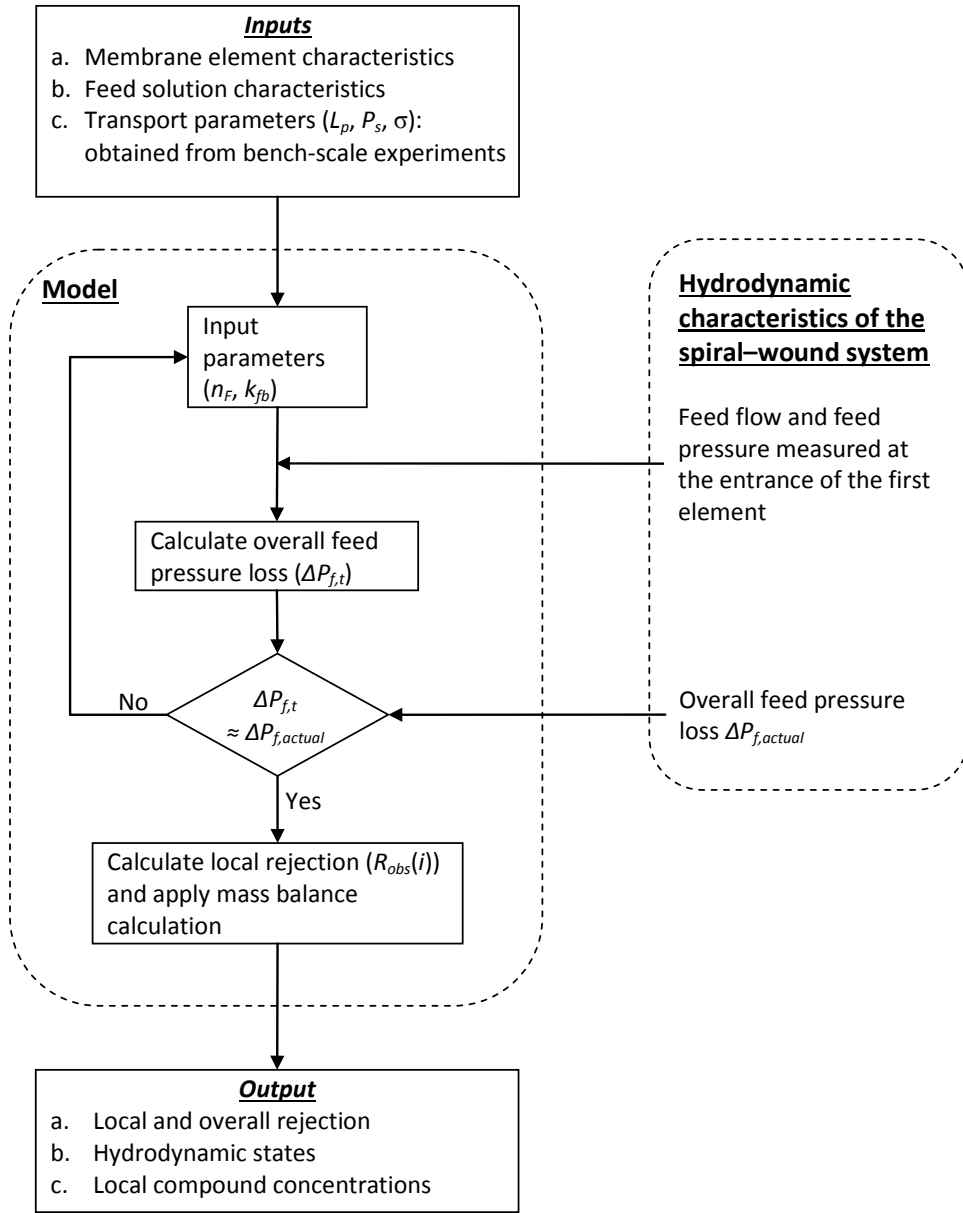


Figure 10.2: Schematic diagram of the iteration procedure to determine the pressure drop in a spiral-wound element and the subsequent rejection calculation.

2.3 Solute permeation through membranes

Local real rejection ($R_{real}(i)$) can be expressed by the Spiegler-Kedem equation [129]:

$$R_{real}(i) = 1 - \frac{C_p(i)}{C_m(i)} = \frac{\sigma(1 - F(i))}{(1 - \sigma F(i))} \quad (16)$$

$$F(i) = \exp\left(-\frac{(1-\sigma)}{P_s} J_p(i)\right) \quad (17)$$

where P_s = permeability coefficient and σ = reflection coefficient both of which can be obtained from bench-scale experiments. Local observed rejection ($R_{obs}(i)$) can be calculated with the local real rejection ($R_{real}(i)$) and local mass transfer coefficient ($k(i)$) as follows [193]:

$$R_{obs}(i) = \frac{R_{real}(i)}{(1 - R_{real}(i)) \times \exp\left(\frac{J_p(i)}{k(i)}\right) + R_{real}(i)} \quad (18)$$

$$k(i) = 0.753 \left(\frac{K}{2-K}\right)^{0.5} \left(\frac{D}{h_b}\right) Sc(i)^{-1/6} \left(\frac{Pe h_b}{\Delta L}\right)^{0.5} \quad (19)$$

where K = efficiency of mixing net ($K = 0.5$), D = diffusion coefficient Sc = Schmidt number ($\mu/\rho(i)D$), Pe = Peclet number ($Pe = 2h_b U_b(i)/D$) and μ = viscosity of feed solution.

$$\mu = 2.141 \times 10^{-5} \times 10^{\frac{247.8}{T-140}} \quad (20)$$

Once the local observed rejection ($R_{obs}(i)$) is determined, the local permeate concentration ($C_p(i)$) can also be calculated using local feed concentration ($C_f(i)$) using equation 21. Then local feed concentration in the following sub-section ($C_f(i+1)$) can be expressed by equation 22. The overall permeate concentration of an element j ($C_p(j)$) can be calculated by totalling mass transport in all sub-sections of the membrane element as described in equation 23.

$$C_p(i) = C_f(i)(1 - R_{obs}(i)) \quad (21)$$

$$C_f(i+1) = \frac{Q_f(i)C_f(i) - Q_p(i)C_p(i)}{Q_f(i+1)} \quad (22)$$

$$C_p(j) = \frac{\sum_{i=1}^m C_p(i) Q_p(i)}{\sum_{i=1}^m Q_p(i)} \quad (23)$$

Because permeate streams from each membrane element blend in the combined permeate stream, solute rejection by a certain number (n) of membrane elements need to be evaluated using the combined concentration. The combined permeate concentration of n elements ($C_p(n)$), combined observed solute rejection of n elements ($R_{obs}(n)$), and recovery of n elements ($R_c(n)$) can be calculated as follows:

$$C_p(n) = \frac{\sum_{j=1}^n C_p(j) Q_p(j)}{\sum_{j=1}^n Q_p(j)} \quad (24)$$

$$R_{obs}(n) = \frac{C_f(j) - C_p(n)}{C_f(j)}, \quad j = 1 \quad (25)$$

$$R_c(n) = \frac{\sum_{j=1}^n Q_p(j)}{Q_f(j)}, \quad j = 1 \quad (26)$$

The iterative procedure to determine the hydrodynamic constants (Eqs 1 – 15) and solute transport following the irreversible thermodynamic principle described Eqs 16 – 26 above provide the basis for this mathematical model as schematically summarised in Figure 10.2.

3 Materials and methods

3.1 Pilot-scale filtration system and RO element

A pilot-scale filtration system was used (Figure 3.2). Specification of the bench-scale filtration system is described in Chapter 3, Section 4.2. Three ESPA2-4040 (Hydranautics, Oceanside, CA, USA) spiral wound elements were used. The ESPA2-4040 membrane element has an equivalent length of 1.016 m, actual membrane sheet length (L) of 0.9 m, membrane area (S) of 7.9 m², and feed channel height (h_b) of 6.60 ×

10^{-4} m. According to the manufacturer, permeability of individual membrane element may vary by up to 25%. It is noteworthy that the ESPA2 membrane is commonly deployed in full-scale RO installations in the USA and Australia for water reuse application [18, 86].

3.2 Chemicals

Properties of eight N-nitrosamines are summarized in Table 3.2 (Chapter 3). Key physicochemical properties and transport parameters (i.e. diffusion coefficient D and permeability coefficient P_s) of these N-nitrosamines through the ESPA2 membrane were obtained from a previous study (Chapter 7).

3.3 Filtration experiments

Prior to the first filtration experiment, the membrane system was operated at approximately 1000 kPa for 12 hours using 100 L Milli-Q water. Following the start-up stage, the Milli-Q water in the feed was conditioned at 20 mM NaCl, 1 mM CaCl_2 and 1 mM NaHCO_3 to simulate the background electrolyte composition typically found in treated wastewater. The stock solution of N-nitrosamines was also introduced into the feed to obtain approximately 250 ng/L of each N-nitrosamine. The permeate flux was then adjusted to 10 $\text{L/m}^2\text{h}$, and stepwise increased up to 30 $\text{L/m}^2\text{h}$. The overall system recovery was adjusted to 25% because only three membrane elements were used. During the experiments, feed pressure was measured at the entrance of the each element and the exit of the third element. The system was operated for at the least 12 h before the first samples were taken for analysis to ensure the separation efficiency has been stabilised. A previous laboratory-scale study revealed no significant changes in the rejection of almost all N-nitrosamines after one hour of filtration [150]. From each sampling point, a sample of 200 mL was collected using amber glass bottles for N-nitrosamine analysis. Immediately after the sample collection, the surrogate stock solution was added to the sampling bottles to obtain 50 ng/L of each isotope labelled N-nitrosamine. The feed temperature during the experiments was kept at $20 \pm 0.1^\circ\text{C}$. It is noteworthy that the overall recovery of each vessel (or stage) which holds six to seven RO elements is about 50% in most full-scale wastewater recycling RO plants.

3.4 Analytical technique

N-nitrosamine concentrations were analysed using an analytical method described in Chapter 3, Section 5.1.

4 Results and discussion

4.1 Determination of model parameters

The pressure of each sub-section within the membrane system was calculated from the pressure of the previous sub-section and the local pressure drop. The local pressure drop ($\Delta P(i)$) was determined using equation 11. The feed friction parameter (f_{fb}), which is dependent upon the geometry of membrane element and operating conditions [190, 191], was obtained using the iteration procedure outline in Figure 10.2 to minimise the difference between the modelled and observed feed pressure to less than 5% at an average permeate flux of 10, 20, and 30 Lm²/h (Figure 10.3). In this study, f_{fb} values of 10, 20 and 30 Lm²/h were 3.9, 4.3 and 5.5, respectively. Knowing the membrane permeability, the local permeate flux can then be calculated based on the local pressure. Subsequently, the overall permeate flux can also be calculated. In fact, the simulated permeate flux only deviated slightly from the observed value at the applied pressure of 1.0 MPa (Figure 10.4). These results indicate that the model can adequately simulate the hydrodynamic condition (i.e. feed pressure and permeate flow) within the RO membrane elements. The small deviation observed in Figure 10.4 may be attributed to the fact that the determined f_{fb} value was used for the entire system as well as the difference in permeability of membranes that were used in the fundamental and pilot-scale experiments. There can be some variation in permeability between different areas of the same membrane element or between different batches of production (Chapter 3, Section 2). As the applied pressure increases, the pressure drop across the membrane element increases resulting in a larger deviation between the simulated and experimentally obtained values.

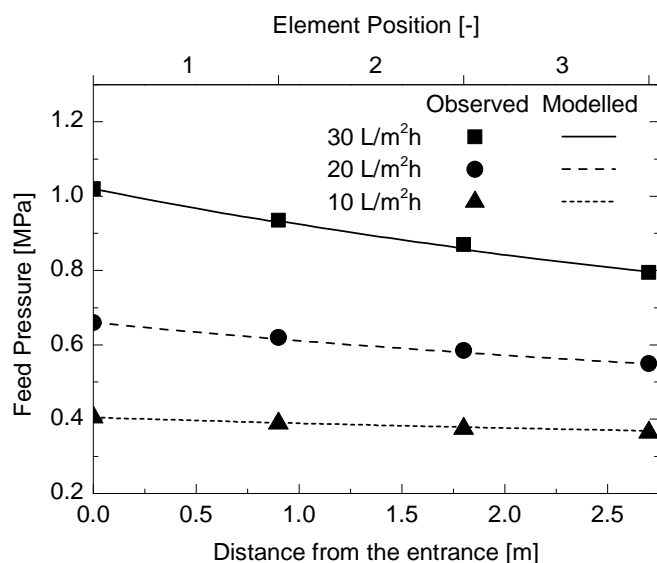


Figure 10.3: Observed and modelled feed pressure within three RO elements (overall permeate flux = 10, 20 and 30 L/m²h; feed solution contains 20 mM NaCl, 1 mM NaHCO₃, and 1 mM CaCl₂; feed temperature = 20.0 ± 0.1 °C).

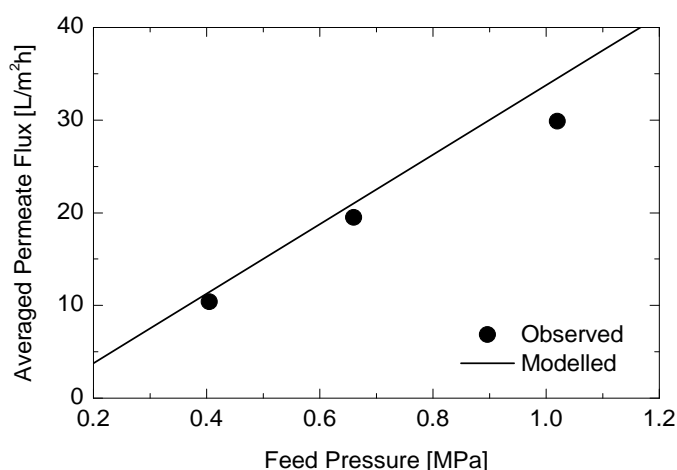


Figure 10.4: Observed and modelled overall permeate flux as a function of the feed pressure at the system entrance (feed solution contains 20 mM NaCl, 1 mM NaHCO₃, and 1 mM CaCl₂; feed temperature = 20.0 ± 0.1 °C).

4.2 N-nitrosamine rejection

All N-nitrosamines used in this study are uncharged in the tested solution (pH 8). In general, the rejection of uncharged solutes by NF/RO membranes generally increases as permeate flux increases [189]. A similar trend using N-nitrosamines was also reported in a previous laboratory-scale study by Fujioka et al. [150]. As expected, the simulated rejection values of three lowest molecular weight N-nitrosamines (i.e. NDMA, NMEA

and NPYR) increased when the overall (system) permeate flux increased (Figure 10.5). Among these three N-nitrosamines, modelled NDMA rejection showed the most significant increase from 31 to 54% with increasing overall permeate flux from 10 to 30 L/m²h, respectively. The impact of permeate flux on N-nitrosamine rejection was less significant as their molecular weights increase. The modelled rejections were comparable with the observed rejections at three different overall permeate fluxes (i.e. 10, 20 and 30 L/m²h) investigated here. Results from Figure 10.5 indicate that the developed model is capable of describing N-nitrosamine rejection at a range of permeate flux. It is also noteworthy that rejection values obtained from the model are conservative. In other word, the modelled rejections of NDMA, NMEA, and NPYR were slightly smaller than values obtained experimentally.

Modelled rejections of the other N-nitrosamines (i.e. NDEA, NPIP, NDPA, NMOR and NDBA) were over 90%. As a result, only a slight increase in rejection was found with increasing overall permeate flux (data not shown). In fact, pilot-scale experiments conducted in this study revealed that the observed rejections of these N-nitrosamines were over 90% and no discernible variation in rejection was observed for changes in permeate flux (Figure 10.6).

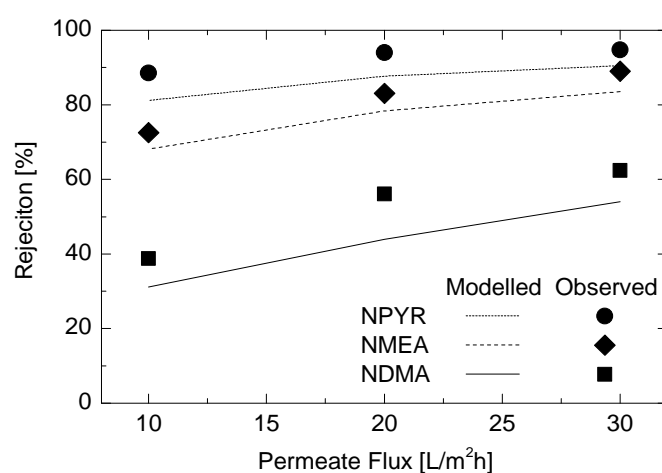


Figure 10.5: Observed and modelled overall rejection of NDMA, NMEA and NDEA (feed solution contains 20 mM NaCl, 1 mM NaHCO₃, 1 mM CaCl₂; feed temperature = 20.0 ± 0.1 °C).

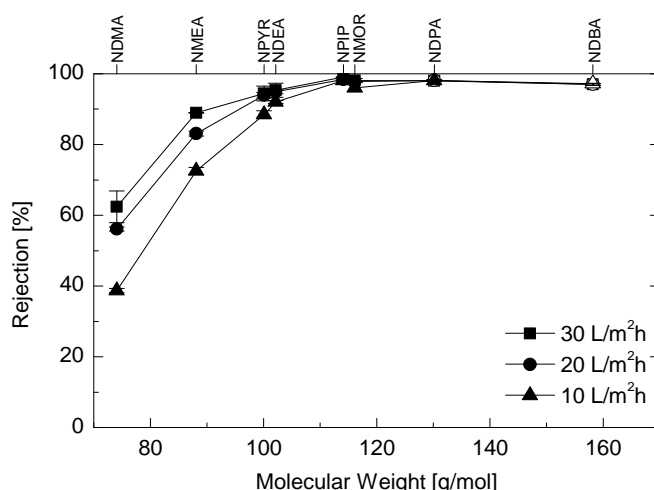


Figure 10.6: Overall rejection of N-nitrosamines by the pilot-scale experiments (overall permeate flux = 10, 20 and 30 L/m²h; feed solution contains 20 mM NaCl, 1 mM NaHCO₃, and 1 mM CaCl₂; feed temperature = 20.0 ± 0.1 °C). Open symbols indicate that the permeate concentration was below the instrumental detection limit. Values reported here are the average and ranges of duplicate results.

4.3 Impact of recoveries

In full-scale RO plants, solute rejection can vary depending on the element position within a vessel and the overall train due to changes in hydrodynamic states and solution characteristics. The variation in solute rejection was investigated by extending the model calculation from three elements to seven elements and the rejections were plotted against recovery (Figure 10.7). The model showed approximately 50% recovery with seven RO membrane elements, which is equivalent to one vessel of the first stage in a full-scale RO train deployed for water reclamation applications. The simulated rejections of the three N-nitrosamines decreased when recovery increased (Figure 10.7). When the recovery of the RO system increased from 10 to 50%, the modelled rejection of NDMA decreased remarkably from 49 to 35%. Likewise, for the same change in recovery, the rejections of NMEA and NPYR also decreased from 81 to 72% and from 89 to 83%, respectively. The observed rejections of these three N-nitrosamines were similar to the modelled rejections (Figure 10.7).

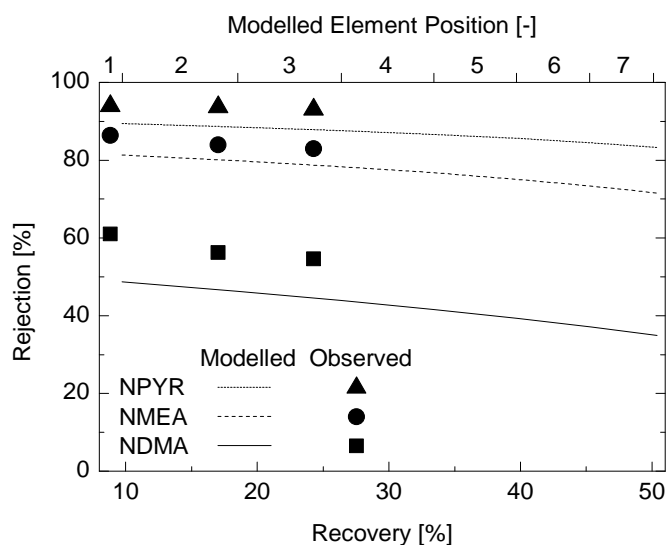


Figure 10.7: Effects of recovery on the rejection of NDMA, NMEA and NPYR (feed solution contains 20 mM NaCl, 1 mM NaHCO₃, and 1 mM CaCl₂; feed temperature = 20.0 ± 0.1 °C).

Changes in the localised rejection of NDMA within a membrane vessel containing several elements were further investigated by examining the variation in hydrodynamic states and mass transfers. As filtration progresses, local feed pressure decreases due to increases in pressure loss and osmotic pressure (Figure 10.8). As a result of the reduced driving force, local permeate flux decreases along with the progress of the filtration. Since permeate flux affects the rejection of N-nitrosamines [183], the local NDMA rejection could also decrease. It is also noteworthy that an increase in TDS along with filtration also causes a slight decrease in N-nitrosamine rejection [183]. In addition, rejected compounds remain in the feed stream, leading to an increase in NDMA concentration in the subsequent feed and permeate. The increased NDMA concentration in the permeate stream contributes to deteriorations in the overall rejection of solutes, since the overall rejection is calculated based on solute concentrations in the feed solution and combined permeate solution as described in equation 25. Thus, the simulation results reported here could explain the discrepancy between laboratory scale results with very low recovery and those from full-scale RO plants for water recycling applications with about 85% recovery [122].

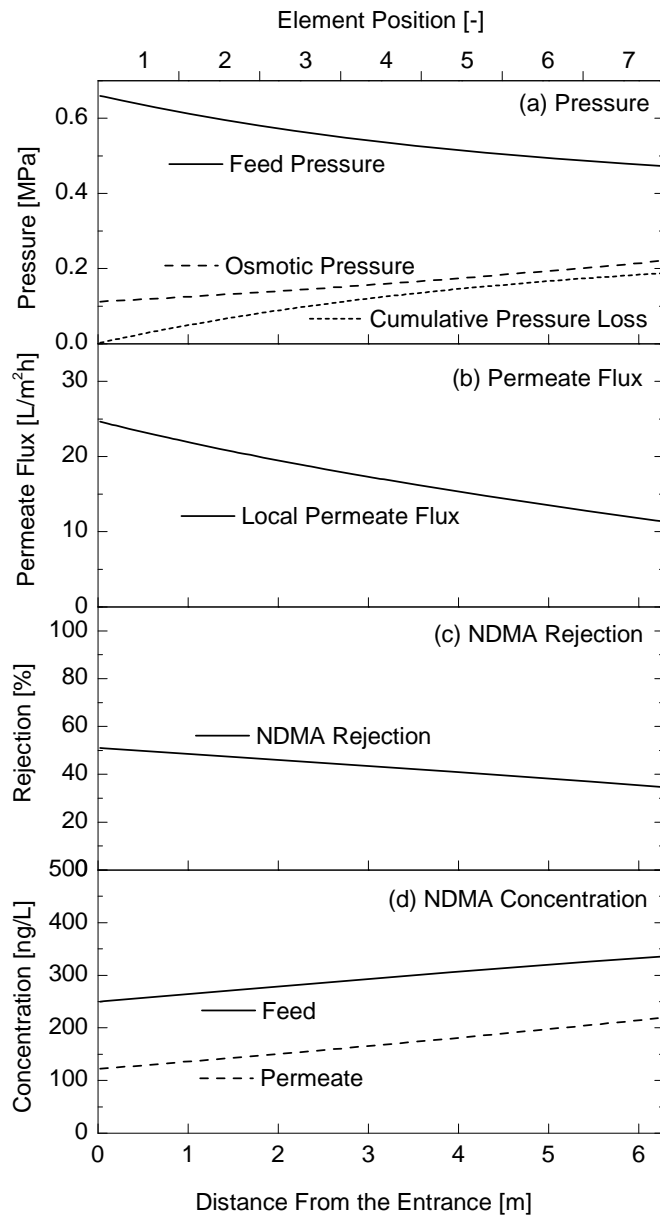


Figure 10.8: Variation in (a) feed pressure, (b) local permeate flux, (c) NDMA rejection and (d) NDMA concentration in the feed and permeate (feed solution contains 20 mM NaCl, 1 mM NaHCO_3 , and 1 mM CaCl_2 ; feed temperature = 20.0 ± 0.1 °C).

5 Conclusions

The developed model successfully simulated the hydrodynamic states (i.e. pressure and permeate flow) of the pilot-scale plant. The modelled results revealed that changes in permeate flux (from 10 to 30 $\text{L}/\text{m}^2\text{h}$) considerably affected the rejection of low molecular weight N-nitrosamines such as NDMA (from 31 to 54%). The modelled N-

nitrosamine rejections at each permeate flux were in a good agreement with experimentally determined N-nitrosamine rejections. Modelling conditions simulating a vessel with seven spiral-wound membrane elements revealed that recovery plays an important role in the rejection of low-molecular weight N-nitrosamines. In particular, when recovery changed from 10 to 50% by increasing the number of elements from one to seven, NDMA rejection decreased considerably from 49 to 35%. Additional simulation using the model revealed that the local NDMA rejection decreased with NDMA concentration increasing along the flow path from the first to the last stage, resulting in a decrease in the overall rejection of NDMA.

Chapter 11

Conclusions

The rejection of N-nitrosamines by RO membranes was systematically investigated in the context of indirect potable water reuse. Specific objectives of this study were to:

- 1) Evaluate the rejection of N-nitrosamines by RO membranes under a range of operating conditions;
- 2) Examine the impact of fouling and chemical cleaning on N-nitrosamine rejection;
- 3) Elucidate the mechanisms of permeation of N-nitrosamines through RO membranes; and
- 4) Develop a full-scale rejection model of N-nitrosamines and validate the model using a pilot-scale RO system.

In chapter 4, the rejection of eight N-nitrosamines was investigated, focusing on the influence of feed solution characteristics on their separation by low pressure RO membranes. In general, the rejection of N-nitrosamines by a given membrane increased in the order of increasing molecular weight, suggesting that steric hindrance was a dominating rejection mechanism of N-nitrosamines. The results presented in this chapter indicate that pH, ionic strength, and temperature of the feed solution can exert an influence on the rejection of NDMA and in some cases other N-nitrosamines. It is striking that an increase in the feed temperature led to a significant decrease in the rejection of all N-nitrosamines.

In chapter 5, the impact of fouling on N-nitrosamine rejection was investigated using tertiary treated effluent and several model fouling solutions. In general, the rejection of N-nitrosamines increased when the membranes were fouled by tertiary effluent. The rejection of small molecular weight N-nitrosamines was most affected by membrane fouling. The effect of membrane fouling caused by model foulants on N-nitrosamine rejection was considerably less than that caused by tertiary effluent. Size exclusion chromatography analyses revealed that the tertiary effluent contains a high fraction of

low molecular weight (< 500 g/mol) organic substances. It appears that these low molecular weight foulants present in the tertiary effluent can restrict the solute pathway within the active skin layer of membranes, resulting in the observed increase of solute rejection.

In chapter 6, the impact of chemical cleaning on the removal of N-nitrosamines was investigated. The results show that caustic chemical cleaning resulted in an increase in membrane permeability but caused a notable decrease in the rejection of N-nitrosamines. The impact was particularly obvious for NDMA and NMEA, which have the lowest molecular weight amongst the N-nitrosamines investigated in this study. The rejection of conductivity also decreased as the membrane permeability increased, indicating that conductivity rejection can be an indicative parameter of predicting changes in NDMA and NMEA rejection during RO plant operation. The impact of caustic cleaning was not permanent and could be significantly reduced by a subsequent acidic cleaning step.

In chapter 7, the influence of membrane characteristics on the rejection of eight N-nitrosamines was investigated using one NF, one SWRO and six LPRO membranes. The rejection of the two lowest molecular weight N-nitrosamines, NDMA and NMEA, varied in the range from 8–82% and 23–94%, respectively. In general, the rejection of NDMA and NMEA increased with decreasing membrane permeability. The impact of membrane characteristics became less important for higher molecular weight N-nitrosamines. Results reported here suggest that membrane characteristics associated with permeability such as the pore size and thickness of the active skin layer might be a key factor determining N-nitrosamine rejection.

In chapter 8, free-volume hole-radii of the active skin layer of one SWRO (SWC5) and two LPRO membranes (ESPA2 and ESPAB) were evaluated using PALS technique to provide insights to the transport of these small solutes through RO membranes. PALS analysis showed that the SWC5 has the smallest mean free-volume hole-radius (0.259 nm) among the three RO membranes investigated here. Correspondingly, the SWC5 membrane exhibited the highest rejection of boric acid and all N-nitrosamines. The ESPA2 and ESPAB were determined to have mean free-volume hole-radius of 0.289 nm. However, the ESPAB membrane had lower water permeability and showed

considerably higher rejection of boric acid and NDMA than the ESPA2 membrane. These results suggest that in addition to the mean free-volume hole-radius, other membrane parameters and properties such as the free-volume hole-radius distribution and thickness of the active skin layer can also play a role in governing the rejection of small and uncharged solutes by RO membranes.

In chapter 9, the rejection of N-nitrosamines was investigated using full-scale RO systems to provide longitudinal and spatial insights during sampling campaigns. Overall rejection of NDMA among the three RO systems varied widely from 4 to 47%. A considerable variation in NDMA rejection across the three RO stages (14-78%) was also observed. Overall NMOR rejections were consistently high ranging from 81 to 84%. On the other hand, overall rejection of NDEA varied from negligible to 53%, which was considerably lower than values reported in previous laboratory-scale studies. A comparison between results reported here and the literature indicates that there can be some discrepancy in N-nitrosamine rejection data between laboratory- and full-scale studies probably due to differences in water recoveries and operating conditions (e.g. temperature, membrane fouling, and hydraulic conditions).

In chapter 10, a mathematical model was developed based on the irreversible thermodynamic principle and hydrodynamic calculation to predict the rejection of N-nitrosamines by spiral-wound RO membrane systems. The developed model is able to accurately describe the rejection of N-nitrosamines under a range of permeate flux and system recovery conditions. The modelled N-nitrosamine rejections were in good agreement with values obtained experimentally using a pilot-scale RO filtration system. Simulation from the model revealed that an increase in permeate flux from 10 to 30 L/m²h led to an increase in the rejection of low molecular weight N-nitrosamines such as NDMA (from 31 to 54%), which was validated by experimental results. The modelling results also revealed that an increase in recovery caused a decrease in the rejection of these N-nitrosamines, which is consistent with the experimental results. Further modelling investigations suggested that NDMA rejection by a spiral-wound system can drop from 49 to 35% when the overall recovery increased from 10 to 50%. The model developed from this study can be a useful tool for water utilities and

regulators for system design and evaluating the removal of N-nitrosamine by RO membranes.

Overall, this thesis provides a comprehensive knowledge and findings with regards to N-nitrosamine rejection by RO membranes. The results reported here indicate that changing operating conditions doesn't sufficiently result in an improvement of N-nitrosamine rejection. Nevertheless, plant operators need to be aware that the rejection of low molecular weight N-nitrosamines can vary significantly over time due to membrane fouling and chemical cleaning. The results reported here also suggest that the rejection of low molecular weight N-nitrosamines (e.g. NDMA) can be improved by selecting appropriate LPRO membranes, indicating that membrane selection is important during RO system design. The last findings with regards to modelling revealed that the RO system designs for N-nitrosamine rejection can be easily extended using simple laboratory-scale experiments which may potentially cut the cost of design and validation and during pilot-scale experiments and full-scale plant commissioning.

Chapter 12

Future research

A comprehensive investigation in regard to the impact of feed solution characteristics, fouling and chemical cleaning was conducted using a laboratory-scale RO system (Chapter 4-6). Although the importance of each factor on the variation of N-nitrosamine rejection during full-scale system operation has been identified through these laboratory-scale studies, the impact of changes in multiple factors still remain unconfirmed using a full-scale RO system (Chapter 9). A long-term investigation with frequent full-scale samplings and monitoring will assist the identification of the importance of each factor during full-scale system operation.

Understanding the mechanism of N-nitrosamine transport within the active skin layer of RO membranes can potentially allow us to improve N-nitrosamine rejection by controlling the important parameters during manufacturing or modifying existing RO membranes. Membrane properties associated with membrane permeability such as the free-volume hole-radius are likely to determine N-nitrosamine rejection (Chapter 7, 8). Nevertheless, free-volume hole-radius is not the only one important factor and there still remain potential membrane properties determining their rejection. Thus, further work is necessary to examine the impact of several other physicochemical properties of RO membranes (e.g. distribution of mean free-volume hole-radius and thickness of the active skin layer) on N-nitrosamine rejection.

A mathematical model simulating hydrodynamic conditions of spiral wound RO membranes was developed and the model was validated under a range of permeate flux conditions using a pilot-scale RO system (Chapter 10). Further work is required to examine the effects of several other factors (e.g. feed water characteristics, fouling and chemical cleaning) on N-nitrosamine rejection using a pilot-scale plant and incorporate these effects into the model. Validating the model using a full-scale RO system, which

generally comprise three stages in series, will also be beneficial to ensure the accuracy of its prediction.

Glossary

CA	Citric acid
CI	Chemical ionization
DMA	Dimethylamine
DOC	Dissolved organic carbon
EDTA	Ethylene diamine tetraacetic acid
ESI	Electrospray ionisation
FTIR	Fourier transform infrared spectroscopy
GC	Gas chromatography
HRMS	High resolution mass spectrometry
IC	Ion chromatography
LC	Liquid chromatography
LC-OCD	Liquid chromatography - organic carbon detection
LPRO	Low pressure reverse osmosis
MF	Microfiltration
MS	Mass spectrometry
MS/MS	Tandem mass spectrometry
NDBA	N-nitrosodi-n-butylamine
NDEA	N-nitrosodiethylamine
NDMA	N-nitrosodimethylamine
NDPA	N-nitrosodipropylamine
NDPhA	N-Nitrosodiphenylamine
NMEA	N-nitrosomethylethylamine
NMOR	N-nitrosomorpholine
NIIP	N-nitrosopiperidine
NPOC	Non-purgeable organic carbon
NPYR	N-nitrosopyrrolidine
PALS	Positron annihilation lifetime spectroscopy
RO	Reverse osmosis
SDS	Sodium dodecyl sulphate
SPE	Solid-phase extraction
SWRO	Sea water reverse osmosis
TDS	Total dissolved solid
TE	Tertiary effluent
TOC	Total organic carbon
UF	Ultrafiltration
WWTP	Wastewater treatment plant

List of symbols

Chapter 4

C_b	concentration in the feed (ng/L)
C_m	membrane concentration (ng/L)
C_p	permeate concentration (ng/L)
d_h	hydraulic diameter (m)
D	diffusion coefficient (m^2/s)
J_s	solute flux (m/s)
J_v	water flux, volume flux, permeate flux (m/s)
k	mass transfer coefficient (m/s)
L^*	length of the entry region (m)
L	the length of the membrane (m)
L_p	pure water permeability ($\text{L}/\text{m}^2\text{h}$)
P_s	solute permeability coefficient (m/s)
Re	Reynolds number (-)
R_{obs}	observed rejection (-)
R_{real}	real rejection (-)
Sc	Schmidt number (-)
Sh	Sherwood number (-)
u	feed velocity (m/s)
ΔP	Pressure difference between the feed and permeate sides (Pa)
Δx	membrane thickness (m)
σ	reflection coefficient (-)
$\Delta\pi$	osmotic pressure difference between the feed and permeate sides (Pa)

Chapter 7

C_b	concentration in the feed (ng/L)
C_m	membrane concentration (ng/L)
C_p	permeate concentration (ng/L)
d_h	hydraulic diameter (m)
D	diffusion coefficient (m^2/s)
J_s	solute flux (m/s)
J_v	water flux, permeate flux (m/s)
k	mass transfer coefficient (m/s)
L	the length of the membrane (m)
L_p	pure water permeability ($\text{L}/\text{m}^2\text{h}$)

P_s	solute permeability coefficient (m/s)
Re	Reynolds number (-)
R_{obs}	observed rejection (-)
R_{real}	real rejection (-)
Sc	Schmidt number (-)
Sh	Sherwood number (-)
u	feed velocity (m/s)
ΔP	pressure difference between the feed and permeate sides (Pa)
x	position in a pore from inlet (m)
Δx	membrane thickness (m)
σ	reflection coefficient (-)
$\Delta \pi$	osmotic pressure difference between the feed and permeate sides (Pa)

Chapter 8

r	the radius of the free volume hole
V_f	free-volume hole-space
τ_{o-Ps}	$o-P_s$ lifetime
V_m	molecular volume

Chapter 9

C_{pi}	solute concentration in the RO permeate of the stage i
C_{fi}	solute concentration in the RO feed of the stage i
C_{pT}	solute concentration in the combined RO permeate

Chapter 10

C_f	feed concentration [kg/m ³]
C_p	permeate concentration [kg/m ³]
d_h	hydraulic diameter [m]
D	diffusion coefficient [m ² /s]
h_b	feed channel height [m]
i	number of sub-section [-]
j	number of element [-]
f_{fb}	feed friction parameter [-]
J_p	permeate flux [m ³ /m ² s]
k	mass transfer coefficient [m/s]
K	efficiency of mixing net [-]
L	membrane sheet length [m]
L_p	pure water permeability [L/m ² hPa]
m	number of sub-sections in a membrane sheet [-]
m_{salt}	molar concentrations of ions [mol/L]

n	quantity of elements [-]
Pe	Peclet number [-]
P_f	feed pressure [Pa]
P_p	permeate pressure [Pa]
ΔP	pressure drop [Pa]
P_s	permeability coefficient of a compound [m/s]
Q_f	feed flow rate [m ³ /s]
Q_p	permeate flow rate [m ³ /s]
R_c	recovery [-]
R_{obs}	observed rejection [-]
R_{real}	real rejection [-]
R_{salt}	salt rejection [-]
ΔS	valid surface area [m]
ΔS_c	cross-section area [m]
Sc	Schmidt number [-]
T	solution temperature [°C]
U_b	bulk velocity of the feed within the feed channel [m/s]
W	membrane sheet width [m]
Δx	sub-section length [m]
ρ	density of solution [kg/m ³]
σ	reflection coefficient [-]
π	osmotic pressure [Pa]
μ	viscosity of feed solution [Pa-s]

References

- [1] M.A. Shannon, P.W. Bohn, M. Elimelech, J.G. Georgiadis, B.J. Marinas, A.M. Mayes, Science and technology for water purification in the coming decades, *Nature*, 452 (2008) 301-310.
- [2] W.H. Traves, E.A. Gardner, B. Dennien, D. Spiller, Towards indirect potable reuse in south east Queensland, *Water Sci. Technol.*, 58 (2008) 153-161.
- [3] C. Bellona, J.E. Drewes, P. Xu, G. Amy, Factors affecting the rejection of organic solutes during NF/RO treatment - A literature review, *Water Res.*, 38 (2004) 2795-2809.
- [4] A.R.D. Verliefde, S.G.J. Heijman, E.R. Cornelissen, G.L. Amy, B. Van der Bruggen, J.C. van Dijk, Rejection of trace organic pollutants with high pressure membranes (NF/RO), *Environ. Prog.*, 27 (2008) 180-188.
- [5] G. Oron, L. Gillerman, A. Bick, N. Buriakovsky, Y. Manor, E. Ben-Yitshak, L. Katz, J. Hagin, A two stage membrane treatment of secondary effluent for unrestricted reuse and sustainable agricultural production, *Desalination*, 187 (2006) 335-345.
- [6] W.A. Mitch, J.O. Sharp, R.R. Trussell, R.L. Valentine, L. Alvarez-Cohen, D.L. Sedlak, N-Nitrosodimethylamine (NDMA) as a drinking water contaminant: A review, *Environ. Eng. Sci.*, 20 (2003) 389-404.
- [7] S.W. Krasner, P. Westerhoff, B. Chen, B.E. Rittmann, G. Amy, Occurrence of disinfection byproducts in United States wastewater treatment plant effluents, *Environ. Sci. Technol.*, 43 (2009) 8320-8325.
- [8] M. Krauss, P. Longrée, E. van Houtte, J. Cauwenberghs, J. Hollender, Assessing the fate of Nitrosamine precursors in wastewater treatment by physicochemical fractionation, *Environ. Sci. Technol.*, 44 (2010) 7871-7877.
- [9] C. Reyes-Contreras, C. Domínguez, J.M. Bayona, Determination of nitrosamines and caffeine metabolites in wastewaters using gas chromatography mass spectrometry and ionic liquid stationary phases, *J. Chromatogr. A*, 1261 (2012) 164-170.
- [10] S. Yoon, N. Nakada, H. Tanaka, A new method for quantifying N-nitrosamines in wastewater samples by gas chromatography—triple quadrupole mass spectrometry, *Talanta*, 97 (2012) 256-261.
- [11] J. Nawrocki, P. Andrzejewski, Nitrosamines and water, *J. Hazard. Mater.*, 189 (2011) 1-18.
- [12] M.J. Farré, K. Döderer, L. Hearn, Y. Poussade, J. Keller, W. Gernjak, Understanding the operational parameters affecting NDMA formation at Advanced Water Treatment Plants, *J. Hazard. Mater.*, 185 (2011) 1575-1581.
- [13] USEPA, N-Nitrosodimethylamine (CASRN 62-75-9) - Integrated risk information system (IRIS), <http://www.epa.gov/iris/subst/0045.htm> (1993).
- [14] NRMCC, EPHC, AHMC, Australian guidelines for water recycling: Managing health and environmental risks (Phase 2): Augmentation of drinking water supplies, Environment Protection and Heritage Council, National Health and

- Medical Research Council, Natural Resource Management Ministerial Council, Canberra, 2008.
- [15] K.O. Agenson, J.-I. Oh, T. Urase, Retention of a wide variety of organic pollutants by different nanofiltration/reverse osmosis membranes: controlling parameters of process, *J. Membr. Sci.*, 225 (2003) 91-103.
 - [16] L.D. Nghiem, A.I. Schäfer, M. Elimelech, Removal of natural hormones by nanofiltration membranes: Measurement, modeling, and mechanisms, *Environ. Sci. Technol.*, 38 (2004) 1888-1896.
 - [17] C. Bellona, J.E. Drewes, G. Oelker, J. Luna, G. Filteau, G. Amy, Comparing nanofiltration and reverse osmosis for drinking water augmentation, *Journal AWWA*, 100 (2008) 102-116.
 - [18] M.H. Plumlee, M. López-Mesas, A. Heidlberger, K.P. Ishida, M. Reinhard, N-nitrosodimethylamine (NDMA) removal by reverse osmosis and UV treatment and analysis via LC-MS/MS, *Water Res.*, 42 (2008) 347-355.
 - [19] T. Wintgens, T. Melin, A. Schäfer, S. Khan, M. Muston, D. Bixio, C. Thoeue, The role of membrane processes in municipal wastewater reclamation and reuse, *Desalination*, 178 (2005) 1-11.
 - [20] J. Drewes, S. Khan, Chapter 16: Water reuse for drinking water augmentation, in: American Water Works Association, J.K. Edzwald (Eds.) *Water Quality & Treatment: A Handbook on Drinking Water*, 6th Edition, McGraw-Hill Professional, 2011.
 - [21] D. Sedlak, M. Kavanaugh, Removal and destruction of NDMA and NDMA precursors during wastewater treatment, *WaterReuse Foundation*, (2006).
 - [22] W.A. Mitch, A.C. Gerecke, D.L. Sedlak, A N-Nitrosodimethylamine (NDMA) precursor analysis for chlorination of water and wastewater, *Water Res.*, 37 (2003) 3733-3741.
 - [23] E. Pehlivanoglu-Mantas, E.L. Hawley, R.A. Deeb, D.L. Sedlak, Formation of nitrosodimethylamine (NDMA) during chlorine disinfection of wastewater effluents prior to use in irrigation systems, *Water Res.*, 40 (2006) 341-347.
 - [24] IARC, IARC monographs on the evaluation of carcinogenic risks to humans: Overall evaluations of carcinogenicity: An updating of IARC monographs volumes 1 - 42: Supplement 7, International agency for research on cancer, (1987).
 - [25] USEPA, Integrated Risk Information System (IRIS), <http://www.epa.gov/iris/> (1993).
 - [26] I.M. Schreiber, W.A. Mitch, Influence of the order of reagent addition on NDMA formation during chloramination, *Environ. Sci. Technol.*, 39 (2005) 3811-3818.
 - [27] W.A. Mitch, G.L. Oelker, E.L. Hawley, R.A. Deeb, D.L. Sedlak, Minimization of NDMA formation during chlorine disinfection of municipal wastewater by application of pre-formed chloramines, *Environ. Eng. Sci.*, 22 (2005) 882-890.
 - [28] D.W. Hawker, J.L. Cumming, P.A. Neale, M.E. Bartkow, B.I. Escher, A screening level fate model of organic contaminants from advanced water treatment in a potable water supply reservoir, *Water Res.*, 45 (2011) 768-780.
 - [29] J.E. Drewes, C. Hoppe, T. Jennings, Fate and transport of N-Nitrosamines under conditions simulating full-scale groundwater recharge operations, *Water Environment Research*, 78 (2006) 2466-2473.

- [30] M. Wilf, S. Alt, Application of low fouling RO membrane elements for reclamation of municipal wastewater, *Desalination*, 132 (2000) 11-19.
- [31] J.E. Drewes, C. Bellona, M. Oedekoven, P. Xu, T.-U. Kim, G. Amy, Rejection of wastewater-derived micropollutants in high-pressure membrane applications leading to indirect potable reuse, *Environ. Prog.*, 24 (2005) 400-409.
- [32] A.A. Alturki, N. Tadkaew, J.A. McDonald, S.J. Khan, W.E. Price, L.D. Nghiem, Combining MBR and NF/RO membrane filtration for the removal of trace organics in indirect potable water reuse applications, *J. Membr. Sci.*, 365 (2010) 206-215.
- [33] L.S. Tam, T.W. Tang, G.N. Lau, K.R. Sharma, G.H. Chen, A pilot study for wastewater reclamation and reuse with MBR/RO and MF/RO systems, *Desalination*, 202 (2007) 106-113.
- [34] S.B. Sadr Ghayeni, P.J. Beatson, R.P. Schneider, A.G. Fane, Water reclamation from municipal wastewater using combined microfiltration-reverse osmosis (ME-RO): Preliminary performance data and microbiological aspects of system operation, *Desalination*, 116 (1998) 65-80.
- [35] R.D. Reardon, SParanjape Sudan V., X.J. Fousseureau, F.A. DiGiano, M.D. Aitken, J.H. Kim, S.-Y. Chang, R. Cramer, Membrane treatment of secondary effluent for subsequent use, in, *Water Environment Research Fondation*, Alexandria, VA, 2005.
- [36] Y. Poussade, A. Roux, T. Walker, V. Zavlanos, Advanced oxidation for indirect potable reuse: a practical application in Australia, *Water Sci. Technol.*, 60 (2009) 2419-2424.
- [37] Y.-Y. Zhao, J. Boyd, S.E. Hrudey, X.-F. Li, Characterization of new Nitrosamines in drinking water using liquid chromatography tandem mass spectrometry, *Environ. Sci. Technol.*, 40 (2006) 7636-7641.
- [38] E. Steinle-Darling, M. Zedda, M.H. Plumlee, H.F. Ridgway, M. Reinhard, Evaluating the impacts of membrane type, coating, fouling, chemical properties and water chemistry on reverse osmosis rejection of seven nitrosoalkylamines, including NDMA, *Water Res.*, 41 (2007) 3959-3967.
- [39] B. Spiegelhalder, R. Preussmann, Contamination of toiletries and cosmetic products with volatile and nonvolatile N-nitroso carcinogens, *J. Cancer Res. Clin. Oncol.*, 108 (1984) 160-163.
- [40] D.L. Sedlak, R.A. Deeb, E.L. Hawley, W.A. Mitch, T.D. Durbin, S. Mowbray, S. Carr, Sources and fate of Nitrosodimethylamine and its precursors in municipal wastewater treatment plants, *Water Environment Research*, 77 (2005) 32-39.
- [41] H. Middleton, M.R. Moore, H. Chapman, F. Leusch, B. Tan, R. Drew, J. Frangos, S. Khan, G. Leslie, G. Shaw, Recycled water quality - A guide to determining, monitoring and achieving safe concentrations of chemicals in recycled water (14655), (2008).
- [42] Z. Chen, R.L. Valentine, Formation of N-Nitrosodimethylamine (NDMA) from humic substances in natural water, *Environ. Sci. Technol.*, 41 (2007) 6059-6065.
- [43] W.A. Mitch, D.L. Sedlak, Characterization and fate of N-Nitrosodimethylamine precursors in municipal wastewater treatment plants, *Environ. Sci. Technol.*, 38 (2004) 1445-1454.

- [44] R. Shen, S.A. Andrews, Demonstration of 20 pharmaceuticals and personal care products (PPCPs) as nitrosamine precursors during chloramine disinfection, *Water Res.*, 45 (2011) 944-952.
- [45] J. Choi, R.L. Valentine, Formation of N-nitrosodimethylamine (NDMA) from reaction of monochloramine: a new disinfection by-product, *Water Res.*, 36 (2002) 817-824.
- [46] A.R. Tricker, B. Pfundstein, T. Kalble, R. Preussmann, Secondary amine precursors to nitrosamines in human saliva, gastric juice, blood, urine and faeces, *Carcinogenesis*, 13 (1992) 563-568.
- [47] W.A. Mitch, D.L. Sedlak, Formation of N-Nitrosodimethylamine (NDMA) from dimethylamine during chlorination, *Environ. Sci. Technol.*, 36 (2002) 588-595.
- [48] A.C. Gerecke, D.L. Sedlak, Precursors of N-Nitrosodimethylamine in natural waters, *Environ. Sci. Technol.*, 37 (2003) 1331-1336.
- [49] W.-J. Zhou, J.M. Boyd, F. Qin, S.E. Hrudey, X.-F. Li, Formation of N-Nitrosodiphenylamine and two new N-containing disinfection byproducts from chloramination of water containing diphenylamine, *Environ. Sci. Technol.*, 43 (2009) 8443-8448.
- [50] P. Andrzejewski, B. Kasprzyk-Hordern, J. Nawrocki, N-nitrosodimethylamine (NDMA) formation during ozonation of dimethylamine-containing waters, *Water Res.*, 42 (2008) 863-870.
- [51] P. Andrzejewski, J. Nawrocki, N-nitrosodimethylamine (NDMA) as a product of potassium permanganate reaction with aqueous solutions of dimethylamine (DMA), *Water Res.*, 43 (2009) 1219-1228.
- [52] J.W.A. Charrois, S.E. Hrudey, Breakpoint chlorination and free-chlorine contact time: Implications for drinking water N-nitrosodimethylamine concentrations, *Water Res.*, 41 (2007) 674-682.
- [53] W. Lee, P. Westerhoff, J.-P. Croué, Dissolved organic nitrogen as a precursor for chloroform, dichloroacetonitrile, N-Nitrosodimethylamine, and trichloronitromethane, *Environ. Sci. Technol.*, 41 (2007) 5485-5490.
- [54] A.D. Shah, W.A. Mitch, Halonitroalkanes, Halonitriles, Haloamides, and N-Nitrosamines: A Critical Review of Nitrogenous Disinfection Byproduct Formation Pathways, *Environ. Sci. Technol.*, 46 (2011) 119-131.
- [55] I.M. Schreiber, W.A. Mitch, Nitrosamine formation pathway revisited: The importance of chloramine speciation and dissolved oxygen, *Environ. Sci. Technol.*, 40 (2006) 6007-6014.
- [56] J. Choi, R.L. Valentine, N-Nitrosodimethylamine formation by free-chlorine-enhanced nitrosation of dimethylamine, *Environ. Sci. Technol.*, 37 (2003) 4871-4876.
- [57] J.W.A. Charrois, J.M. Boyd, K.L. Froese, S.E. Hrudey, Occurrence of N-nitrosamines in Alberta public drinking-water distribution systems *J. Environ. Eng. Sci.*, 6 (2007) 103-114.
- [58] USEPA, Second cycle of the unregulated contaminant monitoring regulation (UCMR2) data summary, in, U.S. Environmental Protection Agency, 2010.
- [59] CDPH, NDMA and other Nitrosamines - Drinking water issues (<http://www.cdph.ca.gov/certlic/drinkingwater/Pages/NDMA.aspx>), California Department of Public Health 2011.

- [60] Ontario MOE, Technical support document for Ontario drinking water standards, objectives and guidelines, Ontario Ministry of the Environment, Ontario, 2003.
- [61] WHO, Guidelines for drinking-water quality 4th edition, in, World Health Organization, Geneva, 2011.
- [62] NHMRC, NRMMC, Australian drinking water guidelines paper 6 national water quality management strategy, National Health and Medical Research Council, National Resource Management Ministerial Council, Commonwealth of Australia, Canberra, 2011.
- [63] USEPA, Contaminant information sheets for the final CCL 3 chemicals, in, EPA, 2009.
- [64] J.A. Roberson, How USEPA Is looking at regulating groups, Journal American Water Works Association, 102 (2010) 16-18.
- [65] J.W.A. Charrois, M.W. Arend, K.L. Froese, S.E. Hrudey, Detecting N-Nitrosamines in drinking water at nanogram per liter levels using ammonia positive chemical ionization, Environ. Sci. Technol., 38 (2004) 4835-4841.
- [66] S. Yoon, N. Nakada, H. Tanaka, Occurrence and removal of NDMA and NDMA formation potential in wastewater treatment plants, J. Hazard. Mater., 190 (2011) 897-902.
- [67] J.W. Munch, M.V. Bassett, METHOD 521 Determination of nitrosamines in drinking water by solid phase extraction and capillary column gas chromatography with large volume injection and chemical ionization tandem mass spectrometry (MS/MS) Version 1.0, in, National Exposure Research Laboratory Office of Research and Development, U.S. Environmental Protection Agency, Cincinnati, 2004.
- [68] A. Llop, F. Borrull, E. Pocurull, Fully automated determination of N-nitrosamines in environmental waters by headspace solid-phase microextraction followed by GC-MS-MS, Journal of Separation Science, 33 (2010) 3692-3700.
- [69] H.-W. Hung, T.-F. Lin, C.-H. Chiu, Y.-C. Chang, T.-Y. Hsieh, Trace analysis of N-Nitrosamines in water using solid-phase microextraction coupled with gas chromatograph-tandem mass spectrometry, Water, Air, Soil Pollut., 213 (2010) 459-469.
- [70] Ontario MOE, Protocol of accepted drinking water testing methods version 2.0, E3388 - The determination of N-nitrosamines in water by gas chromatography-high resolution mass spectrometry (GC/HRMS), Laboratory Services Branch, Ontario Ministry of the Environment Ontario, 2010.
- [71] C. Planas, Ó. Palacios, F. Ventura, J. Rivera, J. Caixach, Analysis of nitrosamines in water by automated SPE and isotope dilution GC/HRMS: Occurrence in the different steps of a drinking water treatment plant, and in chlorinated samples from a reservoir and a sewage treatment plant effluent, Talanta, 76 (2008) 906-913.
- [72] R. Pozzi, P. Bocchini, F. Pinelli, G.C. Galletti, Determination of nitrosamines in water by gas chromatography/chemical ionization/selective ion trapping mass spectrometry, J. Chromatogr. A, 1218 (2011) 1808-1814.
- [73] J.A. McDonald, N.B. Harden, L.D. Nghiem, S.J. Khan, Analysis of N-nitrosamines in water by isotope dilution gas chromatography-electron ionisation tandem mass spectrometry, Talanta, 99 (2012) 146-152.

- [74] Y.Y. Zhao, X. Liu, J.M. Boyd, F. Qin, J. Li, X.-F. Li, Identification of N-Nitrosamines in treated drinking water using nanoelectrospray ionization high-field asymmetric waveform ion mobility spectrometry with quadrupole time-of-flight mass spectrometry, *J. Chromatogr. Sci.*, 47 (2009) 92-96.
- [75] J.M. Boyd, S.E. Hrudey, X.F. Li, S.D. Richardson, Solid-phase extraction and high-performance liquid chromatography mass spectrometry analysis of nitrosamines in treated drinking water and wastewater, *TRAC Trends in Analytical Chemistry*, 30 (2011) 1410-1421.
- [76] M. Krauss, J. Hollender, Analysis of Nitrosamines in wastewater: Exploring the trace level quantification capabilities of a hybrid linear ion trap/orbitrap mass spectrometer, *Anal. Chem.*, 80 (2008) 834-842.
- [77] C. Ripollés, E. Pitarch, J.V. Sancho, F.J. López, F. Hernández, Determination of eight nitrosamines in water at the ngL^{-1} levels by liquid chromatography coupled to atmospheric pressure chemical ionization tandem mass spectrometry, *Anal. Chim. Acta*, 702 (2011) 62-71.
- [78] J. Chung, Y. Yoon, M. Kim, S.-B. Lee, H.-J. Kim, C.-K. Choi, Removal of radio N-nitrosodimethylamine (NDMA) from drinking water by coagulation and Powdered Activated Carbon (PAC) adsorption, *Drinking Water Engineering and Science*, 2 (2009) 49-55.
- [79] E.C. Fleming, J.C. Pennington, B.G. Wachob, R.A. Howe, D.O. Hill, Removal of N-nitrosodimethylamine from waters using physical-chemical techniques, *J. Hazard. Mater.*, 51 (1996) 151-164.
- [80] F. Soroushian, M. Patel, S. Fitzsimmons, M. Wehner, NDMA Removal and Reformation Prevention, in: *Proceedings of the Water Environment Federation*, 2004, pp. 85-112.
- [81] C.K. Schmidt, H.-J. Brauch, N,N-Dimethylsulfamide as precursor for N-Nitrosodimethylamine (NDMA) formation upon ozonation and its fate during drinking water treatment, *Environ. Sci. Technol.*, 42 (2008) 6340-6346.
- [82] Y. Miyashita, S.-H. Park, H. Hyung, C.-H. Huang, J.-H. Kim, Removal of N-Nitrosamines and their precursors by nanofiltration and reverse osmosis membranes, *J. Environ. Eng.*, 135 (2009) 788-795.
- [83] C. Bellona, K. Budgell, D. Ball, K. Spangler, J.E. Drewes, S. Chellam, Models to predict organic contaminant removal by RO and NF membranes, *IDA Journal*, 3 (2011) 40-44.
- [84] S.J. Khan, J.A. McDonald, Quantifying human exposure to contaminants for multiple-barrier water reuse systems, *Water Sci. Technol.*, 61 (2010) 77-83.
- [85] J.E. Drewes, C. Bellona, P. Xu, G. Amy, G. Filteau, G. Oelker, Comparing nanofiltration and reverse osmosis for treating recycled water, *AWWA Research Foundation*, (2008).
- [86] M.J. Farré, J. Keller, N. Holling, Y. Poussade, W. Gernjak, Occurrence of NDMA precursors in wastewater treatment plant effluent and their fate during UF-RO membrane treatment, *Water Sci. Technol.*, 63 (2011) 605-612.
- [87] R. Lugg, Characterising treated wastewater for drinking purposes following reverse osmosis treatment, *Premier's Collaborative Research Program*, (2009).
- [88] E. Pehlivanoglu-Mantas, D.L. Sedlak, Measurement of dissolved organic nitrogen forms in wastewater effluents: Concentrations, size distribution and NDMA formation potential, *Water Res.*, 42 (2008) 3890-3898.

- [89] B. Van der Bruggen, J. Schaep, W. Maes, D. Wilms, C. Vandecasteele, Nanofiltration as a treatment method for the removal of pesticides from ground waters, *Desalination*, 117 (1998) 139-147.
- [90] J.M.K. Timmer, M.P.J. Speelmans, H.C. van der Horst, Separation of amino acids by nanofiltration and ultrafiltration membranes, *Sep. Purif. Technol.*, 14 (1998) 133-144.
- [91] W.R. Bowen, A.W. Mohammad, N. Hilal, Characterisation of nanofiltration membranes for predictive purposes — use of salts, uncharged solutes and atomic force microscopy, *J. Membr. Sci.*, 126 (1997) 91-105.
- [92] Y. Kiso, K. Muroshige, T. Oguchi, M. Hirose, T. Ohara, T. Shintani, Pore radius estimation based on organic solute molecular shape and effects of pressure on pore radius for a reverse osmosis membrane, *J. Membr. Sci.*, 369 (2011) 290-298.
- [93] J.L.C. Santos, P. de Beukelaar, I.F.J. Vankelecom, S. Velizarov, J.G. Crespo, Effect of solute geometry and orientation on the rejection of uncharged compounds by nanofiltration, *Sep. Purif. Technol.*, 50 (2006) 122-131.
- [94] Z. Chen, K. Ito, H. Yanagishita, N. Oshima, R. Suzuki, Y. Kobayashi, Correlation study between free-volume holes and molecular separations of composite membranes for reverse osmosis processes by means of variable-energy positron annihilation techniques, *J. Phys. Chem. C*, 115 (2011) 18055-18060.
- [95] S.H. Kim, S.-Y. Kwak, T. Suzuki, Positron Annihilation Spectroscopic Evidence to Demonstrate the Flux-Enhancement Mechanism in Morphology-Controlled Thin-Film-Composite (TFC) Membrane, *Environ. Sci. Technol.*, 39 (2005) 1764-1770.
- [96] J.G. Wijmans, R.W. Baker, The solution-diffusion model: a review, *J. Membr. Sci.*, 107 (1995) 1-21.
- [97] S.A. Avlonitis, M. Pappas, K. Moutesidis, A unified model for the detailed investigation of membrane modules and RO plants performance, *Desalination*, 203 (2007) 218-228.
- [98] A.R.D. Verliefde, E.R. Cornelissen, S.G.J. Heijman, J.Q.J.C. Verberk, G.L. Amy, B. Van der Bruggen, J.C. van Dijk, The role of electrostatic interactions on the rejection of organic solutes in aqueous solutions with nanofiltration, *J. Membr. Sci.*, 322 (2008) 52-66.
- [99] M.S. Oak, T. Kobayashi, H.Y. Wang, T. Fukaya, N. Fujii, pH effect on molecular size exclusion of polyacrylonitrile ultrafiltration membranes having carboxylic acid groups, *J. Membr. Sci.*, 123 (1997) 185-195.
- [100] A.E. Childress, M. Elimelech, Relating nanofiltration membrane performance to membrane charge (electrokinetic) characteristics, *Environ. Sci. Technol.*, 34 (2000) 3710-3716.
- [101] R.Y. Ning, T.L. Troyer, Colloidal fouling of RO membranes following MF/UF in the reclamation of municipal wastewater, *Desalination*, 208 (2007) 232-237.
- [102] M. Abdel-Jawad, S. Al-Shammari, J. Al-Sulaimi, Non-conventional treatment of treated municipal wastewater for reverse osmosis, *Desalination*, 142 (2002) 11-18.

- [103] J.H. Al-Rifai, H. Khabbaz, A.I. Schäfer, Removal of pharmaceuticals and endocrine disrupting compounds in a water recycling process using reverse osmosis systems, *Sep. Purif. Technol.*, 77 (2011) 60-67.
- [104] W. Won, T. Walker, M. Patel, E. Owens, Comparing membrane operations at three of the world's largest advanced water treatment plants, *IDA Journal*, 2 (2010) 14-19.
- [105] S.L. Ong, W. Zhou, L. Song, W.J. Ng, Evaluation of feed concentration effects on salt/Ion transport through RO/NF membranes with the Nernst-Planck-Donnan model, *Environ. Eng. Sci.*, 19 (2002) 429-439.
- [106] C. Bartels, R. Franks, S. Rybar, M. Schierach, M. Wilf, The effect of feed ionic strength on salt passage through reverse osmosis membranes, *Desalination*, 184 (2005) 185-195.
- [107] V. Freger, Swelling and morphology of the skin layer of polyamide composite membranes: an atomic force microscopy study, *Environ. Sci. Technol.*, 38 (2004) 3168-3175.
- [108] A. Escoda, P. Fievet, S. Lakard, A. Szymczyk, S. Déon, Influence of salts on the rejection of polyethyleneglycol by an NF organic membrane: Pore swelling and salting-out effects, *J. Membr. Sci.*, 347 (2010) 174-182.
- [109] J. Luo, Y. Wan, Effect of highly concentrated salt on retention of organic solutes by nanofiltration polymeric membranes, *J. Membr. Sci.*, 372 (2011) 145-153.
- [110] N. Ben Amar, H. Saidani, J. Palmeri, A. Deratani, Effect of temperature on the rejection of neutral and charged solutes by Desal 5 DK nanofiltration membrane, *Desalination*, 246 (2009) 294-303.
- [111] R.R. Sharma, R. Agrawal, S. Chellam, Temperature effects on sieving characteristics of thin-film composite nanofiltration membranes: pore size distributions and transport parameters, *J. Membr. Sci.*, 223 (2003) 69-87.
- [112] N. Ben Amar, H. Saidani, A. Deratani, J. Palmeri, Effect of temperature on the transport of water and neutral solutes across nanofiltration membranes, *Langmuir*, 23 (2007) 2937-2952.
- [113] E. Van Houtte, J. Verbauwhede, Operational experience with indirect potable reuse at the Flemish Coast, *Desalination*, 218 (2008) 198-207.
- [114] L.D. Nghiem, S. Hawkes, Effects of membrane fouling on the nanofiltration of pharmaceutically active compounds (PhACs): Mechanisms and role of membrane pore size, *Sep. Purif. Technol.*, 57 (2007) 176-184.
- [115] H.Y. Ng, M. Elimelech, Influence of colloidal fouling on rejection of trace organic contaminants by reverse osmosis, *J. Membr. Sci.*, 244 (2004) 215-226.
- [116] P. Xu, C. Bellona, J.E. Drewes, Fouling of nanofiltration and reverse osmosis membranes during municipal wastewater reclamation: Membrane autopsy results from pilot-scale investigations, *J. Membr. Sci.*, 353 (2010) 111-121.
- [117] A.R.D. Verliefde, E.R. Cornelissen, S.G.J. Heijman, I. Petrinic, T. Luxbacher, G.L. Amy, B. Van der Bruggen, J.C. van Dijk, Influence of membrane fouling by (pretreated) surface water on rejection of pharmaceutically active compounds (PhACs) by nanofiltration membranes, *J. Membr. Sci.*, 330 (2009) 90-103.
- [118] E.M.V. Hoek, M. Elimelech, Cake-Enhanced Concentration Polarization: A New Fouling Mechanism for Salt-Rejecting Membranes, *Environ. Sci. Technol.*, 37 (2003) 5581-5588.

- [119] G.-D. Kang, C.-J. Gao, W.-D. Chen, X.-M. Jie, Y.-M. Cao, Q. Yuan, Study on hypochlorite degradation of aromatic polyamide reverse osmosis membrane, *J. Membr. Sci.*, 300 (2007) 165-171.
- [120] A. Simon, L.D. Nghiem, P. Le-Clech, S.J. Khan, J.E. Drewes, Effects of membrane degradation on the removal of pharmaceutically active compounds (PhACs) by NF/RO filtration processes, *J. Membr. Sci.*, 340 (2009) 16-25.
- [121] A. Simon, W.E. Price, L.D. Nghiem, Effects of chemical cleaning on the nanofiltration of pharmaceutically active compounds (PhACs), *Sep. Purif. Technol.*, 88 (2012) 208-215.
- [122] T. Fujioka, S.J. Khan, Y. Poussade, J.E. Drewes, L.D. Nghiem, N-nitrosamine removal by reverse osmosis for indirect potable water reuse – A critical review based on observations from laboratory-, pilot- and full-scale studies, *Sep. Purif. Technol.*, 98 (2012) 503-515.
- [123] G. Kang, Y. Cao, Development of antifouling reverse osmosis membranes for water treatment: A review, *Water Res.*, 46 (2012) 584-600.
- [124] M. Elimelech, W.H. Chen, J.J. Waypa, Measuring the zeta (electrokinetic) potential of reverse osmosis membranes by a streaming potential analyzer, *Desalination*, 95 (1994) 269-286.
- [125] D. Frigon, R. Michael Guthrie, G. Timothy Bachman, J. Royer, B. Bailey, L. Raskin, Long-term analysis of a full-scale activated sludge wastewater treatment system exhibiting seasonal biological foaming, *Water Res.*, 40 (2006) 990-1008.
- [126] P. Berg, G. Hagmeyer, R. Gimbel, Removal of pesticides and other micropollutants by nanofiltration, *Desalination*, 113 (1997) 205-208.
- [127] W.S. Ang, N.Y. Yip, A. Tiraferri, M. Elimelech, Chemical cleaning of RO membranes fouled by wastewater effluent: Achieving higher efficiency with dual-step cleaning, *J. Membr. Sci.*, 382 (2011) 100-106.
- [128] D. Jermann, W. Pronk, M. Boller, A.I. Schäfer, The role of NOM fouling for the retention of estradiol and ibuprofen during ultrafiltration, *J. Membr. Sci.*, 329 (2009) 75-84.
- [129] O. Kedem, A. Katchalsky, Permeability of composite membranes. Part 1.- Electric current, volume flow and flow of solute through membranes, *Trans. Faraday Soc.*, 59 (1963) 1918-1930.
- [130] T. Tsuru, S. Izumi, T. Yoshioka, M. Asaeda, Temperature effect on transport performance by inorganic nanofiltration membranes, *AIChE Journal*, 46 (2000) 565-574.
- [131] K.S. Spiegler, O. Kedem, Thermodynamics of hyperfiltration (reverse osmosis): criteria for efficient membranes, *Desalination*, 1 (1966) 311-326.
- [132] T. Tsuru, K. Ogawa, M. Kanezashi, T. Yoshioka, Permeation characteristics of electrolytes and neutral solutes through titania nanofiltration membranes at high temperatures, *Langmuir*, 26 (2010) 10897-10905.
- [133] G.B. van den Berg, I.G. Rácz, C.A. Smolders, Mass transfer coefficients in cross-flow ultrafiltration, *J. Membr. Sci.*, 47 (1989) 25-51.
- [134] Y. Kiso, K. Muroshige, T. Oguchi, T. Yamada, M. Hhirose, T. Ohara, T. Shintani, Effect of molecular shape on rejection of uncharged organic compounds by nanofiltration membranes and on calculated pore radii, *J. Membr. Sci.*, 358 (2010) 101-113.

- [135] Y. Kiso, Y. Sugiura, T. Kitao, K. Nishimura, Effects of hydrophobicity and molecular size on rejection of aromatic pesticides with nanofiltration membranes, *J. Membr. Sci.*, 192 (2001) 1-10.
- [136] C. Bellona, J.E. Drewes, The role of membrane surface charge and solute physico-chemical properties in the rejection of organic acids by NF membranes, *J. Membr. Sci.*, 249 (2005) 227-234.
- [137] K.O. Agenson, T. Urase, Change in membrane performance due to organic fouling in nanofiltration (NF)/reverse osmosis (RO) applications, *Sep. Purif. Technol.*, 55 (2007) 147-156.
- [138] K. Boussu, A. Belpaire, A. Volodin, C. Van Haesendonck, P. Van der Meeren, C. Vandecasteele, B. Van der Bruggen, Influence of membrane and colloid characteristics on fouling of nanofiltration membranes, *J. Membr. Sci.*, 289 (2007) 220-230.
- [139] R.K. Henderson, N. Subhi, A. Antony, S.J. Khan, K.R. Murphy, G.L. Leslie, V. Chen, R.M. Stuetz, P. Le-Clech, Evaluation of effluent organic matter fouling in ultrafiltration treatment using advanced organic characterisation techniques, *J. Membr. Sci.*, 382 (2011) 50-59.
- [140] S.A. Huber, A. Balz, M. Abert, W. Pronk, Characterisation of aquatic humic and non-humic matter with size-exclusion chromatography – organic carbon detection – organic nitrogen detection (LC-OCD-OND), *Water Res.*, 45 (2011) 879-885.
- [141] R.K. Henderson, R.M. Stuetz, S.J. Khan, Demonstrating ultra-filtration and reverse osmosis performance using size exclusion chromatography, *Water Sci. Technol.*, 62 (2010) 2747-2753.
- [142] J. Haberkamp, M. Ernst, U. Böckelmann, U. Szewzyk, M. Jekel, Complexity of ultrafiltration membrane fouling caused by macromolecular dissolved organic compounds in secondary effluents, *Water Res.*, 42 (2008) 3153-3161.
- [143] H.K. Shon, S. Vigneswaran, R.B. Aim, H.H. Ngo, I.S. Kim, J. Cho, Influence of Flocculation and Adsorption as Pretreatment on the Fouling of Ultrafiltration and Nanofiltration Membranes: Application with Biologically Treated Sewage Effluent, *Environ. Sci. Technol.*, 39 (2005) 3864-3871.
- [144] L.D. Nghiem, P.J. Coleman, C. Espendiller, Mechanisms underlying the effects of membrane fouling on the nanofiltration of trace organic contaminants, *Desalination*, 250 (2010) 682-687.
- [145] C.Y. Tang, Y.-N. Kwon, J.O. Leckie, Fouling of reverse osmosis and nanofiltration membranes by humic acid--Effects of solution composition and hydrodynamic conditions, *J. Membr. Sci.*, 290 (2007) 86-94.
- [146] M. Beyer, B. Lohrengel, L.D. Nghiem, Membrane fouling and chemical cleaning in water recycling applications, *Desalination*, 250 (2010) 977-981.
- [147] S. Lee, W.S. Ang, M. Elimelech, Fouling of reverse osmosis membranes by hydrophilic organic matter: implications for water reuse, *Desalination*, 187 (2006) 313-321.
- [148] C.Y. Tang, Y.-N. Kwon, J.O. Leckie, Characterization of humic acid fouled reverse osmosis and nanofiltration membranes by transmission electron microscopy and streaming potential measurements, *Environ. Sci. Technol.*, 41 (2006) 942-949.

- [149] K.L. Tu, A.R. Chivas, L.D. Nghiem, Effects of membrane fouling and scaling on boron rejection by nanofiltration and reverse osmosis membranes, *Desalination*, 279 (2011) 269-277.
- [150] T. Fujioka, L.D. Nghiem, S.J. Khan, J.A. McDonald, Y. Poussade, J.E. Drewes, Effects of feed solution characteristics on the rejection of N-nitrosamines by reverse osmosis membranes, *J. Membr. Sci.*, 409–410 (2012) 66-74.
- [151] R. Liikanen, J. Yli-Kuivila, R. Laukkanen, Efficiency of various chemical cleanings for nanofiltration membrane fouled by conventionally-treated surface water, *J. Membr. Sci.*, 195 (2002) 265-276.
- [152] Q. Li, M. Elimelech, Organic fouling and chemical cleaning of nanofiltration membranes: measurements and mechanisms, *Environ. Sci. Technol.*, 38 (2004) 4683-4693.
- [153] W.S. Ang, A. Tiraferri, K.L. Chen, M. Elimelech, Fouling and cleaning of RO membranes fouled by mixtures of organic foulants simulating wastewater effluent, *J. Membr. Sci.*, 376 (2011) 196-206.
- [154] W.S. Ang, S. Lee, M. Elimelech, Chemical and physical aspects of cleaning of organic-fouled reverse osmosis membranes, *J. Membr. Sci.*, 272 (2006) 198-210.
- [155] A. Al-Amoudi, P. Williams, S. Mandale, R.W. Lovitt, Cleaning results of new and fouled nanofiltration membrane characterized by zeta potential and permeability, *Sep. Purif. Technol.*, 54 (2007) 234-240.
- [156] J. Benavente, M.I. Vázquez, Effect of age and chemical treatments on characteristic parameters for active and porous sublayers of polymeric composite membranes, *J. Colloid Interface Sci.*, 273 (2004) 547-555.
- [157] C.K. Kim, J.H. Kim, I.J. Roh, J.J. Kim, The changes of membrane performance with polyamide molecular structure in the reverse osmosis process, *J. Membr. Sci.*, 165 (2000) 189-199.
- [158] C.Y. Tang, Y.-N. Kwon, J.O. Leckie, Effect of membrane chemistry and coating layer on physiochemical properties of thin film composite polyamide RO and NF membranes: I. FTIR and XPS characterization of polyamide and coating layer chemistry, *Desalination*, 242 (2009) 149-167.
- [159] Y.-N. Kwon, J.O. Leckie, Hypochlorite degradation of crosslinked polyamide membranes: II. Changes in hydrogen bonding behavior and performance, *J. Membr. Sci.*, 282 (2006) 456-464.
- [160] M.R. Teixeira, M.J. Rosa, M. Nyström, The role of membrane charge on nanofiltration performance, *J. Membr. Sci.*, 265 (2005) 160-166.
- [161] A. Al-Amoudi, Effect of chemical cleaning agents on virgin nanofiltration membrane as characterized by positron annihilation spectroscopy, *Sep. Purif. Technol.*, (2013).
- [162] A. Simon, W.E. Price, L.D. Nghiem, Influence of formulated chemical cleaning reagents on the surface properties and separation efficiency of nanofiltration membranes, *J. Membr. Sci.*, 432 (2013) 73-82.
- [163] T. Fujioka, S.J. Khan, J.A. McDonald, R.K. Henderson, Y. Poussade, J.E. Drewes, L.D. Nghiem, Effects of membrane fouling on N-nitrosamine rejection by nanofiltration and reverse osmosis membranes, *J. Membr. Sci.*, 427 (2013) 311-319.

- [164] S. Sobana, R. Panda, Review on modelling and control of desalination system using reverse osmosis, *Reviews in Environmental Science and Biotechnology*, 10 (2011) 139-150.
- [165] B. Van der Bruggen, A. Verliefde, L. Braeken, E.R. Cornelissen, K. Moons, J.Q.J.C. Verberk, H.J.C. van Dijk, G. Amy, Assessment of a semi-quantitative method for estimation of the rejection of organic compounds in aqueous solution in nanofiltration, *J. Chem. Technol. Biotechnol.*, 81 (2006) 1166-1176.
- [166] B. Van der Bruggen, J. Schaep, D. Wilms, C. Vandecasteele, Influence of molecular size, polarity and charge on the retention of organic molecules by nanofiltration, *J. Membr. Sci.*, 156 (1999) 29-41.
- [167] L.D. Nghiem, A.I. Schäfer, M. Elimelech, Nanofiltration of Hormone Mimicking Trace Organic Contaminants, *Separation Science and Technology*, 40 (2005) 2633-2649.
- [168] L.D. Nghiem, A.I. Schäfer, M. Elimelech, Pharmaceutical Retention Mechanisms by Nanofiltration Membranes, *Environ. Sci. Technol.*, 39 (2005) 7698-7705.
- [169] T. Matsuura, S. Sourirajan, Reverse osmosis transport through capillary pores under the influence of surface forces, *Industrial & Engineering Chemistry Process Design and Development*, 20 (1981) 273-282.
- [170] D. Nanda, K.-L. Tung, W.-S. Hung, C.-H. Lo, Y.-C. Jean, K.-R. Lee, C.-C. Hu, J.-Y. Lai, Characterization of fouled nanofiltration membranes using positron annihilation spectroscopy, *J. Membr. Sci.*, 382 (2011) 124-134.
- [171] K.-L. Tung, Y.-C. Jean, D. Nanda, K.-R. Lee, W.-S. Hung, C.-H. Lo, J.-Y. Lai, Characterization of multilayer nanofiltration membranes using positron annihilation spectroscopy, *J. Membr. Sci.*, 343 (2009) 147-156.
- [172] K. Boussu, J. De Baerdemaeker, C. Dauwe, M. Weber, K.G. Lynn, D. Depla, S. Aldea, I.F.J. Vankelecom, C. Vandecasteele, B. Van der Bruggen, Physico-Chemical Characterization of Nanofiltration Membranes, *ChemPhysChem*, 8 (2007) 370-379.
- [173] T. Shintani, A. Shimazu, S. Yahagi, H. Matsuyama, Characterization of methyl-substituted polyamides used for reverse osmosis membranes by positron annihilation lifetime spectroscopy and MD simulation, *Journal of Applied Polymer Science*, 113 (2009) 1757-1762.
- [174] J. Lee, C.M. Doherty, A.J. Hill, S.E. Kentish, Water vapor sorption and free volume in the aromatic polyamide layer of reverse osmosis membranes, *J. Membr. Sci.*, 425-426 (2013) 217-226.
- [175] R. Suzuki, Y. Kobayashi, T. Mikado, H. Ohgaki, M. Chiwaki, T. Yamazaki, T. Tomimasu, Slow Positron Pulsing System for Variable Energy Positron Lifetime Spectroscopy, *Jpn. J. Appl. Phys.*, 30 (1991) 532-534.
- [176] Y. Ito, H.F.M. Mohamed, V.P. Shantarovich, T. Suzuki, Vacancy Spectroscopy Using Positronium : What are we Looking at by Positronium in Polymers, *Membrane*, 34 (2009) 164-178.
- [177] Y.C. Jean, P.E. Mallon, D.M. Schrader, Principles And Applications Of Positron And Positronium Chemistry, World Scientific, Singapore, 2003.
- [178] M. Eldrup, D. Lightbody, J.N. Sherwood, The temperature dependence of positron lifetimes in solid pivalic acid, *Chem. Phys.*, 63 (1981) 51-58.

- [179] S.J. Tao, Positronium Annihilation in Molecular Substances, *J. Chem. Phys.*, 56 (1972) 5499-5510.
- [180] K. Ito, Z. Chen, W. Zhou, N. Oshima, H. Yanagishita, R. Suzuki, Y. Kobayashi, Subnanoscopic Holes in Composite Membranes for Desalination Elucidated by Energy-Tunable Positron Annihilation, *Jpn. J. Poly. Sci. Technol.*, 69 (2012) 443-447.
- [181] V. Freger, Nanoscale Heterogeneity of Polyamide Membranes Formed by Interfacial Polymerization, *Langmuir*, 19 (2003) 4791-4797.
- [182] A. Prakash Rao, S.V. Joshi, J.J. Trivedi, C.V. Devmurari, V.J. Shah, Structure-performance correlation of polyamide thin film composite membranes: effect of coating conditions on film formation, *J. Membr. Sci.*, 211 (2003) 13-24.
- [183] T. Fujioka, S.J. Khan, J.A. McDonald, A. Roux, Y. Poussade, J.E. Drewes, L.D. Nghiem, N-nitrosamine rejection by nanofiltration and reverse osmosis membranes: The importance of membrane characteristics, *Desalination*, 316 (2013) 67-75.
- [184] C. Bellona, J.E. Drewes, Viability of a low-pressure nanofilter in treating recycled water for water reuse applications: A pilot-scale study, *Water Res.*, 41 (2007) 3948-3958.
- [185] K.L. Tu, L.D. Nghiem, A.R. Chivas, Boron removal by reverse osmosis membranes in seawater desalination applications, *Sep. Purif. Technol.*, 75 (2010) 87-101.
- [186] P.P. Mane, P.-K. Park, H. Hyung, J.C. Brown, J.-H. Kim, Modeling boron rejection in pilot- and full-scale reverse osmosis desalination processes, *J. Membr. Sci.*, 338 (2009) 119-127.
- [187] P.-K. Park, S. Lee, J.-S. Cho, J.-H. Kim, Full-scale simulation of seawater reverse osmosis desalination processes for boron removal: Effect of membrane fouling, *Water Res.*, 46 (2012) 3796-3804.
- [188] H. Hyung, J.-H. Kim, A mechanistic study on boron rejection by sea water reverse osmosis membranes, *J. Membr. Sci.*, 286 (2006) 269-278.
- [189] A.R.D. Verliefde, E.R. Cornelissen, S.G.J. Heijman, J.Q.J.C. Verberk, G.L. Amy, B. Van der Bruggen, J.C. van Dijk, Construction and validation of a full-scale model for rejection of organic micropollutants by NF membranes, *J. Membr. Sci.*, 339 (2009) 10-20.
- [190] G. Schock, A. Miquel, Mass transfer and pressure loss in spiral wound modules, *Desalination*, 64 (1987) 339-352.
- [191] E.M.V. Hoek, J. Allred, T. Knoell, B.-H. Jeong, Modeling the effects of fouling on full-scale reverse osmosis processes, *J. Membr. Sci.*, 314 (2008) 33-49.
- [192] K.M. Sassi, I.M. Mujtaba, Effective design of reverse osmosis based desalination process considering wide range of salinity and seawater temperature, *Desalination*, 306 (2012) 8-16.
- [193] S. Senthilmurugan, A. Ahluwalia, S.K. Gupta, Modeling of a spiral-wound module and estimation of model parameters using numerical techniques, *Desalination*, 173 (2005) 269-286.